NOVIA
UNIVERSITY OF APPLIED SCIENCES

Design of a High-speed Permanent Magnet Synchronous Generator for a Wind Turbine

Syed Danish Mukhtar

Master's Thesis

Master's degree programme in Automation Technology

Vaasa 2022

OPINNÄYTETYÖ

Tekijä: Syed Danish Mukhtar

Koulutusohjelma ja paikkakunta: Automaatiotekniikka, Vaasa

Ohjaaja: Ray Pörn

Nimike: Nopean pysyvän synkronisen magneettigeneraattorin suunnittelu Tuuliturbiinille

---

Päivämäärä: 21.4.2022 Sivumäärä: 152 Liitteet: 4

Tiivistelmä

Tämä opinnäytetyö keskittyy HSPMSG:n (High-Speed Permanent Magnet Synchronous Generator) tuottaman suoritustehokkuuden parantamiseen harjattomien liukurenkaiden ja suuritehoisten tiheyksien ansiosta. Opinnäytetyö huomioi erityisesti tuuliturbiinin mekaanisten ja sähköisten osien välisen vuorovaikutuksen ja pyrkii antamaan pienet häviöt, jotka ovat voimassa generaattorin suunnitteluvaiheessa.

Ensimmäisessä vaiheessa tehtiin yleiskatsaus PMSG:n (Permanent Magnet Synchronous Generator) konesuunnittelusta ja niihin liittyvistä analyyseistä. Tehtiin olemassa olevien konesuunnittelutopologioiden vertaileva analyysi ja pohdittiin generaattorin erilaisten suunnitteluparametrien ja muuttujien vaikutusta. Lopuksi raportoitiin HSPMSG:ssä sovelletut analyyttiset ja elementtimenetelmät (FEM) ja erityisesti sellaiset, joilla pyrittiin täyttämään tuuliturbiinijärjestelmän koneen perusvaatimukset.

Toisessa vaiheessa MATLABissa luotiin täysin integroitu analyyttinen malli HSPMSG:stä ja koneen sähköisistä suureista. Tämän mallin tavoitteena oli laskea koneen ominaisuudet (syöttöteho, hyötysuhde jne.) ja siihen liittyvät parametrit arvioitiin. Jotkut näistä simulaatiotuloksista on validoitu 2-D FEM:llä MotorXP-PM:ssä.

Kolmannessa vaiheessa kahden eri menetelmän prototyyppimalli yhdistettiin validoitujen tulo- ja lähtösuunnitteluparametrien perusteella, jotta voitiin suunnitella uusi tehokas, helposti muunnettavissa oleva generaattori keskikokoiseen ja suureen tuuliturbiinijärjestelmään. Lisäksi tämä uusi prototyyppi saavutti onnistuneesti määritellyn lähtötehon lisäämättä rautahäviöitä tai vaihevirtaa.

Kieli: englanti Avainsanat: HSPMSG, analyyttinen malli, FEM, MATLAB, MotorXP-PM

EXAMENSARBETE

Författare: Syed Danish Mukhtar
Utbildning och ort: Automationsteknik, Vasa
Handledare: Ray Pörn
Titel: Design av High-speed Permanent Magnet Synchronous Generator för Vindkraftverk

---

Datum: 21.4.2022 Sidantal: 152 Bilagor: 4

Abstrakt

Den här avhandlingen fokuserar på förbättringen av prestandaeffektiviteten som genereras av High-Speed Permanent Magnet Synchronous Generator (HSPMSG) på grund av borstlösa släpringar och höga effektdensiteter. Den tar särskilt hänsyn till samverkan mellan de mekaniska och elektriska delarna av vindturbinen och syftar till att ge låga förluster som gäller i generatorns designfas.

I den första fasen görs en översikt över maskinkonstruktionen av Permanent Magnet Synchronous Generator (PMSG) och deras tillhörande analyser. En jämförande analys av de befintliga maskindesigntopologierna görs och generatorns inverkan på olika designparametrar och variabler diskuteras. Slutligen rapporteras den analytiska och finita elementmetoden (FEM) som tillämpas på HSPMSG, och särskilt de som syftar till att uppfylla grundläggande maskinkrav för ett vindturbinsystem.

I den andra fasen etableras en helt integrerad analytisk modell av HSPMSG och maskinens elektriska kvantiteter i MATLAB. Denna modell syftar till att beräkna maskinens egenskaper (ingångseffekt, effektivitet, etc.) och dess närliggande parametrar uppskattas. Vissa av dessa simuleringsresultat är validerade med 2-D FEM i MotorXP-PM.

I den tredje fasen slås prototypmodellen av de två olika metoderna samman baserat på de validerade designparametrarna för input och output för att designa en ny högpresterande lätt konverterbar generator för ett medelstort och storskaligt vindturbinsystem. Dessutom nådde denna nya prototyp framgångsrikt den specificerade uteffekten utan att öka järnförlusterna eller fasströmmen.

Språk: engelska Nyckelord: HSPMSG, analytisk modell, FEM, MATLAB, MotorXP-PM

MASTER'S THESIS

Author: Syed Danish Mukhtar
Degree Programme and Place: Automation Technology, Vaasa
Supervisor: Ray Pörn
Title: Design of a High-speed Permanent Magnet Synchronous Generator for a Wind Turbine

---

Date: 21.4.2022 Number of pages: 152 Appendices: 4

Abstract

This thesis focuses on the enhancement of the performance efficiency generated by the High-speed Permanent Magnet Synchronous Generator (HSPMSG) due to brushless slip rings and high-power densities. It especially accounts for the interaction between the mechanical and electrical parts of the wind turbine and aims to give low losses which apply at the design phase of the generator.

In the first phase, an overview of the machine design of Permanent Magnet Synchronous Generator (PMSG) and their associated analyses are done. A comparative analysis of the existing machine design topologies is done, and the influence of the generator's various design parameters and variables is discussed. Finally, the analytical and finite element method (FEM) applied to the HSPMSG are reported, and especially those aiming to fulfill basic machine requirements for a wind turbine system.

In the second phase, a fully integrated analytical model of the HSPMSG and electrical quantities of the machine is established in MATLAB. This model aims at computing the machine characteristics (input power, efficiency, etc.) and its adjacent parameters are estimated. Some of these simulation results are validated with 2-D FEM in MotorXP-PM.

In the third phase, the prototype model of the two different methods is merged based on the validated input and output design parameters in order to design a new high-performance easily convertible generator for a medium and large-scale wind turbine system. Furthermore, this new prototype successfully reached the specified output power without increasing iron losses or phase current.

Language: English Key words: HSPMSG, analytical model, FEM, MATLAB, MotorXP-PM

Forward

All blessings to almighty ALLAH and its Ahlelbeit (A.S) who enlightened me with the power of wisdom and thought. Ray Pörn starts this campaign from the day first till the last day of this effort as a supervisor without any trembling in his motivation. Under his guidance, I have developed a greater ability to carefully articulate my thoughts, learned to dig deeper, and rediscovered the joys of interesting research. I felt lucky sometimes to have him with me because not only he did provide me with his necessary knowledge in the field of automation technology but also supports me in finding a job in the liquidized Finnish market.

I am grateful to Vladimir Kuptsov who provides me with a MotorXP software license. The work on finite element analysis would not have been possible without his contribution and the time he allotted to me from his busy schedule.

I am thankful to Ronnie Sundsten who interviewed me at the beginning of the course and open a path for me to explore more in the field of automation technology. I would like to mention the name of Hanna Latva with whom I have learned about academic/scientific writing as well as an amazing depth of understanding in the form of homework and assignments.

I want to tribute to the large community of the Novia University of Applied Sciences with whom I have enjoyed a breathtaking experience of learning and support who have enriched my life with generosity and companionship.

Dedicated to my mom & dad for their love & compassion

Table of Contents

List of Figures

List of Tables

Nomenclature

A_s	Area of slot (m^2)
A_{ac}	Winding cross-sectional area (m^2)
A_{st}	Lamination stack length (m)
B	Maximum flux density (T)
B_g	Air-gap flux density (T)
B_b	Back iron flux density (T)
B_t	Tooth flux density (T)
B_{gm}	Air-gap magnetic flux density (T)
B_r	Magnet remnant flux density (T)
B_o	Base flux density (T)
B_{flux}	Radial flux density through coil (T)
B_{sat}	Saturation flux density (T)
B_m	Magnetic flux density (T)
B_n	Magnetic flux density for polyphase windings (T)
$B(\theta)$	Flux density w.r.t magnet physical angle (T)
BH_{max}	Energy product (kJ/m^3)
$C\phi$	Flux concentration factor
C_r	Resistance coefficient
C_h	Coefficient of hysteresis losses
C_c	Coefficient of classical eddy current losses
C_e	Coefficient of excess eddy current losses
C_f	Friction coefficient
CP	Geometrical of permeance coefficient
cov	Conversion factor
D_{mach}	Outer diameter of a machine (m)
D_{in}	Inner diameter (m)
D_s	Strand diameter (m)
dc	Density of conductor (kg/m^3)
ds	Steel density (kg/m^3)
dm	Magnet density (kg/m^3)
E	Electric field (V/m)
E_a	RMS phase excitation voltage/internal voltage (V)
f	Electrical frequency (Hz)
f_e	Electrical frequency “estimated” (Hz)
f_o	Base frequency (Hz)
g	Air gap (m)
g_e	Effective air gap (m)
H	Magnetic field strength (A/m)
H_c	Coercivity or coercive force (A/m)

H_k	Knee magnetization force ($\mathrm{A/m}$)
h_m	Magnet height (m)
h_s	Slot height (m)
h_d	Slot depression height (m)
i	Coil current (A)
I_a	RMS armature/stator current (A)
J	Density of eddy current losses ($\mathrm{A/m^2}$)
J_a	Stator current density "assumed" ($\mathrm{A/m^2}$)
J_o	Stator current density "estimated" ($\mathrm{A/m^2}$)
J_{air}	Density of air ($\mathrm{kg/m^3}$)
k_s	Skew factor
k_d	Breadth or distribution factor
k_w	Winding factor
k_p	Pitch factor
k_g	Magnetic gap factor
k_l	Leakage factor
k_r	Reluctance factor
k_c	Carter's coefficient
k_h	Coefficient of hysteresis losses
k_e	Coefficient of excess eddy current losses
k_z	Surface current density ($\mathrm{A/m^2}$)
l	length of conductor (m)
l_{eh}	Half coil end turn length of an armature conductor (m)
l_{eo}	One end turn length of an armature conductor (m)
L_{ag}	Air-gap inductance (H)
L_{as}	Self-slot leakage inductance (H)
L_{am}	Mutual inductance (H)
L_{slot}	Slot leakage inductance (H)
L_e	End-turn inductance (H)
L_s	Synchronous inductance (H)
L_{st}	Stack length (m)
LDr	Length to diameter ratio
M_{ac}	Mass of the armature conductor (kg)
M_c	Core mass (kg)
M_{cb}	Back iron core mass (kg)
M_{ct}	Tooth core mass (kg)
M_m	Magnet mass (kg)
M_s	Shaft mass (kg)
M_{ser}	Service mass (kg)
M_{tot}	Total mass (kg)
m	Slot per pole per phase

m_w	Magnet width (m)
m_h	Magnet height (m)
m_b	Magnet barrier width (m)
m_{in}	Magnet inset height (m)
N	Rated speed “assumed” (rpm)
N_e	Rated speed “estimated” (rpm)
N_s	Number of slots
N_{sap}	Number of slots with actual pitch of the coil
N_{sfp}	Number of slots with full pitch coil
N_{sp}	Number of slots short pitched
η	Material constant
N_c	Number of turns per coil
n	Flux density exponent
nf	Frequency exponent
N_a	Number of armature turns per coil
N_{cs}	Number of conductors/slots
p	Number of pole pairs
P	Active power (W)
P_b	Base power (W/lb)
P_{cb}	Core back iron losses (W)
P_{ct}	Tooth losses (W)
$Perm$	Slot permeance
P_s	Fundamental machine power (W)
P_{stray}	Stray losses (W)
P_h	Hysteresis losses (W)
p_e	Eddy current losses (W)
P_{iron}	Iron losses (W)
P_{wind}	Windage losses (W)
P_c	Total core losses
P_r	Rotor eddy current losses (W)
P_a	Conductor or copper losses (W)
P_{out}	Power output (W)
P_{in}	Power input (W)
Q	Reactive power (VAR)
q	Number of phases
R_{so}	Stator outside radius (m)
R_{ro}	Rotor outside radius (m)
R_a	Armature/stator resistance (Ω)
R_b	Bottom corner radius (m)
R_t	Top corner radius (m)
R_S	Outer magnet boundary (m)

R_2	Outer boundary of magnet (m)
R_i	Inner magnetic boundary (m)
R_1	Inner boundary of magnet (m)
R_{ci}	Core inside radius (m)
R_{co}	Core outside radius (m)
R_{out}	Outer diameter (m)
R_{in}	Inner radius (m)
r	Radius of rotor (m)
Rey	Reynold's number
S_m	Magnet segments
$sbir$	Stator back iron ratio
$sbid$	Stator core back iron depth (m)
t	Thickness of the material (m)
T	Torque (Nm)
T_f	Peripheral tooth fraction
T_c	Temperature coefficient of the resistance
T_{cog}	Cogging torque (Nm)
τ	Shear stress (psi)
τ_s	Total slot width (m)
u_{rec}	Recoil permeability
μ	Kinematic viscosity of cooling media (m^2/s)
u_0	Permeability of free space
v_{t_ip}	Tip speed (m/s)
V	RMS phase voltage (V)
V_{out}	Output voltage (V)
v	Volume of the material (m^3)
V_a	Terminal voltage (V)
V_{back}	Back-emf (V)
ω	Angular frequency (rad/s)
ω_m	Mechanical frequency (rad/s)
w_t	Width of tooth (m)
ws	Average width of slot (m)
ws_{bottom}	Slot bottom width (m)
ws_{top}	Slot top width (m)
ω_0	Electrical frequency (rad/s)
w_d	Slot depression width (m)
X_s	Synchronous reactance (Ω)
α	Pitch of a winding (electrical degree)
α_{tip}	Tooth tip angle (degree)
β	Efficiency (percentage)
ε	Kinematic viscosity of air (m^2/s)

γ	Coil electrical angle (degree)
γ_{ad}	Advance angle (electrical degree)
Ψ	Torque angle between V_a and E_a (electrical degree)
ϕ	Angle between E_a and I_a or power factor angle (electrical degree)
ϕs	Radial flux through coil (Wb)
ϕ_{pk}	Peak radial flux through coil (Wb)
ϕ_{link}	Flux linkage (Wb)
ϕ_{gm}	Air-gap magnetic flux (Wb)
λ	Length of rotor (m)
λ_s	Slot fill factor
λ_n	Magnetic flux linkage (T)
$\lambda(\theta)$	Total flux linkage w.r.t physical angle (T)
ρ	Electrical resistivity of the material ($\Omega \cdot$ m)
δ	Skin depth
$\hat{\sigma}$	Stator winding conductivity (S/m)
θ_{sk}	Skew angle (electrical degree)
θ_m	Magnet physical angle (radians)
θ_{msk}	Magnet skew angle (mechanical degree)

Chapter 1

1 Introduction

This thesis provides comprehensive research on the topic "Design of a High-speed Permanent Magnet Synchronous Generator for a Wind Turbine" to fulfil the requirements for the master's degree programme in Automation Technology. Based on the results garnered from this research I could gain an insight into the topic that could provide suggestions much needed to the current machine designers working on this topic and ultimately fulfil the purpose of clean and sustainable energy.

1.1 Background

With the substantial growth in the clean and sustainable energy driven by renewable energy resources, such as wind energy is adopted for future electricity generation. In 1990, 16 countries generated a total of about 3.6 billion kWh of wind electricity. In 2017, 129 countries generated a total of about 1.13 trillion kWh of wind electricity [1]. Much of the effort has devoted to further increase the efficiency of the wind turbines. As systems have matured, there is also an increasing demand for low-cost high-performance technologies for renewable energy resources. Designing a high-speed permanent magnet synchronous generator is one area of interest for its potential to significantly reduce the cost of electricity produced by the wind turbines [2].

While the wind energy benefits for electricity generation have been known for about a century [1], only recently have technological advances enabled the use of small-scale wind turbine systems to practically generate electricity on the industrial scale. Existing studies in the literature have focused on large-scale wind turbines within a range of few megawatts of power generation. While there are definite low weight and high-speed benefits to such wind turbine generator design, the existing wind turbine generator design present an unacceptable weight and less efficient electric machine for most wind turbine design. Fortunately, the use of highly efficient electric machines in wind turbines has significantly extended the applications of renewable energy resources in power generation.

This research takes advantage of the permanent magnet (PM) machine and its other necessary characteristics, which offers a wide range of speed and still maintaining good efficiency and power factor for the wind turbine system. As such, many characteristics are crucial for the design of the PM machine which includes a brushless PM machine for the

wind turbine generator. The term “brushless” means that the PM machine does not require brushes, which reduce the weight, cost, and losses. Additionally, the availability of rare-earth magnets making brushless PM machines more popular [3].

There are a number of factors that dictate which type of electric machine is optimal for a wind turbine system such as the high-power density linked mainly to the quality of permanent magnets because of their high magnetic excitation air-gap flux density instead of the size of the PM machine. In addition, current-excited machines, on one hand, have comparatively lower power density due to their lack of space for conductors in a small volume, while on the other hand, the high-frequency design reduces the size and weight of the machine for the same power requirements, respectively. The high-frequency design offers the elimination of power transmission elements. As such, many of the additional components are downsized, and the resulting machine becomes more efficient, lighter, and portable to get maximum benefits from wind energy [4].

1.2 Concept

Natural resources have often been used in solving environmental challenges. The electrical energy produced by the rotation of wind turbine propellers is one predominant way to overcome such challenges. Industry and academia often discuss a wind turbine generator that can fit not only into the renewable energy market easily but are fully capable of producing maximum power without compromising technical features throughout the entire lifecycle of the wind turbine system. When tasked to design a wind turbine generator, the designer will make every effort to keep it simple in design, small in size, and easier to control. In addition, the competitors look for competitive futuristic design, which is fast to enter the market.

Among the many concepts of designing a competitive wind turbine generator, a high-speed completely convertible generator is often used for required power production. High-speed completely convertible generators have lower lifecycle costs and perfectly feasible for the deployment in the rural and sparsely dispersed areas where resources are minimum and large-scale power plants are not feasible as compared to low and medium-speed wind turbine generators. The use of permanent magnet material in electrical machine design has converted the idea of high speed completely convertible generator into a reality. The most important of these, however, is to design a high-speed permanent magnet synchronous generator (HSPMSG) with excellent performance without compromising the technical features [5].

Experimental work on HSPMSG's has yielded a number of advantages such as smaller volume and higher power density over the other type of generators used in wind turbines. Any wind turbine system based on the HSPMSG design concept heavily relies on the electrical, magnetic, and structural performance of the PM machine, for example, the electrical frequency, the voltage waveform, the magnetic flux, the magnet volume, selecting the number of poles, pole size, the magnetic pole pitch, the length-to-diameter ratio, the air-gap size, and stator back iron thickness. All these electromagnetic design parameters must be selected carefully to achieve an excellent performance of the machine [6]. In addition, the design work is conducted to assess the permanent magnet material for the rotor and the properties of the stator accordingly.

A good design concept for HSPMSG relies not only on the electromagnetic design but other technical features as well such as the thermal design of a machine. Common observation shows that, at high speed, the temperature of some of the components of a machine such as the permanent magnets of the rotor increased and close to critical temperature can cause demagnetization. Also, the stator windings are thermally sensitive to the excessive amount of heat and temperature. In short, this research comprises a careful calculation of all the design parameters required for HSPMSG, the selection of appropriate material for the rotor, and properties of the stator by keeping in mind the thermal sensitivity of the material and suitable cooling methods at high-speed without compromising the technical features of a machine.

1.3 Motivation

HSPMSG has the capability to generate a significant amount of electrical energy for wind turbines for a long period of time at an affordable cost. However, some studies suggest that a considerable amount of energy is lost during the operation phase of the wind turbine due to inappropriate choices that have been made during the design phase. The need for a highly efficient generator that can fulfil the demands of the future wind energy market is the main motivation for exploring the concept of HSPMSG in this thesis. The main aim of this research is to calculate the design parameters and selection of permanent magnet material for HSPMSG by keeping the losses at a minimum level. The Analytical Analysis will be carried out in MATLAB software whereas, the Finite Element Analysis will be carried out in MotorXP-PM software. Some suggestions will be given regarding thermal analysis of the machine including designing an appropriate cooling system. This research will represent a

comprehensive design methodology with a prototype model of a brushless high-speed permanent magnet synchronous generator suitable for a wind turbine system.

1.4 Outline

This thesis is structured into the following chapters:

Chapter 2	Literature Review – A literature survey of a high-speed permanent magnet synchronous generator is discussed.
Chapter 3	Methodology – Highlights some of the design layouts used to solve design challenges associated with a brushless high-speed permanent magnet synchronous generator for a wind turbine system.
Chapter 4	Analytical Method – Underlines machine variables/parameters and their values considered to develop a brushless high-speed permanent magnet synchronous generator for a wind turbine system as well as some guidelines to evaluate different parts of a machine.
Chapter 5	Finite Element Method – Identify and evaluate machine variables/parameters to resolve complex geometry of a machine for 2-D field calculation and simulation.
Chapter 6	Modelling and Simulation – Provide a framework to identify input design parameters for the prototype model of a machine and draw output design parameters for the results and analyses purpose.
Chapter 7	Prototype Model – Presents input design parameters/variables used for analytical design parameters estimation from MATLAB and finite element design parameters estimation from MotorXP-PM.
Chapter 8	Results and Analyses – Looks at the simulation results to ensure that the design methodology adopted, fulfil the primary motives of this research work with analyses.
Chapter 9	Conclusion and Future Work – Summarizes the conclusion and discuss potential directions for future research work.

Chapter 2

2 Literature Review

This chapter of the thesis overlooks some of the previous research work carried out on this topic, most of which apply to HSPMSG design driven by wind turbine systems. A literature survey provides a necessary consideration such as the selection of the lamination material, coil construction, and thermal analysis for HSPMSG design, and how the operational efficiency of the machine can be increased by making adequate design choices as compared to other counterparts for the same rated power. By this survey, a detailed prototype modelling of brushless HSPMSG is possible and solving the additional technical challenges associated with thermal sensitivity of the magnet material, and high-temperature design for instance.

2.1 Previous research work

Among the many viable research work from the past, was the observation that the wind turbine can be used to produce electricity. Early researchers correctly hypothesized that by designing highly efficient wind turbine generator, would be able to save energy and reduce losses. However, the reasoning for how to design a highly efficient wind turbine generator was not properly understood. In 1941, Smith-Putnam machine built the world's first large wind turbine using a two-blade propeller downstream system at a constant rotational speed of 28 rpm (revolution per minute). The Smith-Putnam machine's wind turbine produces 1.25 MW of wind electricity that fed directly into the grid using a synchronous electric generator [7].

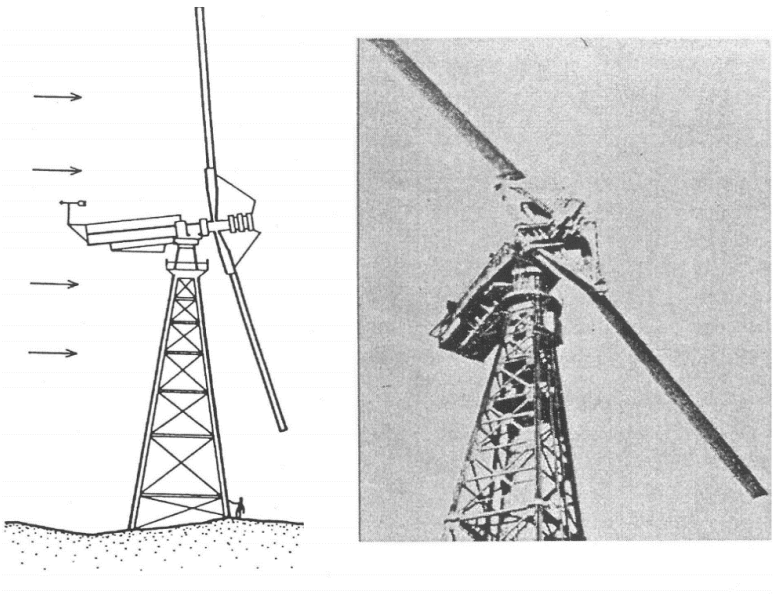

Figure 1. Smith-Putnam wind machine (a) diagrammatic (b) on-site photograph

While the Smith-Putnam machine's idea was correct, the analysis tools were relatively simple, and the generator design was under-predicted. As the machine design theory evolved, the predictions improved as well. During the period 1958 - 1966, France built three-blade propeller design units of a wind-operated electric generator. One unit installed near Paris operated at the constant speed of 47 rpm with its synchronous generator speed of 1000 rpm and 3000 V, connected to a 50 Hz and 60 kW electric grid station via a step-up transformer and a 15 km transmission lines. A further unit, in southern France, operated at the constant speed of 56 rpm with its synchronous generator speed of 1530 rpm [8]. Over the next two decades, a series of global oil crises and environmental concerns increase the needs of renewable energy resources such as wind energy even more demanding for future power production [9].

Figure 2. French wind turbine located near Paris, France; 800 kW (36 mph rated wind speed)

As the idea of electrical energy produced through the wind turbine evolved, the idea of wind turbine generator evolved accordingly. In 1997, Veen et al. [10] published a paper on the design of a high-speed 1400 kW synchronous generator with permanent magnet excitation and loaded by a rectifier, it becomes apparent that rotor losses are a major problem. In this paper, the authors showed that an early choice among several stator windings configuration could improve the problem of rotor losses to an acceptable level, such as 0.1 – 0.2% of the rated power. Ultimately, the cooling of the rotor to an acceptable temperature range become feasible. They computed that an appropriate solution for the rotor losses caused by the asynchronous field components can be found with the help of studying the effect of high frequencies at material properties, dimensions, and harmonics using field equations.

While most previous research works represented the effect of losses occur due to the high-speed and high-frequency of PM machines, in 1999, Proca et al. [11] looked at the analytical modelling of a surface-mount permanent magnet motor. They found that the ripple in the electromagnetic torque is produced due to three main reasons. The first being the non-sinusoidal shape of the current in most brushless direct current (DC) motors, second occurring due to the mismatch in the shape between the back-emf (electromotive force) shape and the current shape, and the third reason is to align with the low reluctance paths (slotting effects). They used a technique of utilizing a great deal of mathematical relationships to calculate the open circuit field, the armature reaction field, the effect of stator slotting, and the magnetic field on load to develop field distribution and relative permeance. In addition to this research work, they extended to include the derivation for the cogging torque and the electromagnetic torque. The analytical model developed in this research work was compared with finite element analysis (FEA) model and a very good correlation was obtained.

Previous research shows that cogging torque, and electromagnetic torque was maximized by considering radial components of magnetization in permanent magnets only. Consequently, this reduced the overall performance of the PM machine. In 1999, Rasmussen [12] showed that by including tangential components of magnetization to calculate the field distribution could enhance the machine performance. The author’s main objective is to represent the analytical prediction of the magnetic field from a surface mount magnet motor. He used this model to calculate the field distribution for three different types of magnetizations such as sine magnetization, radial sine magnetization, and radial magnetization. Additionally, he constructed the Hall probe and encoder test setup in order to measure the radial air-gap flux

density. The author achieved a good agreement between the model developed and the measured results.

Experimental work on brushless permanent magnet synchronous machine has yielded several insights as well. In 2002, Zhu et al. [13] developed a 2-D analytical model with the solution of the Laplacian/quasi-Poissonian field equations in the air-gap/magnet regions, and no simplifying assumptions about the relative recoil permeability of the magnets. They performed analytical calculations for the field distributions from both overlapping and non-overlapping stator windings and compared with FEA predictions from a slotless machine having both radial and tangential magnetization of a rotor as well as for a slotted machine with tangential magnetized rotor having both overlapping and non-overlapping stator windings. This model incorporates the work previously done by Rasmussen [12] and extends the experimental work for internal and external rotor topologies, radial, and tangential magnetization, overlapping and non-overlapping stator winding configurations and slotted and slotless stators [13].

Likewise, Zhu et al. [12], Proca et al. [10] also extended their electromagnetic and cogging torque work from 1999 by publishing a new paper based on Zhu et al. [13] work. In 2003, Proca et al. [14] extend field calculations to include the electromagnetic and cogging torque with the back-emf shape included. A comparison was conducted with FEA and showed excellent agreement.

The previous methods followed an analytical approach by assuming calculations of torque, back-emf, etc. across the macro-elements such as air-gap with permanent magnets. However, in 2000, Zhilichev [15] presents a method of building the numerical-analytical solution of the magnetic problems for slotted and slotless PM machines with surface magnets. In this research work a simple analysis shows that if a hybrid method of magnetic field calculation is adopted then the fast convergence between different types of solutions is achieved by using the Schwartz technique for overlapping sub-regions. This method allows electric machine designers to combine analytical and numerical solutions such as Fourier series, boundary integrals and finite elements in the overlapping sub-regions taking advantage of symmetry, periodicity and linear magnetic properties of airgap and slot areas in PM machines. He validated the method by using different solutions in the slot and by finite element method (FEM) analysis.

As discussed in PM machine design there are several factors that dictate which type of method is optimal for a given set of approaches. The factor includes things like the rotor configuration, windings configurations, type of magnetization, and slotting of a different type. However, examining the design factors of the PM machine more comprehensively, we see that the thermal analysis is essential in terms of the overall performance of an electric machine. In 2011, Mahmoudi et al. [16] analyzed axial-flux permanent-magnet machine with different experimental methods (reducing cogging torque by skewing of slots and magnets, various speed operating conditions through mechanical stress analysis of rotor and lumped-circuit analysis depicts thermal problems through a thermal network similar to an electrical circuit). Because of the machine design's thermal performance according to parameters such as housing heat transfer coefficient, winding current density and machine thermal resistance, we use modern thermal analysis techniques such as experiments, lumped-parameters thermal model and numerical analysis (which are usually FEA-based) for the thermal analysis of a machine. From this research work, the author draws three main conclusions. First, the experimental method, though accurate, is limited to designed-and-constructed machines. Second, the lumped-parameters thermal model is analytical; it quickly estimates machine-temperature distribution. Third and finally, for accurate prediction, numerical analysis is preferred, which includes 3-D-coupled electric, magnetic, and thermal analysis of a machine. A 3-D method, though complex, gives highly accurate results for the thermal behavior of an electric machine.

A number of research works have looked at the computational analysis of electrical machines such as the experimental methods, the analytical methods and the numerical methods. These methods of analysis have been employed to model the electrical machines and to predict their performance accurately at the design stage [17]. In contrast, Guda et al. [18] looked at how a microturbine generation system behaves if it is composed with a permanent magnet synchronous generator (PMSG) for isolated as well as grid-connected operations with the help of modelling and simulation techniques. In this paper, a good description of the system is given with a mathematical modelling method as well as the load analysis of PMSG. The simulation results show that the developed model has met the requirements of load conditions successfully. Their work simplifies the previous studies to include block diagrams describing the system with varying load and specific fuel consumption in MATLAB/Simulink.

So far, we have seen that the computational analysis as well as the modelling and simulation techniques can yield a systematic and sequential optimization for the design of brushless HSPMSG. However, adopting a set of approaches only does not guarantee a high-performance wind turbine generator because these kinds of analyses depend on the tradeoff in losses (eddy current, hysteresis, etc.), general torque, cogging torque, machine design, optimization, sizing, analytical models, general models, performance, and parameter calculations (inductance, resistance, etc.) [19]. Therefore, a simple but cohesive approach is needed who are topic-oriented to address the specific design requirements and permanent magnet material properties simultaneously. In 2014, Hsiao et al. [20] conducted a number of experiments in which design of high performance permanent-magnet synchronous wind generator is analyzed aiming at high induced voltage, low harmonic distortion, high generator efficiency, optimal generator parameters such as pole-arc to pole-pitch ratio and stator-slot-shoes dimension, etc. are determined with the proposed technique using Maxwell 2-D and MATLAB software using Taguchi method. In this paper, the authors proposed double three-phase and six-phase winding configurations, which consist of six windings in the stator, can provide evenly distributed current for high performance operation regarding voltage and current demands. Also, windings are connected in series to increase the output voltage at low wind speed, and in parallel during high wind speed to generate electricity even when either one winding fails, thereby enhancing the reliability. They found that with a 6 Ω load, the output power for the double three-phase winding and six-phase winding were 10.64 and 11.13 kW correspondingly. In addition, they showed that with 24 Ω load, the efficiencies of double three-phase windings and six-phase windings were 96.56 and 98.54% respectively.

While winding configuration is one most important factor to enhance PMSG performance, their importance will be less significant without considering the stator lamination material. In 2004, Paulides et al. [21] proposed an excellent agreement that the iron loss can be reduced considerably by employing 6.5% SiFe (Silicon Iron) lamination rather than 3% SiFe with experimental data. They represented a predicted no-load and full-load stator iron losses which shows the benefits of employing 6.5% SiFe laminations for high speed and high-power PM generators, whose output is rectified by a simple bridge rectifier. They found that 3% SiFe is rarely considered in large electrical machines because of its lower saturation flux density and higher cost. In contrast, 6.5% SiFe is considered due to its higher electrical resistivity at high fundamental frequency.

From this literature survey, we can clearly say that how a number of factors such as the rotor topologies, air-gap flux density, stator windings configurations, and cogging torque, etc. can be used with the help of computational analyses and optimization methods, etc. to predict the possible output of the design process such as the output torque, maximum efficiency, and the size of the machine, etc. Of course, there are many other considerations to consider in optimizing the entire design process of HSPMSG with different prototype models of a machine, but computational analyses and optimization methods are still yielding important insight into the design process. Appropriate design of high-speed machines requires addressing multiple design boundaries simultaneously. For example, Arkkio et al. [22] has presented a design of high-speed permanent magnet synchronous machines but has not done the rotor-dynamics analysis. In another example, Kolondzovski et al. [23] has given an improved design methodology but lacks in thermal analysis. Although different design methodologies are presented by researchers, no one has given fully integrated design which constitutes electrical, mechanical, and thermal analysis of a machine. Therefore, it is necessary to have a set of equations that can be directly calculated from the machine geometry and altered in order to reach an optimal solution [19].

2.2 Topic framing

As discussed previously, past studies have shown that the computational analyses such as analytical analysis, and numerical analysis etc., as well as optimization methods along with modelling and simulation techniques can yield an optimum solution for the design of brushless HSPMSG. This literature survey is then propagated forward to minimize design choices offering significant approach for a particular sort of brushless HSPMSG. The basic machine parameters are:

- For required output power, 660 kW is chosen [24]. The output power is often determined by the type of application in which the generator is being used that can make a difference in output power rating of generator in kVA as well as the referred devices connected with the generator measured in a kW output power.
- The generator rated speed of 15000 rpm is selected for brushless HSPMSG to meet the required performances at the high rotating speed [25]. In the design of high-speed PM machines, the issue is to reduce the iron and eddy current losses due to the high frequency produced by the high speed of the generator respectively [19].

- The output voltage of 690 Volts (DC) is used in this design because it is commonly used in the industry; keeping the losses as minimum as possible [24].
- The number of stator slots of the machine is set to 24. It means that the machine has 24 stator slots to accommodate the machine's armature windings (main windings) and flux path for the magnetic circuit [26].
- Two pole pairs or four poles are selected for this design. The factors involved in the selection of pole pairs are the length of the machine and the fundamental frequency produced by the synchronous speed of the generator. The length of the machine becomes longer if too few poles such as the two poles are chosen. On the contrary, the length of the machine becomes shorter if too many poles such as six poles are used. For optimal design four poles are suitable. Similarly, too few poles produce lower frequency and too many poles produce higher frequency than the required frequency. Therefore, four poles or two pole pairs are chosen to get the shortest possible length of the machine without compromising the performance [27].
- A 3-phase PM machine is chosen for this particular type of generator design because balanced torque is achieved in a 3-phase machine. Higher number of phases can be used if the generator is connected to a DC bus distribution through a power electronics module but with the higher number of phases, we get higher AC line current harmonics [28].
- The number of slots per pole per phase selected for this generator design is 2. This parameter is important not only to determine the connection between rotor poles and stator windings but also to figure out the generated back-emf of the machine. The parameter slots/pole/phase play a vital role to get a balanced sinusoidal voltage waveform and to reduce machine harmonics accordingly [29].
- U-shaped magnets with circular ducts are chosen in this design among many rotor topologies in MotorXP-PM to reduce losses and withstand high temperature. In addition, tooth coil winding pattern is used to get the shortest possible length of the machine.
- A standard double layer overlapping type of winding is used for the design and analysis of a machine. In addition, the number of armature turns per coil is set to 8, and 224 conductors per slot is chosen for the analytical as well as the finite element analysis of the machine, respectively.
- Material used to design rotor and stator lamination is 6.5% SiFe, which is a good choice when it comes to iron losses reduction and operating temperature range accordingly [21].
- The Machine design analysis phase is carried out with the help of analytical and finite element (FE) methods to predict the performance of HSPMSG accurately.

- The analytical, material, basic electrical model, machine size and weight, and basic losses analysis are carried out in MATLAB. MATLAB yields important analytical estimations much needed for the optimal solution of the machine design problems. In other words, MATLAB validates the analytical assumptions carried out in the analytical method of this research work.
- Finally, the FE, electromagnetic, harmonic, and thermal analysis are carried out by using MotorXP-PM. MotorXP-PM model and simulate PM machines in a more detailed manner to study static as well as the dynamic characteristics of a machine in the form of a 2-D simulation [30].

Table 1 below summarizes the basic design considerations and parameters which are assumed in the design of brushless HSPMSG for a wind turbine.

Parameter/design consideration	**Symbol**	**Assumed Value/Detail**
Power output	P_{out}	660 kW
Rated speed	N	15000 rpm
Output voltage	V_{out}	690 V (DC)
Number of stator slots	N_s	24
Pole pairs	p	2
Number of phases	q	3
Number of slots/pole/phase	m	2
Magnet type	-	U-shaped
Type of winding	-	Double layered overlapping
Number of armature turns per coil	N_a	8
Number of conductors/slot	N_{cs}	224
Rotor and stator material	-	6.5% SiFe
Machine design analysis	-	Analytical, material, basic electrical model, machine size & weight, basic losses, FE, electromagnetic, harmonic, and thermal
Machine design analysis methods	-	Analytical, and FE
Software tools for modelling & simulation	-	MATLAB, and MotorXP-PM

Table 1. Basic parameters and considerations assumed for brushless HSPMSG design

These values/details present some basic assumptions that have been made from previous research work carried out on this topic. But detailed generator parameters are presented using in-depth analysis with the help of geometric equations and relationships obtained in chapter 4 on analytical method and chapter 5 on the finite element method of this research work.

2.3 MotorXP-PM

MotorXP-PM enables machine designers to optimize their design for the performance and efficiency, providing crucial link between the electromagnetic as well as the thermal analysis of a wind turbine generator. MotorXP-PM allows fast and easy numerical and graphical results of steady-state as well as the dynamic analysis of an electric machine simultaneously. This software comes with a MATLAB based application and as a standalone program without MATLAB [30]. In this research work MATLAB based application is used for finite element, electromagnetic, harmonic, and performance analysis of the machine. This chapter introduces some of the basic description of MotorXP-PM only. However, the complete functionality of MotorXP-PM is represented in the latter chapter of the thesis when it comes to the finite element analysis of HSPMSG.

Chapter 3

3 Methodology

This chapter introduces some of the basic design methodologies considered in machine design in terms of design phases simultaneously. These include considerations such as how machine design phases can be used to get a detailed design for brushless HSPMSG, and how to achieve overall characteristics, performance, and efficiency for brushless HSPMSG by validating modelling and simulation results based on two different design methodologies such as the analytical method, and finite element method. Once an overall view of two different methods is presented, a machine design process is presented to show how each design variable/parameter is transformed into the performance of a machine to evaluate the impact on the HSPMSG design as a whole.

3.1 Methods

The design parameters assumed in section 2.2 provide a basis to represent an overview of methodology more practical, or at least design centric. Fortunately, because of the previous research work, the methods adopted to design HSPMSG are divided into analytical and finite element methods to solve design challenges associated with electric machine design. This allows the problem to be decomposed into three separable phases which are solved sequentially: machine design analysis, modelling & simulation, and optimal design solution. We explore these two methods for computing the basic generator requirements for wind turbine systems as diagrammed in figure 3.

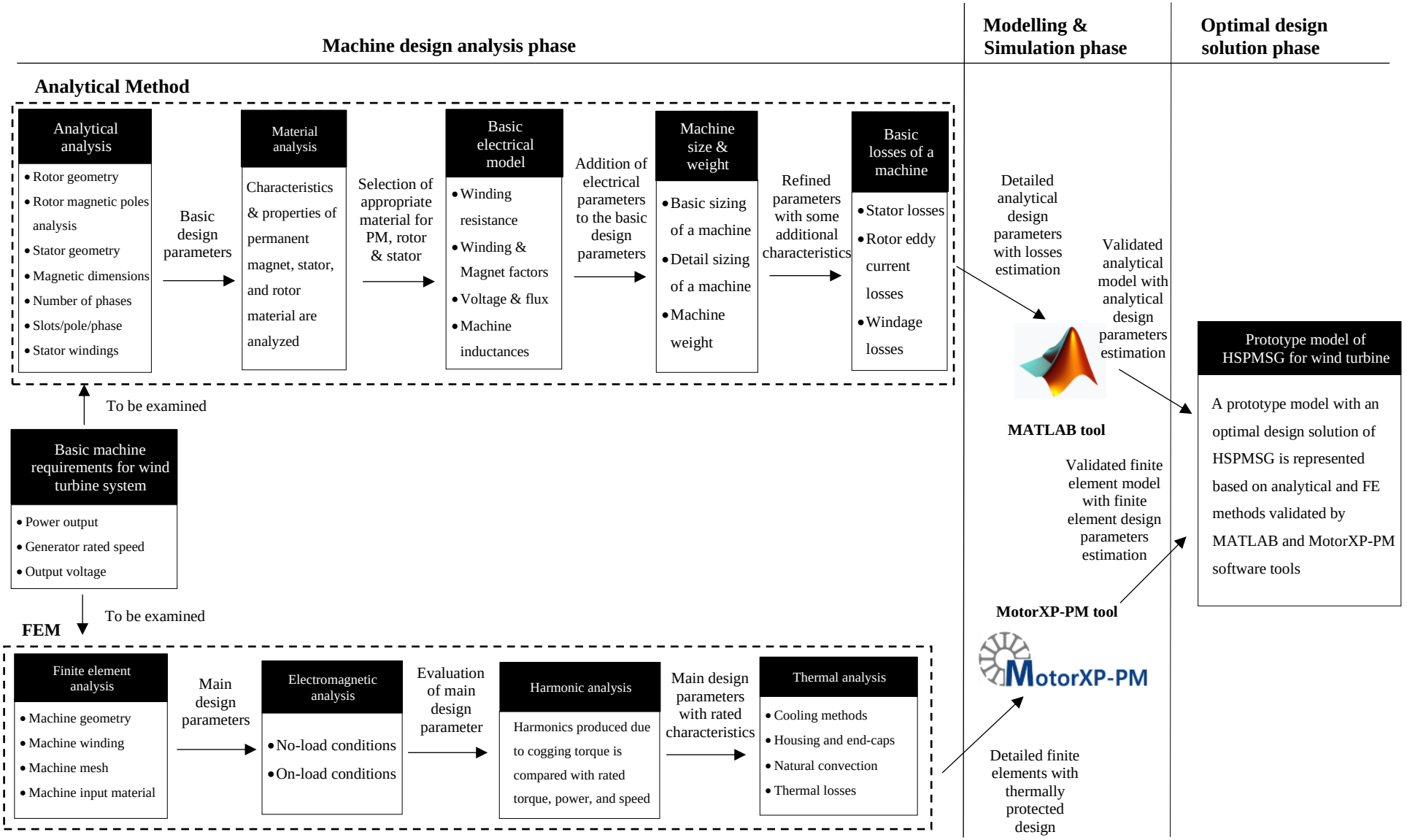

Figure 3. Overview of two different methods adopted for resolving HSPMSG design for wind turbine system

Figure 3 shows an overall view of the methodology adopted to design HSPMSG for wind turbine system. The methods described in this research work provide good correlation between fundamental design consideration and effectiveness of simulation tools to process design parameters effectively. However, the results produced by these methods are still approximate.

3.1.1 Analytical method

The analytical method starts with the analytical analysis of a machine to determine specific design requirements. The basic design parameters are extracted and used to initialize the electrical model of a machine. The electrical model computes several other components and parameters that directly influence the performance of a machine. But before analyzing the basic electrical model of a machine, the characteristics of permanent magnet material properties are analyzed to select an appropriate material for the rotor and stator of a machine. This analytical method is then propagated forward for the detailed analysis of design parameters by evaluating the size and weight of a machine. As discussed previously, past studies have shown that the effect of losses plays a vital role on the performance of machines [10]. Therefore, basic machine losses are examined for the design reliability of a machine. Once the basic as well as the detailed design parameters are determined and evaluated then these parameters are validated further into the modelling and simulation phase of methodology. The design parameters calculated analytically in the machine design analysis phase are executed in the MATLAB tool accordingly. Finally, a prototype model of HSPMSG is represented in the optimal design solution phase based on analytical methods and MATLAB modelling and simulation estimations. Thus, if the design parameters are correctly established then a finite element method (FEM) is applied based on the analytical analysis of a machine.

3.1.2 Finite element method

The second method starts similarly with the analysis of finite elements in its own domain. However, instead of solving design problems analytically only, a dynamic approach is also used to resolve design problems simultaneously [31]. As the FEM is propagated forward to evaluate design problems optimistically, these approximations do not guarantee the performance of the PM machine within the operating range only. In order to understand the impact of many design parameters, materials, rotor, and stator techniques over the

performance of a machine such as electromagnetic torque, back-emf etc., a good calculation of machine electromagnetic analysis is needed for a good control approximation [32]. An electromagnetic analysis is desired in FEM because the effects of the design parameters evaluated in analytical method and FEA on machine performance can be analyzed in terms of no-load and on-load conditions accordingly [33]. Once a good correlation between finite elements and rated machine performance is obtained then harmonic analysis is taken into account based on the various electromagnetic field behavior of the different design characteristics analyzed in analytical and FEA previously. Therefore, the effect of harmonics can be analyzed in the harmonic analysis of a machine. A good design means that it is protected by an excess amount of heat and temperature [19]. Thermal analysis makes sure that the proposed design does not influence the performance of the machine at high-speed [34]. Therefore, a thermal analysis based on the necessary recommendations with cooling process is proposed. After the evaluation of a machine thermally, the machine design analysis phase for FEM is identified to validate in the MotorXP-PM tool in the modelling and simulation phase of the methodology. Once the FEM is examined in MotorXP-PM accurately, it is then meshed with the analytical model in the optimal design solution phase to form a prototype model of a machine as shown in figure 3 above.

3.2 Design process

The analytical as well as the FE approach of the previous section is helpful in visualizing an appropriate design methodology for HSPMSG and the prototype model generated from these software tools would most likely enhance the current machine designer's capabilities to predict design parameters optimistically. We saw that the methodology adopted in this research exhibits the potential for solving design problems by analyzing the design parameters simultaneously. In this section, a visual summary of the research work is discussed in order to estimate possible outputs garnered from different types of analyses performed during the machine design analysis phase.

The design process begins with the grouping of input design parameters collected from previous research work, topic framing, and methods sections as discussed previously. The input design parameters are those who are taken for granted for further analysis of a machine. In addition, these input design parameters may be relevant in establishing the design process effectively.

The design process will be needed to analyze and validate the assumed input design parameters for good performance across a range of factors and conditions selected for HSPMSG design. Each input design parameter is studied under analytical and finite element methods to propose possible output parameters to contribute the desired purpose of this research work accordingly.

The input design parameters analyzed and validated in the design process can yield an estimated output parameter to predict the results estimated from modelling and simulation phase of the research work. The result and analysis as well as the conclusion and future work of this research work depends upon these estimated output parameters. Figure 4 below shows an Input-Process-Output (IPO) diagram for the design process.

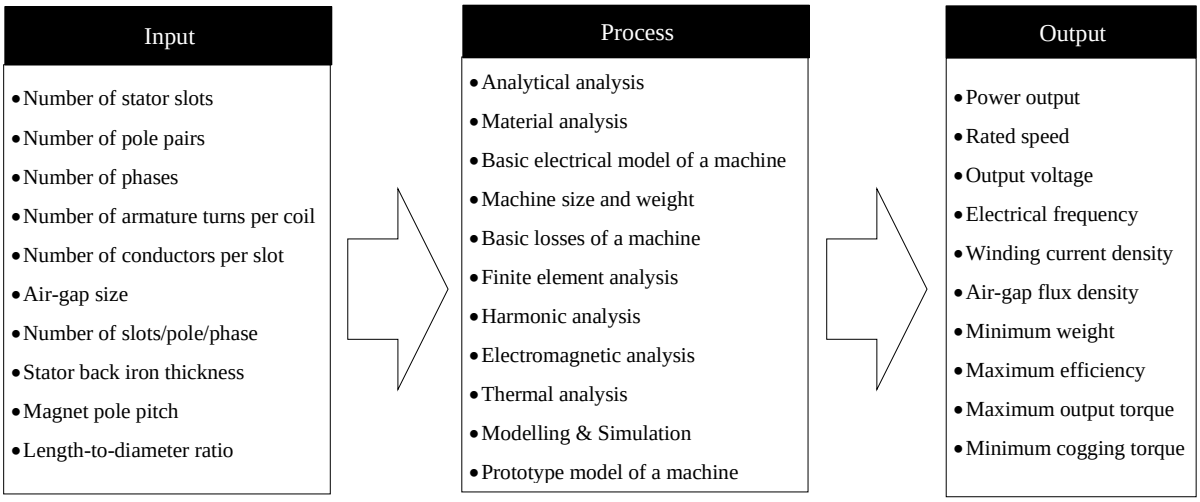

Figure 4. IPO diagram for the design process

Chapter 4

4 Analytical Method

In this chapter of the thesis the machine design analysis based on the analytical method is discussed. These include analysis such as analytical, material, basic electrical model, machine size & weight, and basic losses of a machine in terms of machine parameters, and performance for brushless HSPMSG with relative ease. These analyses can provide guidance for basic prototype models with optimal design solutions, and simulation results. For simplicity, simulation results will focus on machine design variable/parameters derived from analytical, material, basic electrical model, machine size & weight, and basic losses of a machine for instance. Whereas the analysis on these results is based on the simulation results representing the primary motives of this research work in the chapter 8 of the thesis.

4.1 Analytical analysis

This section computes an insight analytical solution to determine the magnetic field distribution of the PM machine and then use this information to calculate several other performance components and parameters [19]. More detail on each section of the analytical analysis of the machine are discussed below.

4.1.1 Rotor geometry

To understand the design of a PM machine in terms of performance and efficiency, the rotor geometry is one factor who can cater for air-gap flux density, induced voltages, and cogging torques etc. [35]. Of course, different combinations of factors and parameters can have important effects, but this factor yields important insight into rotor topologies, and flux distribution, accordingly [19]. In addition, these factors are thoroughly examined with the help of comparative study and a good agreement is represented for the rotor geometry of the PM machine.

4.1.1.1 Rotor topologies

The rotor topologies along with a permanent magnet position is shown in figure 5. PM machines are usually categories in two rotor topologies such as the interior permanent magnet (IPM) and surface-mount permanent magnet (SPM) when it comes to high-speed application. Previous studies show that the air-gap flux density and induced voltages in SPM are less sensitive to rotor irregularities as compared to IPM. In contrast, the cogging torque

decreases in IPM with the increase of rotor eccentricity while in SPM it increases. Moreover, the peak-to-peak ripple torque is high in IPM as compared to SPM [35]. Therefore, IPM rotor topology is selected over SPM for HSPMSG design, respectively.

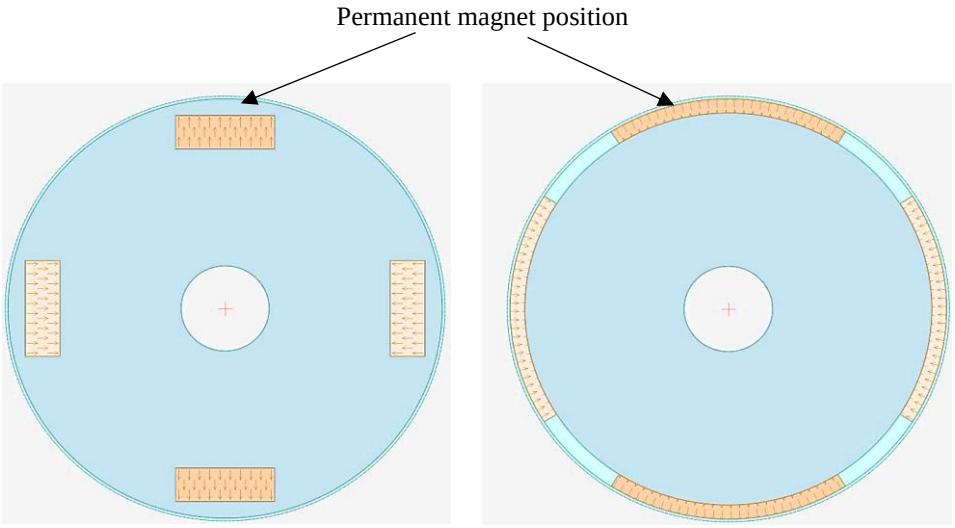

(a) (b)

Figure 5. Permanent magnet rotor topologies (a) IPM (b) SPM

4.1.1.2 Flux distribution

The efficiency and raise operating temperature rely heavily on the distribution of flux at high-speed operations [36]. Thus, a comparative study is used to analyze flux distribution in rotor geometry. An example of what the flux distribution looks like is shown in figure 6.

The distribution of flux is classified by the rotation of flux such as the radial and axial accordingly. Axial flux machines have a smooth rotation of flux. Also, the low eddy current losses and heat removal feature of axial flux machines gave a better choice for wind turbine systems [36].

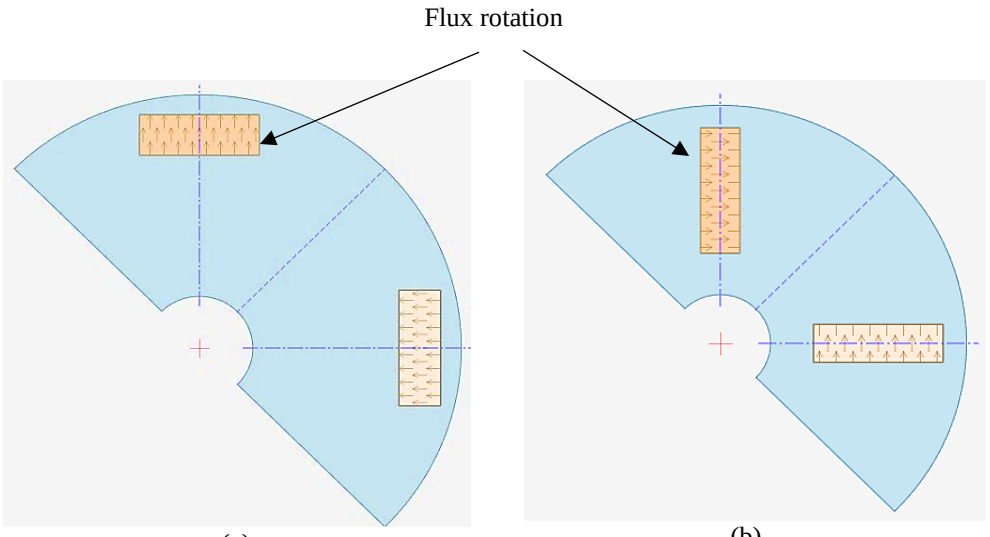

(a) (b)

Figure 6. Permanent magnet flux distribution (a) radial direction (b) axial direction

In contrast, radial flux machines are capable of removing heat and temperature and also provide cooling technique properly. But it has excessive eddy current losses with complicated stator construction. Therefore, radial, or tangential flux distribution is opted for this particular type of HSPMSG design. In addition to rotor topologies and flux distribution, we can also discuss length-to-diameter (L/D) ratio in the rotor stiffness section of the rotor magnetic pole analysis accordingly. Before discussing L/D ratio, we will briefly highlight some more characteristics of flux distribution and rotor topologies to produce reasonable agreement between the choice made and design considerations.

Comparisons are made between the two rotor topologies and flux distribution patterns. IPM is a choice for high-speed application as flux flows radially in magnets to give rotor-to-stator phase advance. This rotor-to-stator phase advance gives smoother torque, and more sinusoidal current as compared to surface mounted topology [37], [38]. In addition, U-shaped buried magnets are used in this particular type of HSPMSG design.

4.1.2 Rotor magnetic poles analysis

As shown in figure 5 (a), 4 magnetic poles or 2 pole pairs are chosen because an even number of poles always provides a balanced rotational design. Similarly, if the number of poles increases, the individual pole pitch decreases which reduces the amount of stator back iron needed to support the magnetic flux. In addition, the required magnetic volume decreases as the number of poles increases for a given power/torque value accordingly [39]. There are a number of factors which dictate which type of arrangement is optimal for the performance of the machine. Among the many factors, number of poles, rotor stiffness, pole arc, and skewing of magnetic poles are selected to analyze rotor magnetic poles.

4.1.2.1 Number of poles

We see that, selecting an appropriate number of poles are essential for structure and performance of the machine. Let us assume that the machine has a constant speed which generate electrical frequency proportional to number of poles accordingly. This effect can be measured in the following expression.

$$N \cdot (2p) = 120 \cdot f \tag{3.1}$$

where N = rated speed in rpm

p = number of pole pairs

f = electrical frequency in Hz

Next, the electrical frequency in rad/sec is determined due to the rotor magnetic poles using equation 3.2 below.

$$\omega_0 = 2 \cdot \pi \cdot f \tag{3.2}$$

where ω_0 = electrical frequency in rad/sec

From the equation 3.2, we can compute that if the number of poles increases then the electrical frequency will be high and as a result there will be higher stator losses because core losses are proportional to frequency squared. Also, the increased number of poles will reduce the number of slots per pole per phase which produces less sinusoidal voltage waveform ultimately [39]. Therefore, a lower number of poles are selected in this research work.

Two possible choices either 2 poles or 4 poles are analyzed in this research work. For 2 poles, lower frequency is produced with lower core and stator losses. Consequently, the generator will be longer due to long endings of the 2 pole stator windings [42]. In contrast, 4 poles design produce higher frequency with an acceptable amount of core and stator losses. In addition, the generator will be shorter in parallel direction accordingly. Therefore, 4 poles or 2 pole pairs design is selected with rated speed of 15000 rpm, and electrical frequency of 500 Hz for this particular type of HSPMSG design.

4.1.2.2 Rotor stiffness

The rotor aspect ratio, defined as length-to-diameter (*L/D*) ratio, is a critical parameter for rotor stiffness and good dynamic performance of a machine. In order to minimize size and weight of a machine while keeping a good rotor stiffness, the "*L/D*" ratio needs to keep relatively low. Higher value of "*L/D*" parameter will make magnet retention extremely difficult. PM machines thus do not have rotor field windings and higher "*L/D*" ratios. Therefore, offers flexibility in selecting pole sizes which allows for smaller diameters. A normal "*L/D*" ratio for a wound rotor machine is 0.5 – 1.0. In contrast, PM machines have 1 – 3 "*L/D*" ratio. Staying close to these ranges usually provides a higher rotor stiffness and a good dynamic performance of a machine [39]. The "*L/D*" value selected for this particular type of HSPMSG design is 2.50 for further analysis of a machine. In addition, the tip speed (v_{tip}) can be calculated by the rotor radius and the rotational speed of the machine.

$$v_{tip} = \frac{r \cdot \omega_0}{p} \tag{3.3}$$

where r = rotor radius in m

For most rotating machines, the upper limit on tip speed is between 100 – 250 m/s depending on the design of the machines [40]. In this design, a range of tip speed is taken to be (50:200). At high-speed operation, the PM rotors can undergo through the centrifugal forces which may weaken their strength. To avoid the effect of these centrifugal forces retaining sleeves can be used on the surface of the rotor. As seen in the equation 3.3, the tip speed in PMSG depends mainly on the rotor radius and electrical frequency. The equation of estimating rotor stack length (L_{st}) can be calculated by equation 3.4 as shows below [39].

$$L_{st} = 2 \cdot LDr \cdot r \tag{3.4}$$

where LDr = L/D ratio

4.1.2.3 Pole arc

The pole arc of the rotor magnetic poles has significant importance to produce flux waveform more sinusoidal. The full pole arc is 180° electrical and produces a full voltage waveform but with high harmonics. Alternatively, if we reduce the pole arc up to 20 – 30% and fill the gaps between the poles with non-magnetic pieces, such as soft-iron, air, or isolation, the resulting flux waveform will be more sinusoidal and has fewer harmonics with lower rotor losses [43].

4.1.2.4 Skewing of magnetic poles

This study includes the impact of skewing factor to reduce cogging torque and smoothen the variations in air-gap reluctance, flux, and voltage waveform of the PM machine. Skewing factor occurs parallelly along the length of the rotor to provide a constant rotational torque and prevent pole pieces from exactly lining up with stator tooth [39]. Following equation is commonly used to determine the skewing of magnetic poles.

$$K_s = \frac{Sin\left(\frac{\theta_{sk}}{2}\right)}{\frac{\theta_{sk}}{2}} \tag{3.5}$$

where K_s = skewing factor

θ_{sk} = skew angle in deg. (elect.)

Skew angle can be measured as;

$$\theta_{sk} = \left((p \cdot \theta_{msk}) + \omega_d\right) \cdot \frac{\pi}{180} \tag{3.6}$$

θ_{msk} = magnet skew angle in deg. (elect.)

The rotor magnetic poles analysis shows several implications resulting from the higher number of poles which reduces stator conductors-per-slot as well as the per-unit inductance

and synchronous reactance accordingly. This can however result in improved performance of the machine since the reactance is lower.

4.1.3 Stator geometry

Similarly, for stator geometry, a comparative study is needed for high power output and an ergonomic design of HSPMSG. A good stator geometry yields low cogging, low vibration, and low noise enabling smooth operation, as well as reduced rotational losses enabling higher speed and reduced heating [41]. It is assumed that the stator carries three-phase windings and produces a near sinusoidal distribution of magnetomotive force for any value of the stator currents [19]. For the comparative purposes, stator topologies, stator slot geometry, and stator current densities, are evaluated using analytical methods.

4.1.3.1 Stator topologies

Stator constitutes the housing for the armature windings (main windings), and flux path for the magnetic circuit [39]. The main consideration of the stator topologies is whether to make it slotted or slotless. Figure 7 below shows the slotted PM stator, with the presence of stator tooth which contains the field windings of the machine on one hand. On the other hand, a slotless stator with no stator tooth is represented. It is assumed that the slotless stator has armature windings fixed on the cylindrical stator core and provides the overall reduced size of the machine accordingly [41].

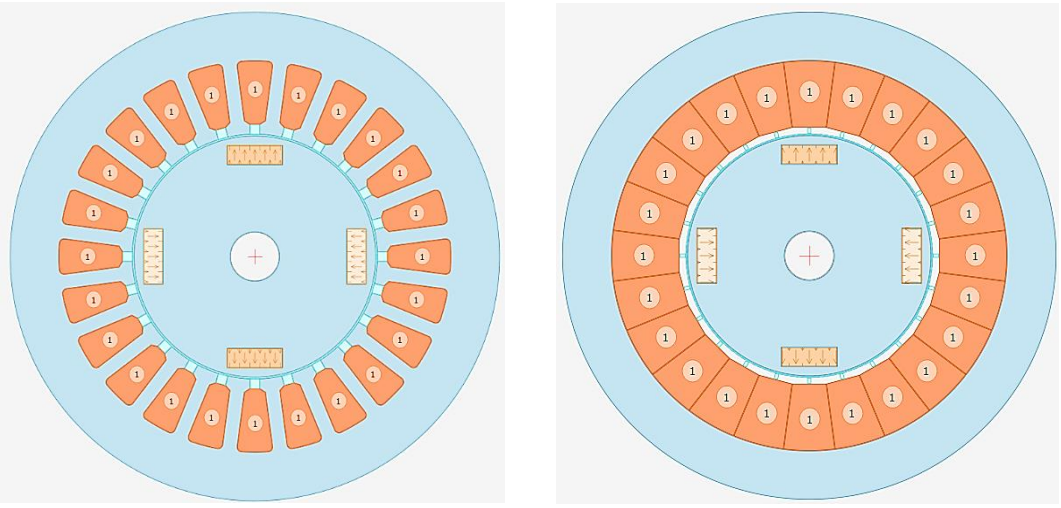

(a) (b)

Figure 7. Permanent magnet stator topologies (a) slotted (b) slotless

Among the topologies represented above for PM stator the slotted topology is selected for this research work. This topology certainly provides a high-power output over the slotless

topology, however that is not the only reason for its selection. The other advantage is that the slotted design has good conduction paths to remove the heat generated from the windings and can increase the allowable current density in the windings for higher output power. In addition, the armature windings are not directly exposed to the rotating flux which decrease the possibilities of additional eddy-current loss in the conductors and further minimize losses due to circulating current in the windings. Overall, the performance of a slotted stator is almost always higher than that of an equivalent slotless stator design and slotless stators do not appear often in high-power applications [39]. Thus, slotted stator is chosen for this particular type of HSPMSG design.

4.1.3.2 Stator slot geometry

Slotted stators are the traditional stator design and consist of opening around the stator for the armature windings as shown in figure 7 (a). The openings provide rigid housings for the conductors and associated insulations, respectively [19]. This analytical analysis is then propagated forward to a stator slot geometry for the slotted PM machine. There are two types of stator slots such as rectangular and trapezoidal as shown in figure 8 [39]. An approximately rectangular type of stator slot is chosen for this particular type of HSPMSG design.

ws_{bottom} – slot bottom width

ws_{top} – slot top width

w_d – slot depression width

h_s – slot height

h_d – slot depression height

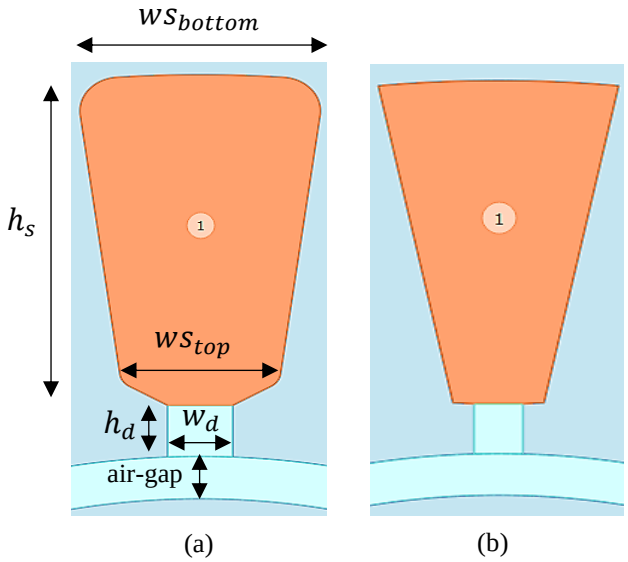

Figure 8. Stator slot geometry (a) rectangular (b) trapezoidal

The rectangular, as well as the trapezoidal stator slot geometries, has shown a good agreement for high-speed applications. But for maximum flux linkages and greater thermal resistivity, the rectangular stator slot geometry is chosen. In addition, the rectangular slot geometry contains form-wound windings so that the depression width is the same as the slot

top width. Because this analysis depends on the tradeoff between reasonable topologies, an estimate of a number of factors is needed. Thus, for this analysis, the average stator slot width can be calculated from equation 3.7 below [39].

$$ws = \frac{ws_{top} + ws_{bottom}}{2} \tag{3.7}$$

where ws = average slot width in m

Additionally, both "ws_{top}" and "ws_{bottom}" can be calculated from a number of parameters as shown in the equation 3.8 and 3.9 simultaneously.

$$ws_{top} = ws_{bottom} \cdot \frac{(r + g + w_d + h_d)}{(r + g + m_w + h_d)} \tag{3.8}$$

$$ws_{bottom} = \frac{2 \cdot \pi \cdot (r + g + w_d + h_d) \cdot (1 - T_f)}{N_S} \tag{3.9}$$

where g = air-gap in m

m_w = magnet width in m

T_f = peripheral tooth fraction

4.1.3.3 Stator current densities

So far, we have seen that the stator geometry has been represented in a comparative way. Thus, a good correlation has been found for stator topologies and stator slot geometries. But the smoothness in the air-gap flux density is important since the slotted topology is used to keep the main field winding conductors close to the field magnets for maximum flux linkage. Therefore, a double layered overlap type of winding is used to support the necessary current density in the windings. A few typical limits for stator current densities (J_a) are shown in table 2 for a variety of cooling methods adopted during the thermal analysis of a machine. For this analysis, the current density limit of 1200 A/cm^2 is used because it tends to be more conservative for our machine design, and it allows uniformity in the air-gap field [41].

Cooling method	**Current density (J_a) in A/cm^2**
Natural Convection	450 – 550
Fan-Cooled	800 – 1200
Liquid-Cooled	2300 – 3200

Table 2. Stator current densities

In this stator geometry of the analytical analysis of a machine, the analytical method is used to compute stator topologies, stator slot geometry, and stator current densities so that it shows a good agreement comparatively. As we see that the slotted stator is a good choice

for high power and high-speed applications. However, one drawback which slotted stator topology has, is that the effect of cogging torque can be high if proper winding technique is not implemented [39]. Therefore, a 3-phase and 24 slots machine design have been selected to limit cogging torque effect for this particular type of HSPMSG design, respectively.

4.1.4 Magnetic dimensions

While the rotor magnetic poles analysis is of course providing a balanced rotational design, for a given number of poles, pole arc, and skewing of magnetic poles. However, the reduce size and weight of the machine would likely be obtained with magnetic dimensions. Two parameters such as air-gap, and magnet height are particularly important in determining the air-gap magnetic field, the air-gap flux density, and the induced voltage in the machine [44]. Equation 3.10 represents an air-gap flux density approximately.

$$B_g = \frac{m_h}{m_h + g} \cdot B_r \tag{3.10}$$

where B_g = air-gap flux density in T

m_h = magnet height in m

B_r = magnet remnant flux density in T

It is clear from equation 3.10 that the air-gap (g) should be kept small as much as possible to maximize the air-gap flux density (B_g) to constitute the largest part of the machine permeance/reluctance. Also, if the magnet height is too large then the "Bg" might be high enough to cause the stator core material to saturate which reduces machine performance. In addition, previous research work shows that the magnet height is usually larger than the air-gap by a factor of 5 – 10 to provide uniform magnetic field respectively [39].

4.1.5 Number of phases

All rotating machines such as motors and generators always need a balanced phase to have an evenly spaced phase distribution around the stator of the machine. However, the generators need higher phase numbers to produce lower ripple in DC bus voltage [39]. Equation 3.11 shows that how the number of phases affects a machine's power, current, and voltage ratings accordingly.

$$|P + jQ| = q \cdot E_a \cdot I_a \tag{3.11}$$

For active power (P);

$$P = E_a \cdot I_a \cdot cos\phi \tag{3.12}$$

For reactive power (Q);

$$Q = E_a \cdot I_a \cdot sin\phi \tag{3.13}$$

where P = real/active power in W

Q = reactive power in VAR

q = number of phases

E_a = RMS phase excitation voltage/internal voltage in V

I_a = RMS armature/stator current in A

ϕ = angle between E_a and I_a in deg. (elect.)

Equation 3.11 provides a reasonable agreement between the number of phases and machine's parameters on one hand, on the other hand, it gives us an important assumption, such as if the power is fixed, and the number of phases increases, then the voltage and/or current decreases, assuming the total number of turns is constant. As the number of phases increases, the AC line current harmonics are also increasing substantially. Therefore, a 3-phase machine is a good choice as it is the industry standard and produces balanced torque without pulsations in rotating machines [39].

4.1.6 Slots per pole per phase

In the previous sections of this research work, it is defined analytically that a 3-phase, and 24 slots are the two main parameters for HSPMSG. However, slots per pole per phase (m) is the one most important parameter to design a generator in such a way that it produces a more sinusoidal voltage waveform and reduces the harmonics [39]. Equation 3.14 helps us to determine the relationship between rotor poles and the stator windings as well as the shape of the generated back voltage of the machine.

$$m = \frac{N_s}{2 \cdot p \cdot q} \tag{3.14}$$

Slots per pole per phase is used to define the type of machine based on net voltage amplitude. In other words, if the back-emf of all the coils making up a phase winding are in phase with each other and add up so that the net voltage amplitude is the sum of the individual coil voltages then this type of machine is called an integral slot machine. In contrast, if the back-emf of all the coils is not in phase so that the net voltage amplitude has a different shape as compared to the individual coil voltages, then this type of machine is called a fractional slot machine [39]. Therefore, an integral slot machine is chosen for this particular type of HSPMSG design.

4.1.7 Stator windings

As noted previously, the voltage produced in the generator relies on slots per pole per phase parameter. The stator windings are the place where the generator voltage is produced or induced. Faraday's law of electromagnetic induction tells us that the voltage is induced in stator windings due to the time-varying magnetic flux caused by the permanent magnets on the rotor. Basically, the windings are distributed in three ways such as pitch, breadth/distribution, and skew in order to produce more sinusoidal waveforms in a slotted machine respectively [46]. In addition to the distribution of windings, the stator windings could benefit from the combination of slot fill factor, skin effect, and winding geometry to focus or limit the scope of this research work so that the desirable windings can be found.

4.1.7.1 Winding pitch

The pitch of a winding (α) is desired for this analysis so that the type of winding can be determined. It is defined as the angular displacement (phase angle) between the edges of the coil. If the angular displacement of induced emf in two coil sides is less than 180 degrees, then this type of winding is known as short-pitched windings. In contrast, if the angular displacement is exactly 180 degrees, then the winding is fully pitched. Additionally, the pitch of a winding is measured in electrical degrees or radians as shown in equation 3.15 below [39].

$$\alpha = \pi \cdot \frac{N_{sap}}{N_{sfp}} \tag{3.15}$$

where N_{sap} = number of slots with actual pitch of the coil

N_{sfp} = number of slots with full pitch coil

Number of slots with actual pitch of the coil, and the number of slots with the full pitch coil can be parameterized in Equations 3.16 and 3.17 simultaneously [39].

$$N_{sap} = N_{sfp} - N_{sp} \tag{3.16}$$

where N_{sp} = number of slot short pitched

and

$$N_{sfp} = \frac{N_S}{2 \cdot p} \tag{3.17}$$

4.1.7.2 Breadth or distribution factor

Each coil of a stator winding occupies a distribution or breadth factor in order to link with rotor flux in such a way that they are slightly out of phase with each other so when they are added together, they produce more sinusoidal waveforms. This type of windings is known as distributed windings. In contrast, the windings are said to be the concentrated one, if the resultant emf would be the arithmetic sum of induced emf. Since the induced emf per coil is not an angle equal to the angular displacement of the slots. Therefore, the resultant emf of the winding is the phasor sum of the induced emf per coil. Equation 3.18 shows the ratio of the phasor sum of the emf's induced in all the coils distributed in a number of slots under one pole to the arithmetic sum of the emf's induced in concentrated windings [46].

$$K_d = \frac{Phasor\ sum\ of\ component\ emfs}{Arithmetic\ sum\ of\ component\ emfs} \tag{3.18}$$

As per definition, the ratio between the emf induced in distributed windings and concentrated windings is measured as the distribution factor [46].

$$K_d = \frac{emf\ induced\ in\ distributed\ windings}{emf\ induced\ in\ concentrated\ windings} \tag{3.19}$$

A stator winding usually consists of several coils each separated by an electrical angle (γ). The electrical angle can be parameterized in equation 3.20 below.

$$\gamma = \frac{2 \cdot \pi \cdot p}{N_s} \tag{3.20}$$

The skewing of a winding is deemed unnecessary to discuss here because it complicates the design and overall size of the machine. However, the skewing of a rotor is employed [39].

4.1.7.3 Slot fill factor

The other significant factor is that how many conductors can be placed in a slot and can easily evaluated by equation 3.21 below [40].

$$A_{ac} = \frac{A_s \cdot \lambda_s}{2 \cdot N_c} \tag{3.21}$$

Where A_{ac} = winding cross-sectional area in m^2

A_s = slot area in m^2

λ_s = slot fill factor

N_c = number of turns per coil

Typically, the slot fill factor used in many generators design vary in value from 0.30 – 0.70, depending on the number and size of the conductors as well as the amount of labour utilized. In this research work, a slot fill factor of 0.50 is assumed [39]. Additionally, the slot area can be parameterized in equation 3.22 below [39].

$$A_s = ws \cdot h_s \tag{3.22}$$

Although the slot fill factor highlights the number and size of the conductors in the slots [40], as the design process proceeds, the factor of stator windings connection is considered accordingly. This factor includes the connection of stator windings in the form of wye or delta patterns as well as series or parallel. The series, wye-connected windings is an industrial choice for most of the design because parallel, delta connected windings can produce back-emf which cause circulating currents and as a result additional losses, heating, or damage [39]. Therefore, wye series connected stator windings are selected for this research work.

4.1.7.4 Skin effect

At high frequency such as the frequency greater than 2 kHz, skin effect is an issue because it causes the current to flow through a smaller cross-sectional area and increase the resistance of the conductor [45]. As discussed in section 4.1.2.1 that the generator electrical frequency chosen for this particular type of HSPMSG design is 500 Hz. Therefore, skin effect is neglected in this research work.

4.1.7.5 Winding geometry

We have seen that considering a number of parameters and factors for stator windings can help us to find an optimal design for HSPMSG. In order to maximize the slot fill factor, the winding layout is considered carefully [19]. Since there are an infinite number of possibilities for windings layout and slot count combinations [46], therefore, we can make some assumptions to focus the scope of desirable windings for our machine design. Some of the main assumptions are as follows:

- All slots are filled. In other words, the number of slots is always a multiple of three for 3 phase machines. Since each coil fills two slots one half full, each coil effectively fills one slot [46]. Therefore, the number of armature turns per coil (N_a) used in this design can be measured as follows.

  $$N_a = 2 \cdot p \cdot m \cdot N_c \tag{3.23}$$

  This arrangement is especially good for three phase machines.

- There are two coils attached to each slot. In other words, the windings can be classified as a double layer winding accordingly.
- For balanced design, a balanced winding is considered. In this case the back-emf of phase B and C is 120-degree electrical offset from the back-emf of phase A simultaneously [46].
- All coils have the same number of spans with respect to the number of slots.
- All coils have the same size. This implies that all the coils have the same resistance and inductance.

These assumptions need to be simplified for further analysis of winding geometry. Before representing the winding layout of HSPMSG, the computed winding pattern is represented in the form of table 3 which indicates coil and slot number with respect to their respective phase.

Coil number	Phase A		Phase B		Phase C	
	Slot number		Slot number		Slot number	
	From	Toward	From	Toward	From	Toward
1	7	1	3	9	11	5
2	8	2	4	10	12	6
3	7	13	15	9	11	17
4	8	14	16	10	12	18
5	19	13	15	21	23	17
6	20	14	16	22	24	18
7	19	1	3	21	23	5
8	20	2	4	22	24	6

Table 3. Winding pattern

The geometrical construction of stator windings of what the winding layout looks like is shown in Figure 9 below.

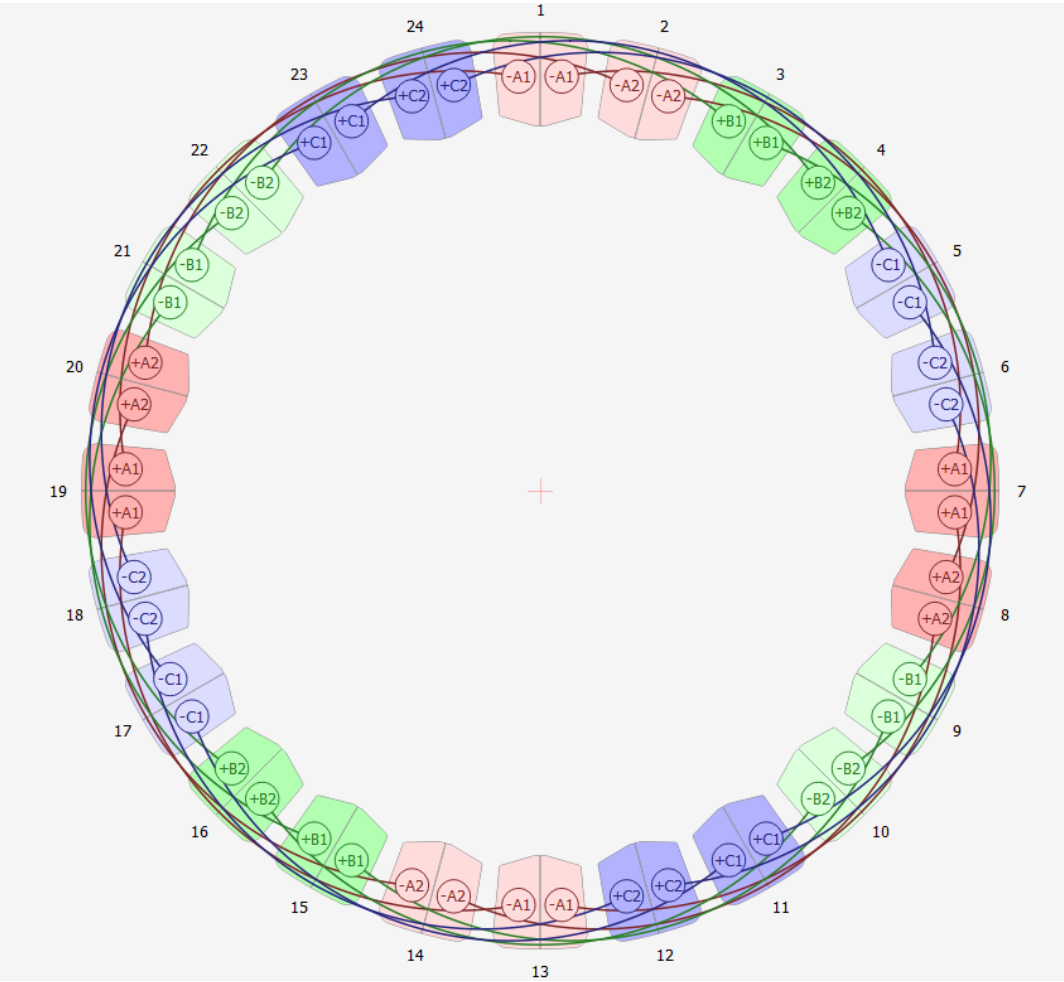

Figure 9. Winding layout

Similarly, figure 9 also gives us important information needed to analyze the performance of the machine. Following are some parameters and their values drawn from figure 9 accordingly.

- The coil span value of 6 is measured, whereas the sign +/- specifies the “from” and “toward” direction of the conductors within a slot. In addition, the letter following the sign specifies the phase and the phase is followed by the parallel path number.
- Double layer winding with two coils on each side of the slot is observed, whereas series wye connection is chosen while constructing the geometrical construction of the stator windings.
- Finally, an angular displacement between the edges of the coil is measured as 120 degrees electrical to minimize the back-emf generated in phase B and C from phase A, respectively.

4.2 Material analysis

Since the analytical analysis only computes the basic design parameters, an appropriate material analysis of the main components of the machine is needed. For this analysis, the main components such as the magnet, rotor, and stator are selected exclusively, because the machine output, heat rise, weight, and cost are directly influenced by the selection of an appropriate material of these components of the machine [47]. Likewise, the analytical analysis, this analysis is also depending on the comparative study based on the properties of different material and their performance for high-speed application.

4.2.1 Permanent magnet material

The size and performance of a high-speed PM generator depend on the permanent magnet material properties [42]. Without proper PM material selection, the cost and weight of the machine is considerably high and has a possibly damaging effect due to ample coercive force and lack of necessary air-gap magnetic field [48].

Most of the permanent magnets used in high-speed generators are made up of ferromagnetic materials [19]. Many different types of ferromagnetic materials are available today. Before discussing these types, we introduce a *B*-*H* curve normally used to define non-linear properties of PM materials by representing the relationship between magnetic flux density (*B*) and magnetic field strength (*H*) [46]. Figure 10 below shows the *B*-*H* curve of the permanent magnet.

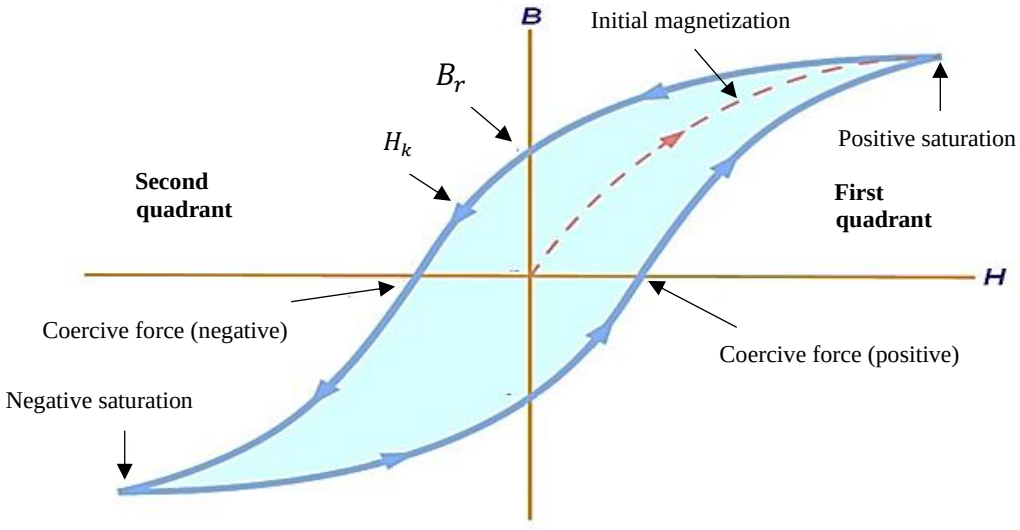

Figure 10. *B*-*H* curve of the permanent magnet

From figure 10 we see that the *B-H* curve offers some unique characteristics and each point on the *B-H* curve represents a dynamic operating condition simultaneously [19]. Following are some basic magnetic properties that are of critical importance for the selection of permanent magnets.

- Remnant flux density (B_r): It is the amount of flux density remaining in a magnet after successful magnetization. It affects the air-gap flux density and magnet size.
- Coercivity or Coercive force (H_c): It is the strength of the magnetic field needed to bring the flux density of the magnet to zero after the saturation of the magnetization.
- Energy product (BH_{max}): It is a product of maximum density of the magnet. Also, it is inversely proportional to the total volume of the magnet required.
- Recoil Permeability (u_{rec}): It is the ability of a magnet to return to its initial magnetization after subjected to damaging forces. If the magnet reaches knee magnetizing force (H_k), then it will allow material to recoil or relax if the value of magnetic flux density reaches to zero as shown in the second quadrant of figure 10 [46].

As discussed previously that PM material comes in a variety of different types subject to machine applications. The most common types include alnico, ferrite (ceramic), samarium-cobalt (SmCo) material, and neodymium-iron-boron (NdFeB). Of these, ferrite types are the most popular because they are inexpensive. In contrast, the rare earth types, SmCo and NdFeB offer the highest performance [46]. Figure 11 beow shows an analytical data of various properties for some common PM materials.

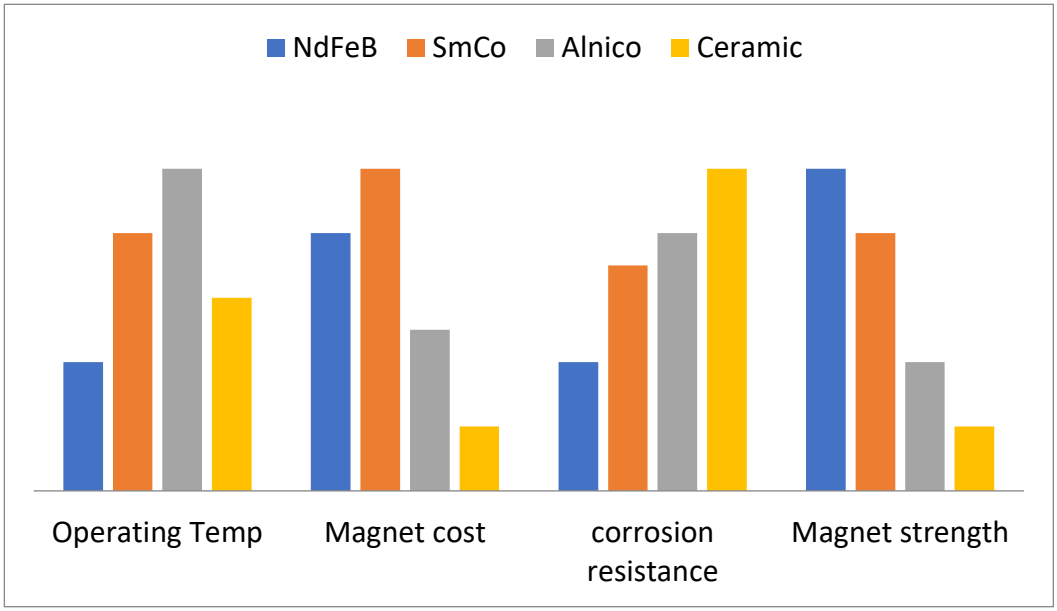

Figure 11. Comparison of different PM material properties

From figure 11 above we see the difference in properties between the various PM material is considerably high. However, it is also of interest to compare the optimal performance value to the worst performance value for each material. Figure 11 shows the percent difference in the properties of rare earth magnets as compared to the alnico and ferrite magnets. Although the operating temperature and corrosion resistance properties of alnico and ferrite magnets are higher, the magnet cost and magnet strength on the other hand is inferior to rare earth magnets relatively. Thus, consideration of how best to select the optimal performance PM material can be important, particularly for high-speed applications with significantly greater power density, high coercivity, high flux density, and linearity of the demagnetization curves [49]. Therefore, the rare earth magnets are considered due to their better properties and *B-H* curves of these materials [41]. Table 4 below shows the magnetic properties of the two rare earth magnets such as NdFeB and SmCo used in this research work.

Property	**Unit**	**Value**	
		NdFeB	**SmCo**
Remanence (B_r)	T	1.0 – 1.3	0.82 – 1.16
Coercivity (H_c)	MA/m	0.875 – 1.99	0.493 – 1.59
Recoil permeability (u_{rec})	-	1.05	1.05
Energy product (BH_{max})	kJ/m^3	260	150
Curie temperature	°C	320	800
Electrical resistivity (ρ)	$\Omega \cdot$ cm	(110 – 170) × 10^{-6}	86 × 10^{-6}

Table 4. Magnetic properties of NdFeB and SmCo

Table 4 depicts that the NdFeB values are relative to optimal performance values. Although, as compared to SmCo, the NdFeB is modest to corrosion and minor confrontation with the effect of temperature, this analysis assumes that this issue can be overcome by using proper cooling methods [50]. By nature, NdFeB is abundant and lower in price as compared to SmCo. Therefore, NdFeB is selected for this particular type of HSPMSG design.

4.2.2 Rotor and Stator material

While the generator performance will be affected by the magnetic properties of PM material, their relevant components such as the rotor and stator have an impact on machine losses and efficiency [41]. For this reason, rotor and stator material selection are likely of great interest. As discussed earlier there are a number of factors which dictate which type of material is

optimal for a particular type of machine. However, examining the material for rotor and stator, we see that saturation flux density, core losses, and temperature are essentially important to minimize core losses including hysteresis and eddy current losses. In addition, the material must act as a flux guide and absorb the minimum amount of magnetomotive force (MMF) to concentrate flux in the air-gap [39].

Typically, rotor and stator are made up of same material for ease of construction and cost effectiveness. Besides that, another significant factor is that the material can be of high-quality, non-oriented, electrical grade lamination steels to minimize losses [47].

There are a number of lamination steels to impact the performance and efficiency of the machine, however the four main materials are used accordingly. These are low carbon steel, silicon (Si) steel, nickel (Ni) alloy steel, and cobalt (Co) alloy steel. Low carbon steels are the lowest cost and are used in high volume applications where high core losses are acceptable. Silicon steels usually have a content of 3.5% silicon which increases the resistivity to reduce eddy current losses. Nickel alloys have lower losses than the silicon steel but are much more expensive. Finally, the cobalt alloys are only used in extreme high-performance situations such as military aircraft and space applications due to the high cost [39]. Also, the lamination thickness is one factor that can play a significant role in performance. Thus, silicon steel is selected for the HSPMSG design because it is economical, its thin lamination minimizes losses, and it has a stator saturation flux density of 1.8 T approximately [41], [47].

Silicon steel with 3.5% silicon contents does not provide the performance and efficiency required from this type of generator accordingly [21]. In 1993 JFE steel developed the world's first thin steel sheet with 6.5% silicon contents and superior high-frequency characteristics [51]. Table 5 below summarizes the laminated steel properties of two silicon steel such as 3.5% silicon Iron (SiFe) and 6.5% silicon Iron (SiFe) used in this analysis.

Property	**Unit**	**Value**	
		6.5% SiFe	**3.5% SiFe**
Stator Saturation flux density	T	1.8	2.0
Typical core losses at 50 Hz	W/kg	0.5	0.7
Operating temperature range	℃	-55 to +200	-55 to +200
Maximum temperature	℃	700	400

Table 5. Laminated steel properties of 6.5% SiFe and 3.5% SiFe

Table 5 above indicates some of the properties contribute the most to the performance and efficiency of the generator. The saturation flux density value of 3.5% SiFe is relatively better than 6.5% SiFe, but typical core losses and maximum temperature values are fairly better for 6.5% SiFe as compared to 3.5% SiFe. Thus, a 6.5% SiFe lamination material is used as a rotor and stator material in this machine design analysis. The manufacturing process and some other material properties are given in the appendix 2 of this thesis.

4.3 Basic electrical model

The analytical and material analysis of the machine give good insight into the basic design parameters and a more realistic comparative study to determine an appropriate material. Even still, an electrical circuit analysis of the machine is much significant to determine the additional electrical parameters using the analytical analysis and material characteristics of the generator [52]. Thus, in many cases, an electrical equivalent model could determine the additional electrical parameters of a machine using basic circuit analysis. Figure 12 depicts the per-phase electrical equivalent model of a PMSG as a phasor circuit.

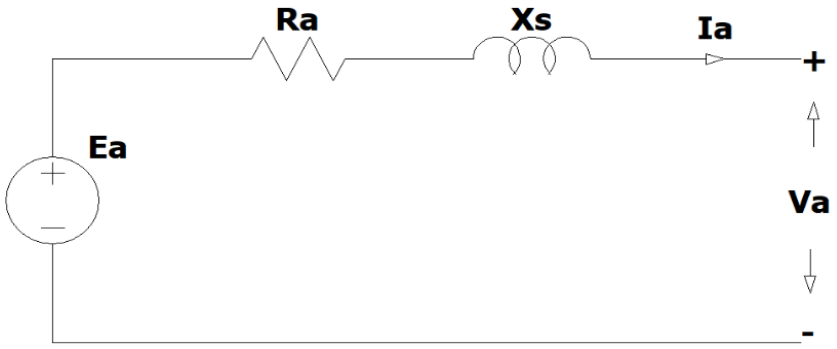

Figure 12. Per phase electrical equivalent model of a PMSG

where R_a = armature/stator resistance in ohms

X_s = synchronous reactance in ohms

V_a = terminal voltage in V

Since we make the assumption as before, that the machine has 3-phases. Therefore, all these basic parameters such as E_a, R_a, X_s, etc. can be determined for one phase and then applied to the other two phases. The following study computes these basic parameters using the dimensions and material characteristics of the generator analytically [52].

4.3.1 Winding resistance

The stator coils are made of copper and have some resistance to the current flow [40]. We can calculate the resistance of the copper phase windings by using the following equation.

$$R_a = \frac{l}{\hat{\sigma} \cdot A_{ac}} \tag{3.24}$$

where l = length of an armature conductor in m

$\hat{\sigma}$ = stator winding conductivity

The length of an armature conductor normally measured by the equation 3.25 below [39].

$$l = 2 \cdot N_a \cdot (L_{st} + 2 \cdot l_{eh}) \tag{3.25}$$

where l_{eh} = end turn length of an armature conductor (half coil) in m

The end turn length of an armature conductor is proportional to the end turn length of an armature conductor from one end as shown in equation 3.26 below [39].

$$l_{eh} = \pi \cdot l_{eo} \tag{3.26}$$

where l_{eo}= end turn length of an armature conductor (one end) in m

Equation 3.27 below help us to calculate the end turn length of an armature conductor from one end in order to determine the basic electrical as well as the geometry of a machine exclusively [39].

$$l_{eo} = \frac{\pi \cdot (r + g + m_w + h_d + 0.5 \cdot h_s) \cdot N_{sap}}{N_S} \tag{3.27}$$

4.3.2 Winding and Magnet factors

As discussed in section 4.1.7.2, windings are short pitched and have a breadth connected to produce more sinusoidal waveforms. This phenomenon is shown more explicitly with the help of winding factor. In a nutshell, the winding factor can be calculated as the product of pitch factor and breadth/distribution factor as shown in equation 3.28 below.

$$k_w = k_p \cdot k_d \tag{3.28}$$

Where k_w = winding factor

k_p = pitch factor

Similarly, the breadth/distribution factor is defined as the ratio between the voltage induced in distribution winding under the same phase belt to the voltage induced in concentrated winding. Breadth/distribution factor can be derived in equation 3.29 below.

$$k_d = \frac{sin\left(\frac{m \cdot \gamma}{2}\right)}{m \cdot sin\left(\frac{\gamma}{2}\right)} \tag{3.29}$$

Additionally, short pitching is an important means to eliminate harmonics and improve power quality of the HSPMSG [39]. Therefore, the pitch factor is defined as the ratio between the flux produced by the short pitch coil to the flux produced by a full pitch coil. The pitch factor can be determined by equation 3.30 below.

$$k_p = sin\left(\frac{\alpha}{2}\right) \cdot sin\left(\frac{\pi}{2}\right) \tag{3.30}$$

These winding factors are especially advantageous for the basic electrical modelling of a machine on one hand. On the other hand, the magnetic factors such as the magnetic gap factor is highly desirable because the air-gap flux density is affected by the magnet geometry in the air-gap [39]. The equation 3.31 below represents the magnetic gap factor for the slotted stator with IPM rotor configuration, respectively [40].

$$k_g = \frac{{R_i}^{p-1}}{{R_s}^{2p} - {R_i}^{2p}} \cdot \left[\left(\frac{p}{p+1}\right) \cdot \left({R_2}^{p+1} - {R_1}^{p+1}\right) + \frac{p}{p-1} \cdot {R_s}^{2p} \cdot \left({R_1}^{1-p} - {R_2}^{1-p}\right) \right] \tag{3.31}$$

where k_g = magnet gap factor

R_i = inner magnet boundary in m

R_s = outer magnet boundary in m

R_1 = inner boundary of magnet in m

R_2 = outer boundary of magnet in m

4.3.3 Flux and Voltage

As described in equation 3.10 that the air-gap magnetic flux density is affected by the magnet geometry in the air-gap but since the magnetic field rotate north/south, it needs to be represented as a Fourier series, with considering odd components only because of the half-wave symmetry as shown in figure 13 below [39].

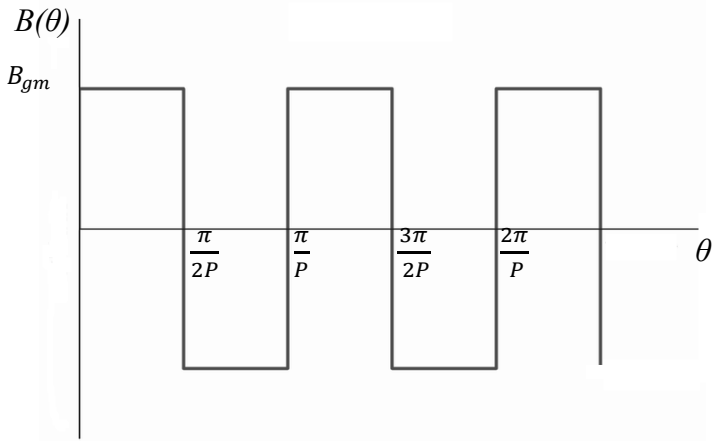

Figure 13. Air-gap magnetic flux density (B_{gm})

A simple Faraday's law of electromagnetic induction tells us that the voltage is induced across a winding whenever the flux varies with time. For simplicity, we highlight three factors such as the leakage factor, reluctance factor, and Carter's coefficient to determine the air-gap magnetic flux density. Leakage factor accounted for the flux leak when the flux lines from the magnetic poles crossed the air-gap to the stator windings. Reluctance factor is used to compensate for the small effects of the steel reluctance on the air-gap flux. Carter's coefficient is used to account the effects of air-gap magnetic flux density due to the difference in permeance caused by the slots before reaching the highly permeable stator back iron [39]. Overall, air-gap flux density is calculated using equation 3.32 through equation 3.40 below.

$$k_c = \left[1 - \frac{1}{\frac{\tau_s}{w_s}\left(5 \cdot \frac{g}{w_s} + 1\right)}\right]^{-1} \tag{3.32}$$

where k_c = carter's coefficient

τ_s = total slot width in m

For total slot width (τ_s);

τ_s = average slot width + tooth width

or $\tau_s = ws + wt$ (3.33)

where wt = tooth width in m

For tooth width (wt);

$$wt = \frac{2 \cdot \pi \cdot (r + g + m_w + h_d) \cdot T_f}{N_S} \tag{3.34}$$

For effective air-gap (g_e);

$$g_e = k_c \cdot g \tag{3.35}$$

For permeance coefficient (CP);

$$CP = \frac{m_h}{g_e \cdot c\phi} \tag{3.36}$$

where $C\phi$ = flux concentration factor

For flux concentration factor ($C\phi$);

$$C\phi = \frac{p \cdot \theta m}{180} \tag{3.37}$$

where θm = magnet physical angle in rad.

Air-gap magnetic flux density (B_{gm}) can be calculated as;

$$B_{gm} = \frac{k_l \cdot c_\emptyset}{1 + k_r \cdot \frac{u_{rec}}{CP}} \cdot B_r \tag{3.38}$$

where B_{gm} = air-gap magnetic flux density in T

k_l = leakage factor

k_r = reluctance factor

Magnetic flux density w.r.t magnet physical angle can be calculated as;

$$B(\theta) = \sum_{n=1}^{\infty} B_m \cdot sin\,(n \cdot p \cdot \theta) \tag{3.39}$$

where $B(\theta)$ = flux density w.r.t. magnet physical angle in T

B_m = magnetic flux density in T

Magnetic flux density (B_m)can be calculated as;

$$B_m = \frac{4}{\pi} \cdot B_{gm} \cdot k_g \cdot sin\left(\frac{p \cdot \theta m}{2}\right) \cdot sin\left(\frac{\pi}{2}\right) \tag{3.40}$$

The equations from 3.32 to 3.40 can certainly be used to validate the HSPMSG model in modelling and simulation phase, and the prototype model of a machine, but flux linked by a single, full-pitched coil which spans an angle from 0 to π/p must be presented here. The equation 3.41 represents flux in radial direction and equation 3.42 presents the peak flux for this ideal coil.

$$\phi s = \int_0^{\pi/p} B_{flux} \cdot R_s \cdot L_{st}\, d\theta \tag{3.41}$$

where ϕs = radial flux through coil in Wb

B_{flux} = radial flux density through coil in T

$$\phi_{pk} = \frac{2 \cdot R_s \cdot L_{st} \cdot B_{flux}}{p} \tag{3.42}$$

ϕ_{pk} = peak radial flux through coil in Wb

Since there are a number of armature turns and coils in a stator phase winding, therefore the total flux linkage is calculated with the help of equation 3.43 below.

$$\lambda(\theta) = \sum_{n=1}^{\infty} \lambda_n \cdot sin\,(n\ \cdot p\ \cdot \theta) \tag{3.43}$$

Where $\lambda(\theta)$ = total flux linkage w.r.t physical angle in T

λ_n = magnetic flux linkage in T

Magnetic flux linkage can be calculated as;

$$\lambda_n = \frac{2 \cdot R_s \cdot L_{st} \cdot N_a \cdot B_m \cdot k_\omega \cdot k_s}{p} \tag{3.44}$$

Finally, the RMS phase excitation voltage or internal voltage, and armature or stator current are determined by using equation 3.45, and 3.46 below.

$$E_a = \frac{d}{dt}\lambda_n = \frac{wo \cdot \lambda_n}{\sqrt{2}} \tag{3.45}$$

and $$I_a = \frac{P_{out}}{q \cdot E_a} \quad (3.46)$$

4.3.4 Machine inductances

In a slotted PM machine, three types of machine inductances such as the air-gap inductance, slot leakage inductance, and end-turn inductance are used to determine the electrical parameters of the HSPMSG [53]. The Following study computes all these machine inductances analytically.

4.3.4.1 Air-gap inductance

Since large amount of flux crossing the air-gap, therefore the air-gap inductance constitutes the major portion of the machine inductances due to the interaction of the stator windings. In order to calculate air-gap inductance, a current carrying full pitched concentrated winding is considered. It means that we need to re-write the equation for flux density "*B(θ)*" from section 4.3.3 accordingly.

$$B_{flux} = \sum_{n=1}^{\infty} B_m \cdot sin\,(n \cdot p \cdot \theta) \quad (3.47)$$

Magnetic flux density (B_m) from flux and voltage can be re-calculated as;

$$B_m = \frac{4}{\pi} \cdot \frac{u_0}{(g + m_w)} + \frac{N_a \cdot I_a}{2 \cdot p} \quad (3.48)$$

where u_0 = permeability of free space

For polyphase[1] windings;

$$B_n = \frac{q}{2} \cdot \frac{4}{\pi} \cdot \frac{u_0}{(g + m_w)} + \frac{N_a \cdot I_a}{2 \cdot p} \quad (3.49)$$

$$\lambda(\theta) = N_a \cdot \phi \quad (3.50)$$

With all real winding effect included;

$$L_{ag} = \frac{\lambda(\theta)}{i} = \frac{q}{2} \cdot \frac{4}{\pi} \cdot \frac{u_0 \cdot R_s \cdot L_{st} \cdot N_a^2 \cdot K_w^2}{p^2 \cdot (g + m_w)} \quad (3.51)$$

where L_{ag} = air-gap inductance in H

i = coil current in A

[1] Polyphase windings are armature windings arranged in such a way that the first and third segments in each belt are connected in series with one another and the remaining segment is series-connected with a corresponding segment of the opposite phase belt. More detail can be found in appendix 4.

4.3.4.2 Slot leakage inductance

We see from air-gap inductance that the coil current generates a magnetic field that crosses slots from one side to another produces a slot leakage inductance. Slot leakage inductance for rectangular slot geometry is measured with slot depression which results in a slot permeance per unit length as shown in equation 3.52 [41], [46].

$$perm = u_0 \cdot \frac{1}{3} \cdot \frac{h_s}{ws_{top}} + \frac{h_d}{ws_{top}} \tag{3.52}$$

where $perm$ = slot permeance

If we consider the "m" number of slots/pole/phase with standard double layer windings, then the slot leakage inductance is represented from equation 3.53 through equation 3.56 accordingly.

For self-inductance;

$$L_{as} = 2 \cdot p \cdot Lst \cdot perm \left[4 \cdot N_c^2 \left(m - N_{sp}\right) + 2 \cdot N_{sp} \cdot Nc^2\right] \tag{3.53}$$

where L_{as} = slot leakage inductance in H

For mutual-inductance;

$$L_{am} = 2 \cdot p \cdot Lst \cdot perm \cdot N_{sp} \cdot Nc^2 \tag{3.54}$$

where L_{am} = mutual inductance in H

For 3-phase inductance;

$$L_{slot} = L_{as} + 2 \cdot L_{am} \cdot cos\left(\frac{2\pi}{q}\right) \tag{3.55}$$

where L_{slot} = slot leakage inductance in H

For multiple phase inductance;

$$L_{slot} = L_{as} - 2 \cdot L_{am} \cdot cos\left(\frac{2\pi}{q}\right) \tag{3.56}$$

4.3.4.3 End-turn inductance

A small proportion of end-turn inductance is created around a coil after leaving one slot and before entering another slot due to magnetic field effect. Since it is difficult to measure end-turn inductance due to complex winding patterns, therefore a rough estimation is used by considering end-turn are semi-circular with a radius equal to one-half the mean coil pitch intuitively. The total end-turn inductance per phase is represented in equation 3.57 below [46].

$$L_e = \frac{u_o \cdot N_C \cdot N_a^2 \cdot \tau_s}{2} \cdot ln\left(\frac{wt \cdot \sqrt{\pi}}{\sqrt{2 \cdot As}}\right) \tag{3.57}$$

where L_e = end-turn inductance in H

For all machine inductances discussed above subsequently equation 3.58 compute the total inductance for the phase by adding equation 3.51, equation 3.55, and equation 3.57 below, while ignoring other small factors.

$$L_s = L_{ag} + L_{slot} + L_e \quad (3.58)$$

where L_s = synchronous inductance in H

Whereas the synchronous reactance can be calculated with the help of equation 3.59.

$$X_s = \omega_0 \cdot L_s \quad (3.59)$$

4.4 Machine size and weight analysis

When designing a relatively new machine, brief work is needed to further evaluate the design, which builds the relationship between the geometry and the performance of the machine. Machine sizing discusses the possible potential on how to implement the analytical equations into an optimized machine performance on the basis of rated torque capabilities rather than power. For machine sizing, the potential directions include basic sizing from shear stress value [40], and detailed sizing based on the phasor diagram of the generator is discussed [57]. For an optimal design solution, machine weights are computed to imply that the machine is applicable to the given purpose. Machine weight analysis is performed using the calculation of the analytical parameters of armature conductor mass, core mass, magnet mass, shaft mass, services mass, and total mass of a machine, with the help of parameters determined previously. It provides a reasonable agreement between the chosen variables and expected output values to determine the remaining performance parameters of HSPMSG in the modelling and simulation part of this thesis eventually.

4.4.1 Basic sizing

Although the rotor tip speed discussed in section 4.1.2.2 provides the basis of the design, air-gap magnetic shear stress is another parameter used in basic sizing of the most generator design. Air-gap magnetic shear stress is the magnetic shear force developed per unit gap area and is constrained by magnetic design and thermal management. It is proportional to the product of the surface current density and magnetic flux density as represented in equation 3.60 below [39].

$$\tau = k_z \cdot B_m \quad (3.60)$$

where τ = shear stress in psi

k_z = surface current density in A/cm^2

Typical shear stress value range for different types of generators are represented in table 6 [39].

Generator Type	Shear stress in psi
Small air-cooled	1 – 5
Large air-cooled	5 – 10
Large liquid-cooled	10 – 20
High-temperature superconducting	30 – 50

Table 6. Shear stress values

Since the generator is a large air-cooled machine, therefore the value of shear stress selected for this particular type of HSPMSG design is between 5 – 10 psi accordingly.

In addition, the machine power equation is utilized to derive the rotor radius and stack length of the machine as shown in equation 3.61 below [40].

$$P_s = 2 \cdot \pi \cdot r \cdot L_{st} \cdot v_{tip} \cdot \tau \tag{3.61}$$

where P_s = fundamental machine power in W

4.4.2 Detail sizing

Once the fundamental machine power expression has been derived in a basic sizing of the machine, then the relationship between phase excitation voltage and terminal voltage is derived from the phasor diagram of a synchronous generator to present the final expression of a detail sizing of an HSPMSG. Two factors such as the leading and lagging power factors would be important to consider if balanced torque is required.

As we know that the phase excitation voltage differs from the terminal voltage by the resistance and inductance. And if we consider that our generator is supplying a purely resistive load at unity power factor then maximum efficiency is easily obtained. In contrast if the load is lagging then it requires large phase voltage. Thus, it is always preferred that the load is leading so that the minimum internal generated voltage is required for maximum efficiency [57]. In real synchronous generators, the winding resistance is much smaller than the synchronous reactance ($X_s >> R_a$). Therefore, the armature resistance is ignored. Figure 14 below shows the simplified phasor diagram when armature resistance is neglected.

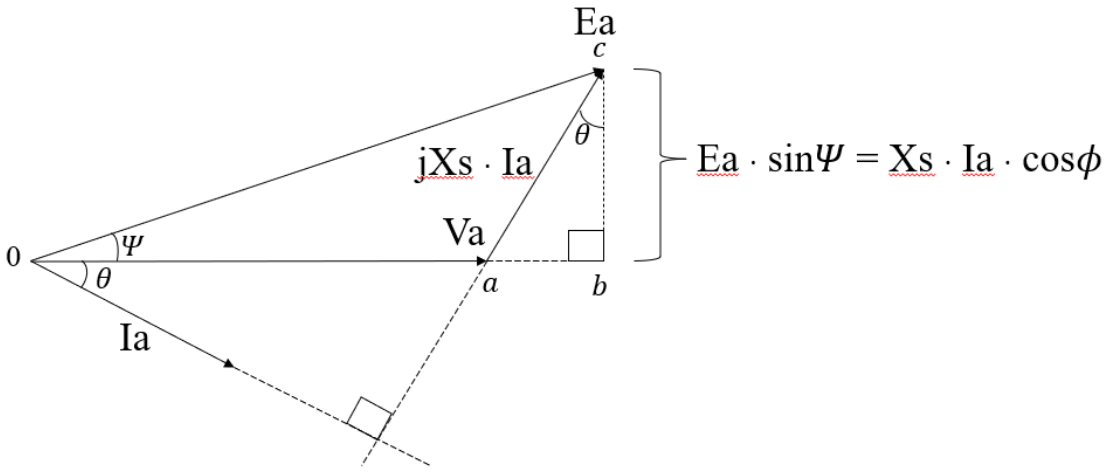

Figure 14. Phasor diagram of a synchronous generator when armature resistance is neglected

The relationship between phase excitation voltage and terminal voltage can be expressed after some rearranging in equation 3.62 below.

$$V_a = \sqrt{E_a^2 - ((X_s + R_a) \cdot I_a \cdot cos\phi)^2} - (X_s + R_a) \cdot I_a \cdot sin\phi \qquad (3.62)$$

where Ψ = torque angle between V_a and E_a in deg. (elect.)

4.4.3 Machine weight

For a large brushless liquid-cooled generator, there are five possible mass combinations (armature conductor mass, core mass, magnet mass, shaft mass, and services mass) are calculated to compute the total mass of a machine. For each calculation, material density is assumed such that their ferromagnetic material properties are aligned with the basic machine requirements. While only three components such as permanent magnet, rotor, and stator material of a machine are analyzed in section 4.2, therefore only three material densities can be logged to calculate the weight of the machine. In this research work, the material density of steel (7700 kg/m^3), magnet (7400 kg/m^3), and conductor (8900 kg/m^3) is chosen from the existing database of the same kind of machines [59]. Utilizing machine design parameters computed from the previous sections, the total mass of the machine is established using equation 3.63 through equation 3.74 respectively.

For armature conductor mass (M_{ac});

$$M_{ac} = q \cdot l \cdot A_{ac} \cdot dc \qquad (3.63)$$

where dc = conductor density in kg/m^3

Equation derivation for core mass (M_c);

$$R_{ci} = r + mw + g + h_d + h_s \quad (3.64)$$

where R_{ci} = core inside radius in m

$$R_{co} = R_{ci} + sbid \quad (3.65)$$

where R_{co} = core outside radius in m

sbid = stator core back iron depth in m

Overall diameter of a machine (D_{mach}) can be calculated as;

$$D_{mach} = 2 \cdot R_{co} \quad (3.66)$$

$$sbid = \frac{sbir \cdot r}{p} \quad (3.67)$$

where *sbir* = stator back iron ratio

$$M_{cb} = ds \cdot \pi \cdot (Rco^2 - Rci^2) \cdot L_{st} \quad (3.68)$$

where M_{cb} = back iron core mass in kg

ds = steel density in kg/m^3

For tooth core mass (M_{ct});

$$M_{ct} = ds \cdot L_{st} \cdot (N_s \cdot wt \cdot h_s + 2 \cdot \pi \cdot r \cdot h_d - N_s \cdot h_d \cdot w_d) \quad (3.69)$$

where M_{ct} = tooth core mass in kg

$$M_c = M_{cb} + M_{ct} \quad (3.70)$$

For magnet mass (M_m);

$$M_m = 0.5 \cdot (\pi \cdot \theta m) \cdot [\,(r + m_w)^2 - r^2\,] \cdot L_{st} \cdot dm \quad (3.71)$$

where *dm* = magnet density in kg/m^3

For shaft mass (M_s);

$$M_s = \pi \cdot r^2 \cdot L_{st} \cdot ds \quad (3.72)$$

For service mass (M_{ser});

$$M_{ser} = 0.15 \cdot (M_{ac} + M_c + M_m + M_s) \quad (3.73)$$

As noted previously, the generator used in this research work is a large fan-cooled, for this analysis we will add a 15% service mass friction to the total service mass calculation to account for the additional services associated with large fan-cooled machines as shown in equation 3.73 above [62].

Total mass (M_{tot}) can be calculated as;

$$M_{tot} = M_{ac} + M_c + M_m + M_s + M_{ser} \quad (3.74)$$

4.5 Basic losses of a machine

Most past studies of wind turbine generator design have been done using analytical, material, electrical modelling, or size and weight analysis, leaving the impact of losses on machines not well understood. This research describes a methodology which allows to predict system performance and reliable operation by identifying basic losses of a machine. Losses in PM machines can be roughly divided within three categories such as stator losses, rotor eddy current losses, and windage losses [54]. The following study examines the basic losses in HSPMSG in depth using analytical methods.

4.5.1 Stator losses

The stator losses in high-speed generators are higher than other machines due to its higher frequencies [39]. These losses can be minimized by generating frequencies that are not too high and by selecting appropriate lamination material as discussed in section 4.2.

Stator losses consist of conductor and iron losses. Conductor losses arise when the current flows through the stator windings. Using the conventional power equation for a resistance, conductor losses can be determined by equation 3.75 below.

$$P_a = q \cdot Ia^2 \cdot R_a \tag{3.75}$$

where P_a = conductor or armature losses in W

Conductor losses are sometimes called as I^2R losses or copper losses. Conductor losses can be further divided into stray losses caused by skin effect and proximity effect[2]. The skin effect is caused by the electromagnetic induction in the conducting material, which opposes the current due to the electromagnetic field [54]. The intensity of skin effect can be measured by skin depth[3]. The skin depth can be determined by the equation 3.76 below.

$$\delta = \sqrt{\frac{2}{\omega_o \cdot \mu_o \cdot \hat{\sigma}}} \tag{3.76}$$

where δ = skin depth

[2] The proximity effect resulting from the field induced from adjacent conductors sharing the same slot.

[3] The skin depth is the distance in which the main electromagnetic field entering a conductor surface is damped and reduced by a factor of 1/e, where “e” is equal to 2.71828… [54]

Losses due to the proximity effects known as the stray losses of the conductor located in the slots of an electric machine can be determined by the equation 3.77 below [54].

$$P_{stray} = P_a \cdot (C_r - 1) \quad (3.77)$$

where P_{stray} = stray losses in W

C_r = resistance coefficient

Similarly, iron losses can be divided into hysteresis losses and eddy current losses. Hysteresis losses is due to the steel not wanting to change magnetic state [55].

In other words, if the magnetic field increases, the hysteresis losses increase and vice versa [54]. The hysteresis losses in terms of maximum flux density (*B*) and frequency (*f*) can be determined by the equation 3.78 below.

$$P_h = \eta \cdot Bsat^n \cdot f \quad (3.78)$$

where P_h = hysteresis losses in W

B_{sat} = maximum or saturation flux density in T

η = material constant

n = flux density exponent (between 1.8 – 2.2)

Also, the eddy current losses can be caused by the variation in flux density. The eddy current losses are represented by the equation 3.79 below.

$$P_e = \frac{\pi^2 \cdot Bsat^2 \cdot t^2 \cdot f^2}{\rho \cdot CP} \quad (3.79)$$

where P_e = eddy current losses in W

t = thickness of the material in m

ρ = electrical resistivity of the material in $\Omega \cdot$ cm

CP = geometrical or permeance coefficient

For a more accurate analysis, the eddy current losses are further divided into classical eddy current losses and excess eddy current losses [54]. Therefore, the cumulative iron losses for electrical steel can be calculated by the equation 3.80 below.

$$P_{iron} = C_h \cdot Bsat^2 \cdot f + C_c (B_{sat} \cdot f)^2 + C_e (B_{sat} \cdot f)^{\frac{3}{2}} \quad (3.80)$$

where P_{iron} = iron losses in W

C_h = coefficient of hysteresis losses

C_c = coefficient of classical eddy current losses

C_e = coefficient of excess eddy current losses

The stator losses discussed above are estimated analytically, but the best way to approximate the stator losses is to use the empirical core loss data. This empirical core loss data can be used to estimate the total losses if the flux density is estimated for each part of a machine and the mass of the steel is determined previously. Table 7 below shows the core loss parameters applied to the core losses equations to obtain an estimated machine's core losses [39].

Core loss parameter	Value
Base power (P_b) in W/lb	36.79
Base flux density (B_o) in T	1.0
Flux density exponent (n)	2.12
Frequency exponent (nf)	1.68
Base frequency (f_o) in Hz	1000

Table 7. Core loss parameters

By utilizing equations 3.81 to 3.85 the total core losses of the generator are calculated as shown in the equations below.

For tooth flux density (B_t);

$$B_t = \frac{B_g}{T_f} \tag{3.81}$$

For back iron flux density (B_b);

$$B_b = B_g \cdot r \cdot p \cdot sbir \tag{3.82}$$

For core back iron losses (P_{cb});

$$P_{cb} = M_{cb} \cdot P_b \cdot \left(\left|\frac{B_b}{B_o}\right|\right)^n \cdot \left(\left|\frac{f}{f_o}\right|\right)^{nf} \tag{3.83}$$

For tooth losses (P_{ct});

$$P_{ct} = M_{ct} \cdot P_b \cdot \left(\left|\frac{B_t}{B_o}\right|\right)^n \cdot \left(\left|\frac{f}{f_o}\right|\right)^{nf} \tag{3.84}$$

Total core losses (P_c) can be calculated as;

$$P_c = P_{cb} + P_{ct} \tag{3.85}$$

4.5.2 Rotor eddy current losses

Although, as compared to stator losses, the rotor eddy current losses do not have much significant in machines total losses. However, this analysis is likely required to predict losses accurately and to get reasonable operating temperature at high-speed operations. Likewise, stator losses, rotor eddy current losses can be categorized into three groups such as the no-load rotor eddy current losses – caused by the existence of slots, on-load rotor eddy current losses – induced by winding harmonics, and on-load rotor eddy current losses – induced by the time harmonics of the phase currents due to Pulse Width Modulation (PWM) [54]. General expression used to calculate the eddy current losses can be determined by the equation 3.86 below.

$$P_r = \int_v \sigma \cdot E^2 \, dv = \int_v J^2 \, / \, \sigma \, dv \tag{3.86}$$

where P_r = rotor eddy current losses in W

E = electric field in V/m

J = density of eddy current losses in A/m^2

v = volume of the material in m^3

4.5.3 Windage losses

A final consideration relating to analyze basic machine losses, is the estimation of windage losses. The inclusion of these losses causes inefficiency and heat production in HSPMSG [54]. These losses are calculated using power necessary to overcome the drag resistance of a rotating cylinder as given by the equation 3.87 below [56].

$$P_{wind} = C_f \cdot \pi \cdot J_{air} \cdot \ {\omega_m}^3 \cdot r^4 \cdot L_{st} \tag{3.87}$$

where P_{wind} = windage losses in W

C_f = friction coefficient

J_{air} = density of air in kg/m^3

ω_m = mechanical frequency in rad/s

Mechanical frequency is determined by using equation 3.88 below [39].

$$\omega_m = \frac{\omega_0}{p} \tag{3.88}$$

The friction coefficient parameter used in the equation 3.47 depends upon the surface roughness and flow region. As it is assumed that the air in the gap is in the turbulent region and the rotor is spinning at high speed, therefore, the coefficient of friction can be approximated by the equation 3.89 below [39].

$$C_f \approx 0.0725 \cdot Rey^{-0.20} \quad (3.89)$$

where Rey = Reynold's number

Using equation 3.90 below, we can determine the value of Reynold's number accordingly [54].

$$Rey = \frac{\omega_m \cdot r \cdot g}{\varepsilon} \quad (3.90)$$

where ε = Kinematic viscosity of air at 20°C in m^2/s

At this stage, the analytical method is implemented by gather all essential parameters needed for machine design analysis phase of this research work. But it is more advantageous to measure the efficiency of the machine. For this purpose, stator current density, and machine input power are estimated to understand the overall performance of the machine [63]. Following equations are used to determine the remaining performance parameters of a machine accordingly.

For stator current density (J_a);

$$J_a = 10 \cdot \frac{k_z}{h_s \cdot \lambda_s} \quad (3.91)$$

For power input (P_{in});

$$P_{in} = P_{out} + P_a + P_c + P_{wind} \quad (3.92)$$

Finally, the efficiency (β) of the machine can be calculated as;

$$\beta = \frac{P_{out}}{P_{in}} \quad (3.93)$$

Chapter 5

5 Finite Element Method

In this chapter of the thesis the finite element method of the machine design analysis phase is discussed. One fundamental difference between the analytical and finite element method is that the modelling of non-linear design problem associated with the electric machines are not possible except for simple problems where transformation methods are used [17]. In contrast, the FEM will provide better estimates of the performance of the machine in the form of 2-D simulation on one hand. On the other hand, it will validate the design parameters assumed and estimated in the analytical method previously. Likewise analytical method, this method can also provide guidance for basic prototype models with optimal design solutions and simulation results. Whereas the analysis part is based on these simulation results garnered from FEM representing the primary motives of this research work in the latter part of the thesis. The following headlines examine the effect of geometrical arrangement and characteristics to find the best optimal design solution for the prototype model of a machine.

5.1 Finite element analysis

The second approach starts similarly with the finite element analysis in its own domain. However, instead of extracting design parameters analytically, field calculations of an electric machine are resolved. These field calculations are then fed into the modelling and simulation phase of the methodology, and finally an optimal design solution is represented in the form of a validated prototype model of HSPMSG using MotorXP-PM. More details on each step of the FEA are discussed below.

5.1.1 Machine geometry

Since we are interested in building prototype models and results obtained from the assumptions made in the modelling and simulation phase, we first set up a machine geometry. The geometry editor of MotorXP-PM provides us an opportunity to set up desired geometry in the form of 2-D FEA [59]. The geometry editor allows us to edit geometry parameters into three separable dimensional geometry such as stator dimensions, rotor dimensions, and axial dimensions, as well as the machine type to configure rotor, stator, and axial dimensions according to the design parameters chosen for this particular type of HSPMSG. Figure 15 below shows the geometry editor of the MotorXP for the stator, rotor, and axial dimensions with corresponding parameters.

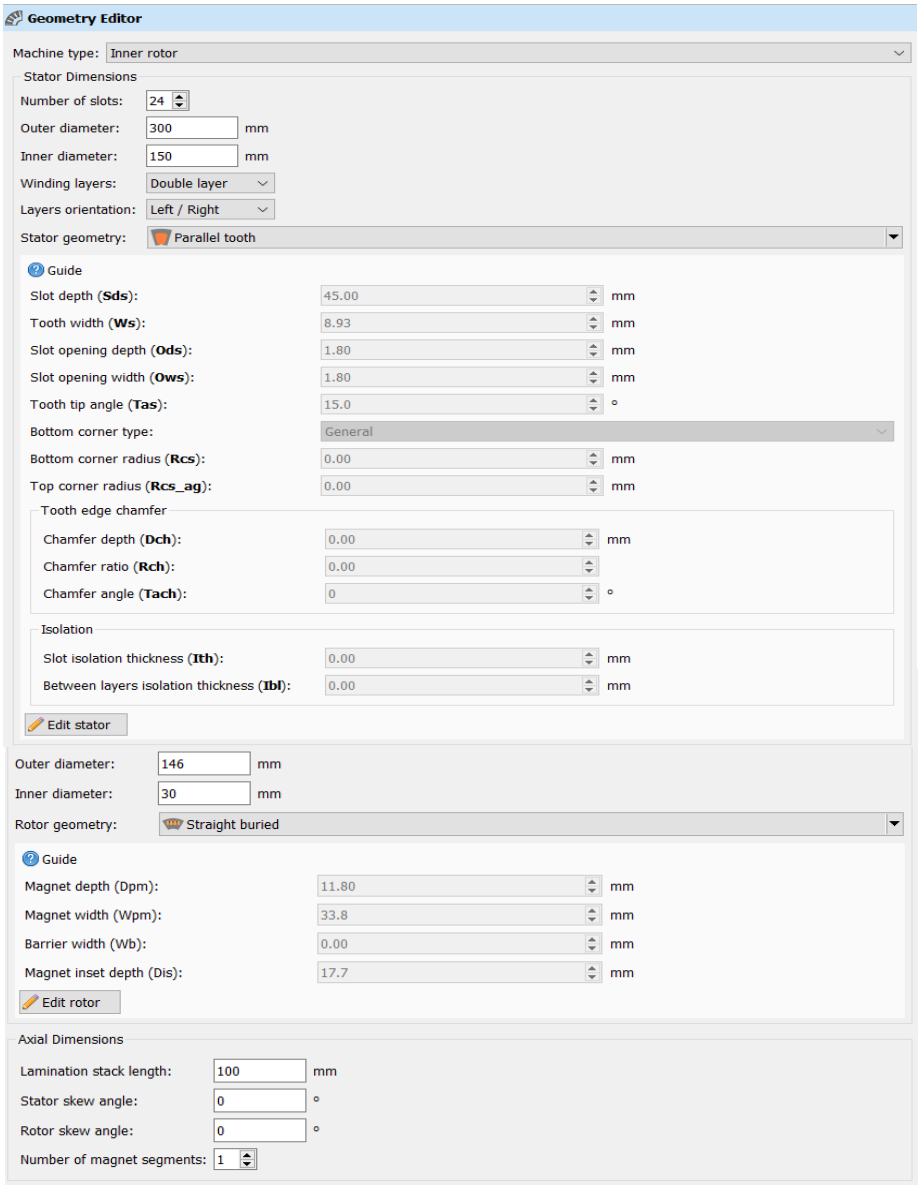

Figure 15. Geometry editor of MotorXP design studio for rotor, stator, and axial dimensions

5.1.2 Machine windings

The winding editor tab of the MotorXP design studio allows us to set up parameters of the stator windings. Parameters of winding editor such as number of slots, number of pole pairs, winding layers and layers orientation are the same as in geometry editor, but wire size method, winding layers type, winding layout, fundamental winding factors and other parameters provide better estimate to the performance of entire finite element analysis of a machine [59]. Figure 16 below shows the winding editor of the MotorXP with a number of machine winding parameters much needed in the modelling and simulation phase of the thesis.

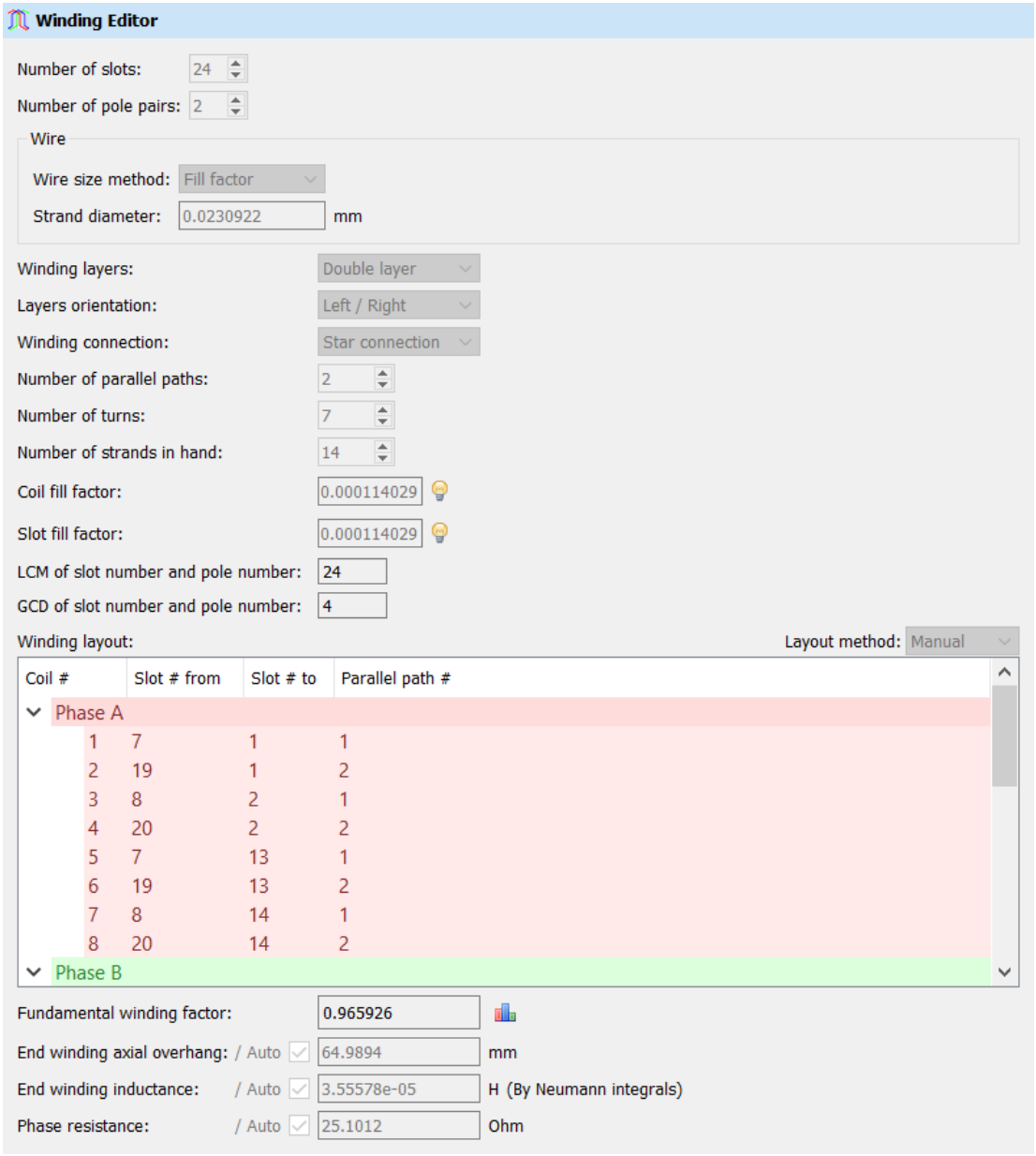

Figure 16. Winding editor of MotorXP for stator winding configuration

5.1.3 Machine mesh

In order to get more realistic finite element analysis of a machine, the machine or finite element mesh is used for a good quality simulation result. Mesh editor tab of MotorXP design studio is used to properly align the mesh parameters of the machine accordingly. In addition, the triangles of the mesh should be close to an equilateral triangle as much as possible in order to enhance the accuracy of the simulation result [59]. Figure 17 below represents the mesh editor tab includes mesh parameters much important to further evaluate the FE analysis of the machine.

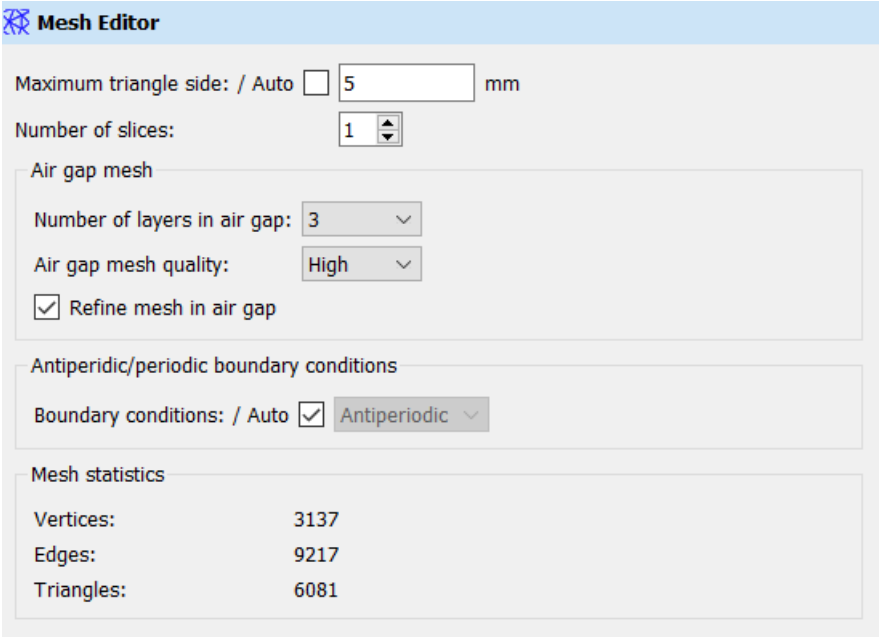

Figure 17. Mesh editor of MotorXP design studio

5.1.4 Machine material

MotorXP-PM tool highlights five different types of materials such as General, Iron, Winding, Magnet, and Conductor assigned to different parts of the machine in its database is shown in figure 18. As seen, each material is designated with stacking factor and temperature field because stacking factor can play a significant role in the performance of the machine when it comes to rotor and stator on one hand. On the other hand, the iron losses, and eddy current losses can be measured at different temperature values under no-load and on-load conditions [21]. Figure 18 below shows the material input panel for assigning materials in MotorXP-PM design studio.

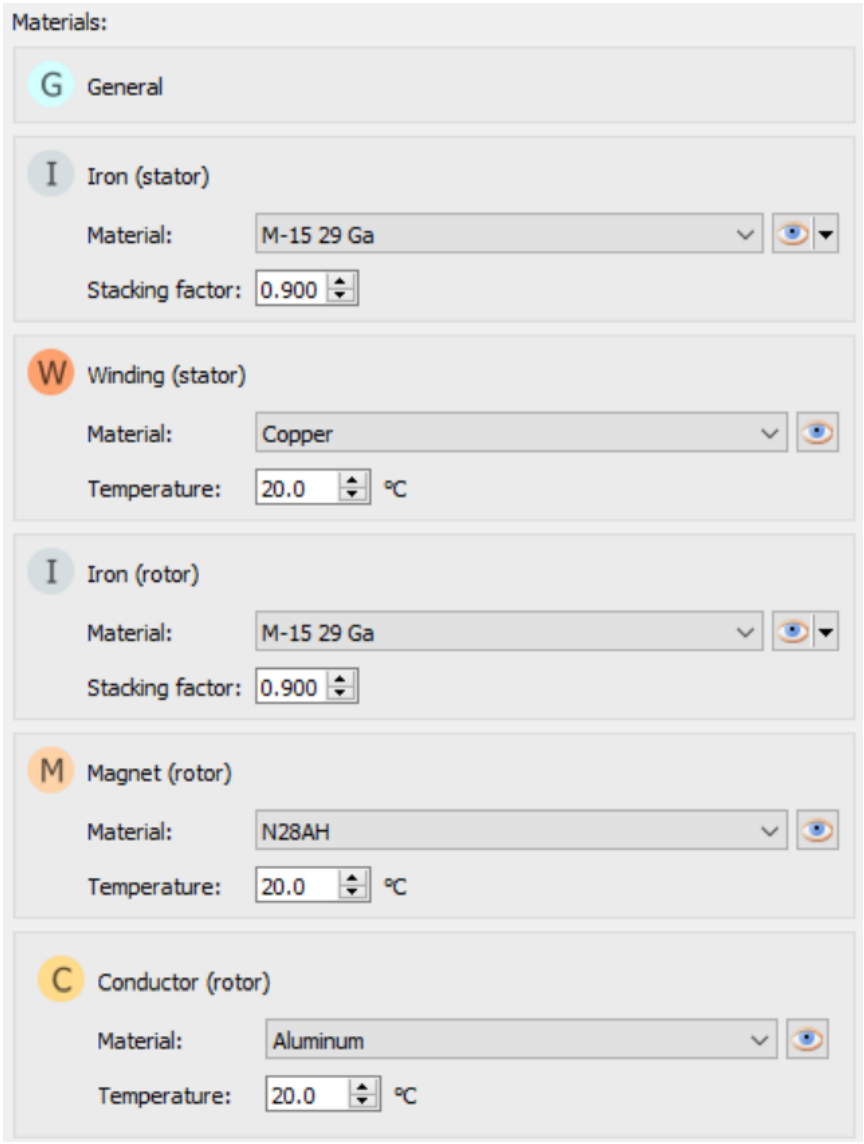

Figure 18. Material assigning panel of MotorXP design studio

The stacking factor specifies the ratio of the volume filled by electrical steel to the total volume of the iron core. The total volume of the iron core consists of the volume of lamination steel sheets and the volume of the coating between the sheets [59].

Temperature of the stator winding specifies the temperature of the winding conductors. Whereas the temperature of the magnet has its effect on the permanent magnet properties such as the remanence flux density and intrinsic coercivity. In addition, the temperature of the conductor material affects the resistance of the conductor according to its temperature coefficient of the resistance (T_c). However, it is also of interest to examine the properties of the material. For this purpose, the MotorXP-PM tool provides an eye shape button next to the material tab to better judge the properties of the existing material in the form of a graph or text in its database [59].

5.2 Electromagnetic analysis

For all design parameters and variables discussed briefly in the previous section to formulate the optimal design solution for HSPMSG have been investigated under no-load and on-load conditions of the electromagnetic analysis of a machine. Under no-load condition, the prototype model is investigated in two-dimensional magnetostatic FEA to solve time-stepping computational analysis with zero stator current [17]. Whereas a three-phase balanced current is fed into the armature windings to find a good agreement between the chosen design parameters/variables and computed results under on-load condition. The magnetostatic FEA of MotorXP is chosen because it allows us to estimate generator parameters like voltage, current, back-emf, power, torque, flux linkage, and losses etc. over different plot wizards by assuming an ideal sinusoidal or trapezoidal current waveform respectively [59]. For more detailed electromagnetic analysis, no-load and on-load conditions are further discussed to obtain good agreement between estimated parameters and simulation plots.

5.2.1 No-load conditions

Normally, the electromagnetic analysis begins with the field calculations of the design parameters such as terminal voltage, flux linkage, cogging torque, flux density, and losses in the machine under no-load conditions. In other words, a magnetostatic FEA is performed to compute the main design parameters under no-load condition. Here, it is important to mention that only terminal voltage, flux density, cogging torque, flux linkage, and losses of the machine are evaluated in no-load conditions. Whereas the back-emf, stator phase current, and stator losses are evaluated under on-load condition. The reason for using this form of combination is that the value of impedance, current, and voltage calculated from a no-load condition is utilized to calculate back-emf, and stator phase current, and stator losses in order to evaluate the impact of experimental values on the machine performance [54].

Magnetostatic FEA consists of a number of field solutions such as General Results, Machine Constants, and Flux Density Levels of the finite element simulations with predefined currents and geometrical construction. Figure 19 shows the main window of magnetostatic FEA in MotorXP-PM. It includes a plot wizard button to display quantities to be plotted into the selected axes, and a simulation button to start the simulation process over electrical periods or user choice [59].

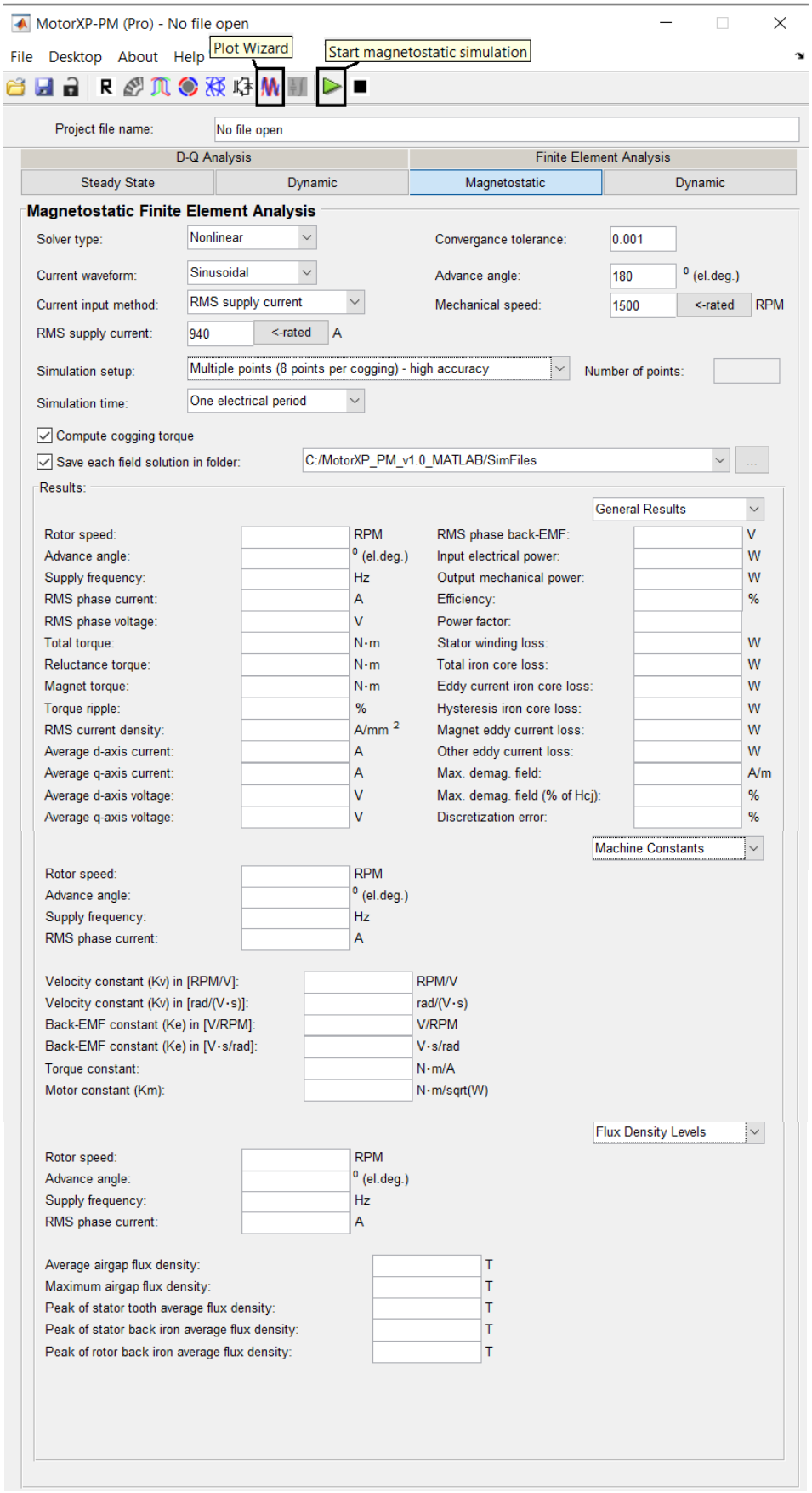

Figure 19. Magnetostatic FEA main window with General Results, Machine Constants, and Flux Density Levels in MotorXP-PM

Terminal voltage is a fundamental output parameter in the optimal design solution phase of this research work. MotorXP provides more accurate terminal voltage waveforms by subtracting line-to-line phase value from another. One goal of this study is to obtain a more sinusoidal terminal voltage waveform by reducing torque ripples, noise, and vibrations.

The pole pitch ratio is of interest during the FEA modelling of a machine. For a good design choice, the pole pitch ratio is considered to be 1 for maximum flux linkage. But the flux leakage due to adjacent permanent magnets is then high. To increase flux linkage and decrease flux leakage, the pole pitch ratio is reduced slightly from 1 for a good correlation [61]. Therefore, a flux linkage waveform is computed to ensure more sinusoidal wave shape for a good correlation with the analytical model of a machine.

For a good correlation between analytical and FEA design choices, if the machine is slotted, we must also consider the effect of cogging torque from time-stepping magnetostatic FEA. In a nutshell, cogging torque is undesirable and needs to be eliminated. For this purpose, the skew factor should be kept half of the slot pitch. In this research work, the cogging torque is computed by Maxwell's stress tensor method with respect to time scale [17].

As mentioned in section 4.1.1.2, axial flux distribution in the rotor and stator can lead to improving the performance of the machine. However, it is of interest to analyze flux density by solving electromagnetic models to verify that the flux lines are leaving rotor poles nearly perpendicular to meet design goals. It is possible when tooth and stator yoke dimensions are good to meet design requirements and all the flux from the rotor enter into the stator tooth simultaneously [60]. Therefore, the flux density, as well as the rotor and stator losses of a machine is calculated in the result and analysis part of this thesis to get an optimal design solution correctly.

5.2.2 On-load conditions

One of the characteristics of this particular type of HSPMSG is to produce a balanced torque at the rated speed [17]. For this purpose, a good estimate of back-emf is required to determine the ability of a machine by subtracting line-to-line phase value from another in MotorXP. Likewise terminal voltage, we are interested in a more sinusoidal waveform of the back-emf with fewer harmonics accordingly.

Similarly, for stator phase current waveform, a sinusoidal output stator current waveform is needed at on-load condition. Unlike terminal voltage, phase current can be computed

according to their respective input stator voltage waveforms without subtracting line-to-line phase current value. For a good agreement between the prototype model and simulation results, the current waveform should be approximately sinusoidal and closely match with the back-emf waveform [17].

In addition, on-load stator tooth losses "P_{ct}" are also verified to ensure that the machine is not saturated, and the value of "P_{ct}" is within a calculated range. Thus, FEA parameters of a machine geometry represented in section 5.1 are verified particularly in an on-load condition and how best they are arranged to achieve maximum phase current and lower losses for maximum performance of a machine.

5.3 Harmonic analysis

While the magnetostatic FEA discussed in section 5.1 yields time-stepping computational electromagnetic analysis, practical implementation of a prototype model of a machine would need to include harmonics study of the performance parameters of a machine such as speed, torque, and power. In MotorXP, the harmonic components of the selected quantities are plotted w.r.t the frequency spectrum by selecting "spectrum" in the corresponding "plot type" pop-up menu [59]. Higher-order harmonics in the currents and in the magnetic field can play a significant role in the machine output torque and the corresponding performances [17]. The computation of cogging torque is another significant factor associated with the measurements of performance parameters that can be used to help predict the steady-state and dynamic performance of the machine [59]. In this research work, the harmonic spectrum of torque and cogging torque is obtained against higher-order harmonics in the MotorXP software tool. Once the computation of torque and cogging torque is calculated accurately then the torque and power are plotted against the speed in the performance analysis part of this thesis simultaneously. One goal of this research work is to optimize the performance of the machine within the operating range.

Another challenge in high-performance wind turbine drives associated with the PM generators is to produce smooth torque with very low components of cogging torque. An improper design of any PMSG constitutes inadmissibly high cogging torque w.r.t the rated torque. High-performance applications such as the production of sustainable energy due to the propulsion of wind turbine blades rotation require minimization of cogging torque by carefully choosing a number of design parameters, materials, and assembly imperfections such as the combination of rotor and stator techniques on one hand. On the other hand, the

control methods can be used for the drives to create a difference between assumed and measured cogging torque accordingly. Another goal of this research work is to limit cogging torque value below 1% of the rated torque in order to obtain more power and smooth torque at higher RPM [64].

5.4 Thermal analysis

The most basic machine requirement for this particular type of HSPMSG is to ensure that the machine has enough torque at all speeds, from zero to full speed, to energize the referred devices connected with the generator without exceeding any thermal limits [17]. The thermal analysis of conventional PM machines is relatively easier as compared to the high-speed PM machines because it has smaller size and larger power density. An irreversible demagnetization induced in the PM rotor can easily create overheat and temperature rise issues to its integral parts such as the stator, air-gap, and rotor. Owing to the rapid temperature rise in the PM rotor, the indirect method of cooling the rotor does not protect the PM rotor from overheating [34]. Therefore, we will mainly use the self-ventilated cooling method to control the temperature in the winding and machine rotor in this research work.

MotorXP does not offer the thermal analysis of a machine. However, it is necessary to develop and analyze the thermal performance of the 24/4 (Ns/number of magnets) prototype model of a machine to overcome technical challenges such as magnet demagnetization, degradation of insulation materials, and loss of generator efficiency [65]. As mentioned previously in sections 4.1.3, and 4.4.1, that the cooling method selected for this particular type of HSPMSG is a large air-cooled. Thus, the critical cooling paths are discussed in the housing and end-caps of the machine, and heat transfer between housing and ambient is discussed in natural convection [66]. In addition, though not modeled in this analysis, the thermal losses of the machine are briefly discussed with few possible topologies adopted in the industry.

5.4.1 Cooling methods

Generally, the cooling methods used primarily for thermal analysis of PM machines are liquid and self-ventilated. Air-cooled generators come with self-ventilated hoses fitted to meet high torque densities and desired overload capabilities. However, a self-ventilated hose alone is often inadequate to remove heat from rotor and stator windings due to the high

thermal resistivity between heat source and coolant. It should be kept in mind that the thermal resistivity of the stator yoke, the low thermal conductivity of insulated stator windings, and internal air caused by the rotor together form a significant temperature difference between the air coolant and the stator windings. Consequently, self-ventilation alone become ineffective at high-speed operations of HSPMSG. To overcome this challenge, a forced air-flow mechanism is used to cool the rotor structure. In this case, one or more cooling fans are used to lowering the temperature and avoiding overheating issues in the machine [65].

5.4.2 Housing and end-caps

Housing and end-caps are the mechanical compositions of the machine to protect it from moisture, dirt, and chemicals on one hand. On the other hand, it is the combination of air ducts, lids, sleeves, and jackets to improve the thermal conductivity of the windings and to reduce the hot-spot value. In order to reduce the overall weight of the machine, Aluminum is chosen for the housing and end-caps material. One implication of this is that the mechanical composition of housing and end-caps becomes complicated and more expensive by using the combination of air ducts, lids, sleeves, and jackets simultaneously. One possibility is to use an air-ventilation jacket in the rotor parts and end windings rather than stator parts in order to extract heat from active windings and end windings in the end space region accordingly. By implementing an air-ventilation jacket in the housing and end-caps, the final prototype model of the machine become more cheaper and lightweight to implement the cooling process in the industry [66].

5.4.3 Natural convection

Natural convection is a process referred to as heat transfer between housing and ambient. It is applied to different parts of the machine, depending on their geometry. In other words, the correlation of a horizontal cylindrical type of structure is applied to the housing, and radial areas of the end caps. Whereas a correlation of a vertical flat plate type of structure is applied to the axial areas of the end-caps of a machine accordingly. In a large air-cooled generator, the air is blown over the wind turbine due to its height, which could be considered as natural convection between housing and ambient. This composition is much effective when the forced air-flow mechanism is used simultaneously [66].

5.4.4 Thermal losses

The major sources of heat and temperature rise are copper losses in the windings, eddy current and hysteresis losses in the stator steel, and friction and windage losses [19]. Iron losses rise in teeth and yoke. This means that the stator iron losses are the combination of teeth and yoke losses respectively. Whereas the rotor iron losses are measured with magnet losses. Copper losses can also be split between active and end-windings according to the winding geometry discusses in section 4.1.7. End-windings has front and rare sides, and losses are divided between them according to their volumes. The best approach is to measure the thermal losses of the machine at constant torque and at a steady state. In this way, the losses variation is taken into account with temperature (as shown in section 4.2) and load according to the basic requirements of the machine [66].

Finally, it is important to mention that the self-ventilation along with the air-forced cooling method chosen in this research work is actually the finite element method (FEM). Generally, four methods are adopted for the thermal analysis of an electrical machine. These are the lumped parameter network method, the finite element method (FEM), the computational fluid dynamics (CFD) method, and the experimental method [65]. The lumped parameter network method is used to solve convection heat transfer problems where the temperature at all nodes in the thermal network is calculated together with the power through all the thermal resistances [67]. The FEM is used to solve conduction heat transfer problems. Whereas the CFD method is used to solve both conduction and convection phenomena which dictate that it usually takes a little more time and effort than the lumped and FEM. The experimental method is the most effective method, but the test facilities required can be costly and time-consuming [65].

At this stage of the machine design analysis phase, the finite element methodology is completed with an overview of some key field calculations in MotorXP along with the thermally protected design of an HSPMSG is represented. But the optimal design solution of the prototype model is validated only if the field calculation of the performance parameters is estimated correctly in the MotorXP software tool. Thus, the performance graphs such as the torque-speed characteristics, iron losses, and efficiency map of the machine are represented in the result and analysis part of this research work exclusively.

Chapter 6

6 Modelling and Simulation

The HSPMSG design process depends mainly on modelling and simulation and how analytical and finite element methods are transformed into the prototype model of HSPMSG. In this section, an optimal modelling and simulation approach is used for each method to characterize the design challenges associated with the development of the machine used in MATLAB and MotorXP-PM software tools. The model is built around this approach and simulation tools take input design parameters as a starting point to develop prototype model of the machine.

The values obtained from this framework easily allow us to analyze and draw results and fulfilment to the basic machine requirement for the wind turbine system. These values are rationally motivated but are not necessarily meant to be universally applicable. This modelling and simulation framework is explored further to evaluate each design method in MATLAB and MotorXP-PM simultaneously.

6.1 Analytical design parameters estimation in MATLAB

While the design parameters identified in the analytical method of the machine design analysis phase serve to estimate output parameters for analytical, material, basic electrical model, machine size & weight, and basic losses of the machine. Practical implementation of analytical modelling and simulation would need to include a few common design parameter considerations. The common design parameters and their values are fairly straightforward to predict if the machine type is known, as it applies to all those electric machine designs that have the same ratings, purpose, or configurations.

However, it is always clear whether the values of these common design parameters will remain relevant to retrieve the basic machine requirements or may not apply to this particular type of HSPMSG.

Fortunately, because of the extensive analyses, and previous research work, we can assume the common design parameters to begin modelling and simulation of HSPMSG. The common design parameters are those parameters normally serve as an input to all type of analyses to estimate the output design parameters of the analytical design of a machine in MATLAB. The common design parameters and input design parameters are presented in the

prototype model of a machine. While the output design parameters are presented in the result and analysis part of the thesis.

The common design parameters will enable us to establish necessary output design parameters when analyzing an electric machine. However, as mentioned previously in chapter 3, an optimal modelling and simulation approach is needed to correctly estimate parameters discussed in the machine design analysis phase of this research work. Thus, an optimal modelling and simulation approach is discussed to correctly establish design parameters in MATLAB according to their respective analyses.

6.1.1 Modelling and Simulation approach in MATLAB

In order to obtain analytical design parameters correctly, a stepwise approach is used to aid in the input and output parameters in MATLAB. This approach allows tracing design parameters of HSPMSG. This approach combines the functionality of the MATLAB software tool along with the machine design analyses performed in the analytical method to estimate the performance of the machine accurately. Following steps are taken into account based on analytical, material, basic electrical model, machine size & weight, and basic losses of the machine simultaneously.

i. Each analysis is divided into two sections according to their respective input and output parameters. The common design and input parameters are examined in the prototype model, while the output parameters are examined in the results and analysis part of the thesis.

ii. Each parameter and its value are collected from their respective analyses and labelled as an input and output parameter. Each parameter is designated according to their respective analyses. Input parameters are those whose values are given in the thesis. Whereas output parameters are those whose values are calculated from equations only.

iii. The common design parameters and their values are entered first in chronological order to calculate the unknown parameters of the machine. This is done in order to calculate the output parameters of the machine.

iv. The parameters are arranged in such a way that the output parameter from one analysis will serve as an input parameter of another analysis. For example, the addition of electrical parameters to the basic design parameters (output parameters) estimated from the basic electrical model will serve as an input design parameter of the machine size & weight and so on. While for the material analysis the output parameters are not considered as they do not contain any equation.

v. For some parameters such as the rated speed, and stator current density, the values are assumed first as an input parameter and then estimated as an output parameter in order to validate design using the appropriate equations.

vi. Once all the parameters are modeled and simulated according to the methodology adopted in part 3 of the thesis then this approach can lead to the performance parameters estimation to judge whether HSPMSG design is feasible or not.

vii. Finally, the finite element design parameters are estimated in MotorXP-PM and compared with the analytical design parameters estimated from MATLAB to complete the design process eventually.

6.2 Finite element design parameters estimation in MotorXP-PM

Analytical design parameters estimation depends on the common design parameters assumed and collected from the analytical method. Whereas the finite element design parameters estimation relies heavily on the data assumed and collected from the prototype of a machine based on the analytical method. The modelling and simulation of FEM deal with the formulation of magnetostatic modelling of HSPMSG using nonlinear electromagnetic and geometrical construction in a time domain and solved simultaneously in each time step. In other words, the magnetostatic model is used to validate analytical design parameters of the HSPMSG at step voltage variation, load torque and changing rotor positions which are very difficult to include using the analytical approach [17].

Due to the direct coupling of the machine geometry, winding, mesh, and input material, the results can take into account the terminal voltage, flux linkage, back-emf, stator phase current, losses, cogging torque, and magnetic flux density are proposed using time-stepping FEM combined with 2-D FEA in MotorXP-PM. In addition, high-order harmonics, and

steady-state D-Q analysis[4] can be developed to conclude the performance analysis of a machine to fulfil the primary objective of the research work [59]. The following approach outline some of the steps required to carry out FEM useful to investigate HSPMSG in MotorXP-PM.

6.2.1 Modelling and Simulation approach in MotorXP-PM

MotorXP-PM is a leading software tool for electric machine design [59]. Here some stepwise approach to this software is summarized, with emphasis on the initial dimensioning of the PM generator to meet the basic machine requirements for the wind turbine system.

i. The modelling and simulation of FEM can be roughly divided into two main sections (such as the magnetostatic FEA and steady-state D-Q analysis). The initial dimensioning and geometrical construction of a machine is carried out in the magnetostatic FEA. While the performance analysis of a machine is carried out in the steady-state D-Q analysis.

ii. In the magnetostatic FEA of the FEM modelling and simulation, the input design parameters for finite element analysis, and electromagnetic analysis, are grouped together to form the prototype model of a machine.

iii. The input design parameters depend mainly on the analytical prototype model or the basic machine requirements according to their respective no-load and on-load conditions.

iv. Once the input design parameters are correctly established in the geometry editor tab of the MotorXP-PM then the input design parameters for the electromagnetic analysis are established to analyze the time-stepping 2-D FEA model of a machine at multiple-point simulation setup for high accuracy and precision of the results.

---

[4] A traditional analysis of permanent magnet synchronous machines which focused upon establishing a relationship between the Quadrature (Q) and Direct (D) axis stator current or voltage and the electromagnetic force created to establish rotation torque [76].

v. Next, the generator parameters are plotted for no-load and on-load conditions under the plot wizard tab of the MotorXP-PM. The quantities such as the terminal voltage, flux linkage, cogging torque, core losses, and magnetic flux density are plotted under no-load conditions. Whereas, the stator phase current, back-emf, and stator tooth losses are plotted under on-load conditions.

vi. Likewise magnetostatic FEA, the harmonic analysis is performed by plotting air-gap magnetic flux distribution, and air-gap magnetic flux spectrum plot. In addition, the harmonic spectrum of torque and cogging torque is also plotted to judge the suitability of the prototype model of a machine simultaneously.

vii. The performance analysis of a machine can be measured by setting up input design parameters in steady state D-Q analysis. The quantities such as the speed versus torque and speed versus power are plotted to fulfil the basic requirements of the wind turbine system. Here, it is important to mention that the input design parameters for the performance analysis of a machine are mentioned to plot speed versus torque and power in the steady state D-Q analysis. Whereas the air-gap magnetic flux distribution, air-gap magnetic flux spectrum, the harmonic spectrum of torque and cogging torque are plotted in the magnetostatic FEA plot wizard.

viii. Finally, the performance analysis of a machine is examined in the steady state D-Q analysis of the MotorXP-PM. For this purpose, iron losses, and performance efficiency of a machine is plotted by adjusting input design parameters according to the basic requirements of the wind turbine system.

Once the prototype model of a machine is examined in the results and analyses chapter of the thesis then the conclusion is represented to summarize the analytical and finite element methods and highlight which parameters contribute the most to design, and some of the fundamental differences in the two different types of methods.

Chapter 7

7 Prototype Model

Two methods such as the analytical & finite element are examined in this study. Both are validated with their respective software tools to form a prototype model of a machine. In this part of the thesis, few common design parameters are first assumed to start prototype modelling for each design method (analytical and FE). In addition, the input design parameters are also considered from different analyses to form an optimal design solution of an HSPMSG.

7.1 Prototype model for analytical method

In this section, the input design parameters along with some common design parameters are presented and analyzed in such a way that each parameter is grouped into its own respective machine design analysis, and then some detail on their values are discussed simultaneously. The development of a prototype model of a machine is explored further to establish how performance is impacted by selecting each parameter and its value from their respective analysis and the equations presented in the machine design analysis phase of the thesis.

7.1.1 Common design parameters

The first related consideration is the commonly used design parameters that contribute most to the output design parameters of the result and analysis part of the thesis. The overall machine performance depends on the appropriate selection of the common design parameter values, as well as solving the analytical equations efficiently which are ideally suited for this type of design problem. A summary of the various commonly used design parameters is provided in Table 8 below.

Common Design Parameter	Value	Machine Part or Section	Analysis Type	Output Parameter/s
Free-space permeability (u_0)	1.256×10^{-6}	Air-gap	Basic electrical model	L_{ag}, $perm$, L_e
			Basic losses	δ
Pole pairs (p)	2	Stator slots	Analytical	f, r, N_e, θ_{sk}, m, N_{sfp}, γ, N_a
			Basic electrical model	K_g, $C\phi$, B_m, λ_n, L_{ag}, L_{as}, L_{am}
			Machine size & weight	$sbid$, M_m
			Basic losses	t, B_b, ω_m
Number of phases (q)	3	Stator	Analytical	m
			Basic electrical model	I_a, L_{ag}, L_{slot}
			Machine size & weight	M_{ac}
			Basic losses	P_a
Number of stator slots (N_s)	24	Stator slots	Analytical	ws_{bottom}, m, N_{sfp}, γ
			Basic electrical model	leo, w_t
			Machine size & weight	M_{ct}
Slot depression width (w_d) in μm	1.0	Stator slots	Analytical	θ_{sk}, ws_{bottom}, ws_{top}
			Machine size & weight	M_{ct}

(To be continued)

Air-gap (g) in mm	4.0	Air-gap	Analytical	ws_{bottom}, ws_{top}, B_g
			Basic electrical model	leo, w_t, K_c, g_e, L_{ag}
			Machine size & weight	R_{ci}
			Basic losses	Rey
Magnet height (m_h) in mm	40.0	Rotor geometry	Analytical	B_g
			Basic electrical model	CP
Slot depression height (h_d) in mm	0.1	Stator slot geometry	Analytical	ws_{bottom}, ws_{top}
			Basic electrical model	leo, w_t, $perm$
			Machine size & weight	R_{ci}, M_{ct}
Magnet width (m_w) in mm	25.0	Rotor geometry	Analytical	ws_{top}
			Basic electrical model	leo, w_t, L_{ag}
			Machine size & weight	R_{ci}, M_m
Peripheral tooth fraction (*tf*)	0.5	Stator slots	Analytical	ws_{bottom}
			Basic electrical model	w_t
			Basic losses	B_t
Power factor angle (ϕ) in deg. (elect.)	0	Phase	Analytical	pf
			Machine size & weight	V_a
No. of turns/coil (N_c)	1	Stator windings	Analytical	A_{ac}, N_a
			Basic electrical model	L_{as}, L_{am}, L_e

(To be continued)

Slot height (h_s) in mm	25.0	Stator slot geometry	Analytical	A_s
			Basic electrical model	$leo, perm$
			Machine size & weight	R_{ci}, M_{ct}
No. of slots short-pitched (N_{sp})	1	Stator slots	Analytical	N_{sap}
			Basic electrical model	L_{as}, L_{am}
Magnet remnant flux density (B_r) in T	1.2	PM material	Analytical	B_g
			Basic electrical model	B_{gm}
Stator winding conductivity ($\hat{\sigma}$) in S/m	6.0×10^7	Stator windings	Basic electrical model	R_a
			Basic losses	δ
Stator back iron ratio ($sbir$)	0.7	Stator	Machine size & weight	$sbid$
			Basic losses	t, B_b

Table 8. Common design parameters for analytical modelling & simulation

From Table 8 above we see that the common design parameters serve to estimate the output design parameters for all types of analyses previously discussed in the analytical method. This is not too surprising, as the parameters chosen to present as a common design parameter are either fetched from the analytical method discussed in this thesis or the previous research work carried out on this topic. In other words, the values of pole pairs, number of phases, number of stator slots, and magnet remnant flux density are collected from the analytical method assumed from this thesis. Whereas, the values of slot depression width, air-gap, magnet height, slot depression height, magnet width, peripheral tooth fraction, power factor angle, number of turns per coil, slot height, number of slots short-pitched, stator winding conductivity, and stator back iron ratio are collected from previous research work accordingly. In addition, free-space permeability is a constant parameter available from the resource database. In a nutshell, common design parameters are considered as input parameters to solve equations for analytical design parameters estimation in MATLAB.

As noted in Table 8 above that each parameter is expressed according to its relevant machine part or section. This additional detail gives a more realistic understanding of parameters across the design process so that the entire machine can be designed around the actual physical parts of a machine or section accordingly. For example, the stator represents a section of a machine that includes stator slots, stator windings and other parts relevant to the stator of a machine. Whereas all those parameters which belong to air-gap, stator slots, phase, stator windings, and PM material are considered to be a specific part of a machine accordingly. In addition, the parameters belonging to rotor or stator slot geometry are considered to be used as a measuring parameter to construct the geometry of a specific part or section. The reason behind representing each parameter w.r.t its relevant part or machine is to give a good guideline for the engineers and designers working on the PMSG design.

7.1.2 Input design parameters for analytical analysis

The analytical method presented in the machine design analysis phase contains five analyses: analytical, material, basic electrical model, machine size & weight, and the basic losses of the machine. Each analysis contains a number of parameters and adjacent equations in order to calculate unknown output parameters accordingly. In this section, input design parameters for analytical analysis are presented to estimate the output design parameters for the analytical analysis. Table 9 below outlines the main input design parameters and their values for analytical analysis w.r.t their adjacent machine part or section, and how it helps increase machine performance.

Input Parameter	Value	Machine Part or Section	Output Parameter
Rated speed (*N*) in rpm	15000	Rotor	f_e
Tip speed (v_{tip}) in m/s	200	Rotor	r
Length to diameter ratio (*LDr*)	2.50	Rotor geometry	L_{st}
Magnetic skew angle (θ_{msk}) in deg. (mech.)	10	Rotor magnetic poles	θ_{sk}
Stator current density (J_a) in A/cm^2 "max."	1200	Stator	-
Number of conductors/slot (N_{cs})	224	Stator geometry	-

Slot fill factor (λ_s)	0.5	Stator slot conductor	A_{ac}
Electrical frequency (f) in Hz	500	Phase	-

Table 9. Input parameters for analytical analysis

Table 9 above shows fewer input parameters as compared to the actual number of parameters that can be fetched from the analytical analysis of the machine, because most of the parameters are already summarized in common design parameters, and these input design parameters are solely for the analytical analysis of the machine.

While only five types of analysis are conducted for the prototype modelling of a machine, the practicality of this research work can only be validated by presenting each design parameter according to their respective sections or physical parts of a machine accordingly. A number of various parts or sections used in this prototype model are provided in Table 9. The input design parameters associated with its adjacent part or section are meant to compute the output design parameters of a machine relative to their respective part/section or some other part/section. In other words, the rated speed (N) of the rotor is used to determine the estimated electrical frequency (f_e) of phase, and tip speed (v_{tip}) of the rotor is used to determine the rotor radius (r) of its own machine part accordingly.

Likewise, common design parameters, the values of the input design parameters for analytical analysis can also be fetched from the analytical part of this thesis or from the previous research work accordingly. For this purpose, the values of rated speed, electrical frequency, L/D ratio, tip speed, and slot fill factor are collected from the analytical analysis. Whereas the value of the magnetic skew angle is assumed from the previous research work. In contrast, the electrical frequency (f), number of conductors per slot (N_{cs}), and stator current density (J_a) are not used to estimate the output design parameters but are rather mentioned to give good design consideration for machine designers and to validate electrical frequency, and stator current density in the results and analyses chapter of this thesis respectively.

7.1.3 Input design parameters for material analysis

Of the 5-analyses, the material analysis seems to have input design parameters only than the others. The reason for this is, as discussed in chapter 6, that the analysis has no equation to estimate any of the output parameters of the machine, whereas in the other type of analyses

such as the basic electrical model, and basic losses the material input design parameters should be accountable for. Table 10 below presents the input design parameters for material analysis and its values used in modelling and simulation adjacent to their respective analysis type.

Input Parameter	Machine Part or Section	Analysis Type	Value	Output Parameter/s
Stator saturation flux density (B_{sat}) in T	Stator	Basic losses	1.8	P_h, P_e, P_{iron}
Recoil permeability (u_{rec})	Rotor magnetic poles	Basic electrical model	1.05	B_{gm}
Electrical resistivity (ρ) in $\mu\Omega \cdot$ m	Rotor magnetic poles	Basic losses	1.43	P_e

Table 10. Input parameters for material analysis

All input design parameters and their values presented are used to compute the output design parameters of their respective analysis type as shown in Table 10. The input design parameters for material analysis can be presented in common design parameters and some other input design parameters but it is taken for granted that each parameter and its associated value must be mentioned here in order to better predict the properties of the material accordingly. In addition, all input design parameters for material analysis are collected from their respective analysis accordingly.

7.1.4 Input parameters for basic electrical model

Likewise analytical analysis, the input design parameters for basic electrical model are solely used to estimate the output design parameters of the basic electrical model of the machine. More detail of each input design parameter is discussed in the Table 11 below.

Input Parameter	Machine Part or Section	Value	Output Parameter/s
Power output (P_{out}) in kW	Phase	660	I_a
Inner magnetic boundary (R_i) in m	Rotor magnetic poles	r [5]	k_g
Outer magnetic boundary (R_s) in m	Rotor magnet poles	$r + mw + g$ [6]	k_g, λ_n, L_{ag}
Inner boundary of magnet (R_1) in m	Rotor magnetic poles	r[5]	k_g
Outer boundary of magnet (R_2) in m	Rotor magnetic poles	$r + mw$ [7]	k_g
Magnet physical angle (θ_m) in deg. (mech.)	Rotor magnetic poles	50.0	$C\phi,\ \theta m$ in rad.
Leakage factor (k_l)	Air-gap between rotor and stator	0.95	B_{gm}
Reluctance factor (k_r)	Air-gap between rotor and stator	1.05	B_{gm}

Table 11. Input parameters for basic electrical model

As we see from Table 11 above that there are a number of input design parameters collected to analyze the basic electrical model of a machine. One of them is the power output of the machine. Actually, power output is a basic requirement of a machine, and machine designers always built a machine around the output power requirement of a machine. Other parameters such as the inner magnetic boundary, inner boundary of the magnet, outer magnetic boundary, and outer boundary of the magnet are calculated with the help of the analytical analysis of the machine. Whereas the other three parameters such as the magnet physical angle, leakage factor, and reluctance factor are collected from the previous research work carried out on this topic accordingly.

---

[5] For a 2-pole pair machine, the length of each pole innermost part of each magnet is considered to be the same as the rotor radius of a machine. Similarly, for the inner magnetic boundary, the length of the innermost part of the magnetic flux for each magnet pole is also the same as the rotor radius of the machine.

[6] The value of the outer magnetic boundary is the sum of rotor radius, magnet width, and air-gap because the magnetic flux lines passing from one pole toward another covers the air-gap outermost edges and the width of the magnet is also increased at the outer edges of the rotor.

[7] The value of the outer boundary of the magnet is the sum of rotor radius, and magnet width as the width of the magnet is also increased at the outer edges of the rotor.

7.1.5 Input parameters for machine size and weight

The input parameters assumed for machine size and weight analysis are used to estimate the output design parameters of a machine in its own analysis. Table 12 below presents input parameters and their values identified and evaluated for analytical modelling & simulation.

Input Parameter	Machine Part or Section	Value	Output Parameter/s
Conversion factor (*cov*)	Air-gap between rotor and stator	703.069	k_z
Shear stress (τ) in psi	Air-gap between rotor and stator	10	k_z
Magnetic flux density (B_m) in cT	Air-gap between rotor and stator	64.37	k_z
Steel density (*ds*) in kg/m^3	Rotor and stator material	7700	M_{cb}, M_{ct}, M_s
Magnet density (*dm*) in kg/m^3	Rotor magnetic poles	7400	M_m
Conductor density (*dc*) in kg/m^3	Stator windings	8900	M_{ac}

Table 12. Input parameters for machine size and weight

From Table 12 above we see that there are a number of parameters that contribute to estimating the output parameters of a machine. Among them is the conversion factor which is used to estimate the surface current density (k_z). The value of conversion factor is applicable for this particular type of large air-cooled machine accordingly [39]. Another parameter that significantly affects the performance of the machine is the magnetic flux density (B_m). This parameter is actually an output parameter estimated from the basic electrical model where it is converted first (m→cm) in order to compare it with the stator current density (J_a) of a machine. Next, the remaining parameters such as the shear stress, steel density, magnet density, and conductor density are collected from the machine size and weight analysis of the thesis accordingly.

7.1.6 Input parameters for basic losses of a machine

Finally, the input design parameters and their values are collected from the basic losses analysis and the previous research work carried out on this topic. Table 13 below presents the values of input design parameters used in analytical modelling and simulation of the output design parameters estimation accordingly.

Input Parameter	Machine Part or Section	Value	Output Parameter/s
Coefficient of resistance (C_r)	Stator slots	1.12	P_{stray}
Material constant (η)	Rotor + stator material	0.1	P_h
Air density (J_{air}) in kg/m^3	Air-gap between rotor and stator	1.205	P_{wind}
Coefficient of hysteresis losses (C_h)	Rotor + stator material	0.0275	P_{iron}
Coefficient of excess eddy current losses (C_e)	Rotor + stator material	0.000277	P_{iron}
Coefficient of classical eddy current losses (C_c)	Rotor + stator material	1.83	P_{iron}
Kinematic viscosity of air (ε) in m^2/s	Air-gap	1.5×10^{-5}	Rey
Base power (P_b) in W/lb	PM material	36.79	P_{cb}, P_{ct}
Base flux density (B_o) in T	PM material	1.0	P_{cb}, P_{ct}
Flux density exponent (n)	PM material	2.12	P_h, P_{cb}, P_{ct}
Base frequency (f_o) in Hz	PM material	1000	P_{cb}, P_{ct}
Frequency exponent (nf)	PM material	1.68	P_{cb}, P_{ct}

Table 13. Input parameters for the basic losses of a machine

Similarly, for basic losses analysis, input design parameters are assumed from either previous research work or from this thesis accordingly. For instance, the coefficient of resistance, material constant, air density, coefficient of hysteresis losses, coefficient of excess eddy current losses, coefficient of classical eddy current losses, and kinematic viscosity of air are assumed from previous research work carried out on this topic. Whereas the base power, base flux density, flux density exponent, base frequency, and frequency exponent are collected from the basic losses of a machine.

Once the input design parameters and their values are established correctly, then the optimal design solution based on the analytical method is propagated forward to validate these input design values in the MATLAB tool. The MATLAB tool will then use these input values to estimate output design parameters with the help of their adjacent equations presented in the analytical method according to their respective analysis type. The output design parameters and their values are presented in the results and analyses part of this thesis along with some brief overviews on data obtained from analytical design parameters estimations and their suitability for this particular type of HSPMSG design.

7.2 Prototype model for finite element method

The analytical prototype model of the previous section is helpful in visualizing each parameter according to its relevant machine parts or sections. However, it is not clear how to visualize machine parts or sections in a manner such that each part or section are relatively adjacent to one another physically. The geometrical construction of HSPMSG in MotorXP-PM provide us with an overview to illustrate the relative machine parts or sections of a machine for analysis purpose. Figure 20 below shows a 2-D model of HSPMSG along with numbers to highlight the relevant machine parts or sections for easier visualization.

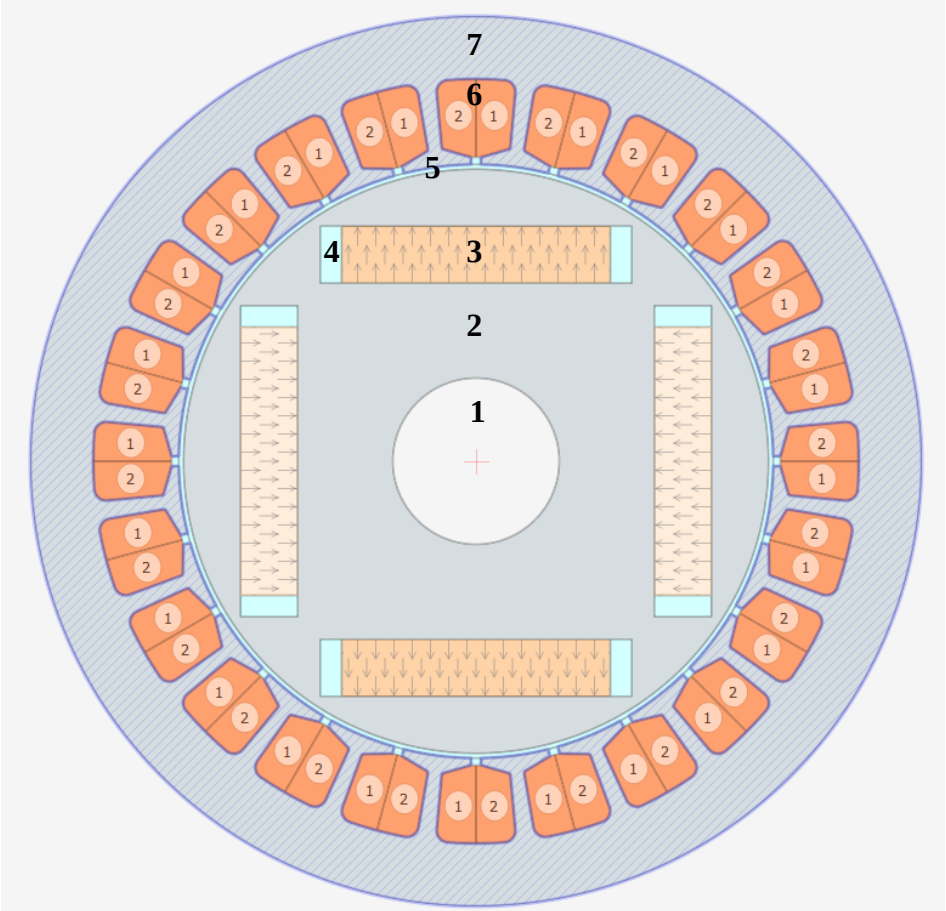

Figure 20. Overview of 2-D prototype FE model of HSPMSG

1. **Rotor shaft** – Rotor shaft inserted directly into the rotor
2. **Rotor** – Rotating part of a machine accommodate PM, general, and rotor shaft
3. **PM** – Interior or straight buried permanent magnets
4. **General** – Space between PM's and rotor body, normally denoted as air or insulation
5. **Air-gap** – Gap between rotor and stator
6. **Stator slot** – House double layered armature and phase windings
7. **Stator/armature** – A large fixed cylindrical structure for balancing rotor

7.2.1 Input parameters for finite element analysis

The input design parameters for finite element analysis contribute most to the variation in performance and describe some of the fundamental considerations in the optimal design solution of the FEM prototype model. For this purpose, input design parameters for machine geometry, machine winding, machine mesh, and machine input material are considered to construct the geometry for the magnetostatic FEA of HSPMSG. Choosing proper input design parameters can have a significant impact on the selected quantities and the performance analysis of the machine. The following detail specifies the number of input design parameters and their value along with the adjacent output parameters to which they impact the most to develop the prototype model of a machine respectively.

7.2.1.1 Input design parameters for machine geometry

There are a number of physical parts or sections of a machine that can be seen in Figure 20. The Figure does not depict machine parameters used to construct the geometry of the machine. The input design parameters for machine geometry will not only specify the values of individual parts or sections but can also specify the outcome of modelling in the form of results and performance analysis of a machine. Table 14 below shows the input parameters for the stator, rotor, and axial dimensions of the machine geometry simultaneously.

Machine Type: Inner rotor		
Stator Dimensions		
Input Parameter	**Value/Detail**	**Output Parameter/s**
No. of stator slots (N_s)	24	V_a, I_a
Outer diameter (D_{mach}) in mm	450.0	P_{out}, P_{in}, pf
Inner diameter (D_{in}) in mm	300.0	P_{out}, P_{in}, pf
Winding layers	Double layer	V_a, I_a
Layers orientation	Left/Right	β, I_a, V_a
Stator geometry	General slot	P_{out}, P_{in}, T, N
Slot depth (h_s) in mm	25.0	B_m, V_{back}, ϕ_{link}
Slot bottom width (ws_{bottom}) in mm	17.0	B_m, V_{back}, ϕ_{link}
Slot top width (ws_{top}) in mm	15.0	B_m, V_{back}, ϕ_{link}
Slot opening depth (h_d) in mm	0.1	B_m, V_{back}, ϕ_{link}
Slot opening width (w_d) in mm	0.0001	B_m, V_{back}, ϕ_{link}

Tooth tip angle (α_{tip}) in deg.	16.0	$B_m, V_{back}, \phi_{link}$
Bottom corner radius (R_b) in mm	5.0	$B_m, V_{back}, \phi_{link}$
Top corner radius (R_t) in mm	1.0	$B_m, V_{back}, \phi_{link}$
Rotor Dimensions		
No. of pole pairs (p)	2	β
Air-gap (g) in mm	4.0	$B_m, V_{back}, \phi_{link}$
Outer diameter (R_{out}) in mm	296.0	P_{out}, P_{in}, pf
Inner diameter (R_{in}) in mm	98.0	P_{out}, P_{in}, pf
Rotor geometry	Straight buried	β
Magnet height (m_h) in mm	50.0	$B_m, V_{back}, \phi_{link}$
Magnet width (m_w) in mm	25.0	$B_m, V_{back}, \phi_{link}$
Magnet barrier width (m_b) in mm	5.0	$B_m, V_{back}, \phi_{link}$
Magnet inset height (m_{in}) in mm	100.0	$B_m, V_{back}, \phi_{link}$
Axial Dimensions		
Lamination stack length (A_{st}) in mm	134.0	P_{out}, P_{in}, T, N
Stator skew angle (θ_{sk}) in deg. (elect.)	0.35	$B_m, V_{back}, \phi_{link}$
Magnetic skew angle (θ_{msk}) in deg. (mech.)	10.0	$B_m, V_{back}, \phi_{link}$
No. of magnet segments (S_m)	1	$B_m, V_{back}, \phi_{link}$

Table 14. Input design parameters for machine geometry

It is certain from the previous research work carried out on a wind turbine generator design that the machine is an inner rotor type [70]. For all the input parameters presented here, only the newly assumed parameters are analyzed because the rest of the parameters are already analyzed in the analytical model appropriately.

The FEM prototype modelling starts with the parameterization of a stator dimension. From table 14 we see that the value of D_{in} is almost two-thirds of the D_{mach} because it is a common standard to design an inner rotor electric machine for construction and performance purposes [71]. MotorXP offers three types of stator geometry templates such as “parallel tooth”, “parallel slot”, and “general slot” simultaneously [59]. The “general slot” is selected to create proper dimensions for ws_{bottom}, and ws_{top}. Finally, the values of α_{tip}, R_b, and R_t needs to be in a limit range to accommodate 224 conductors/slot and to provide smoothness

to the stator tooth. In other words, the higher the value of α_{tip}, R_b, and R_t the more will be the values of ϕ_{link}, and B_m quantities.

Similarly, the value of R_{out} of the rotor dimension must be kept smaller (4 mm) from D_{in} due to the air-gap factor. Whereas the value of R_{in} must be one-third to the value R_{out} as we need space to insert permanent magnets into the rotor. The geometry of the rotor can also be straight buried to receive the maximum number of flux linkage for this particular type of HSPMSG. Similarly, the value m_h is double than m_w to cover the height between the rotor, and stator accordingly. In addition, the value of m_{in} is double as compared to m_h to cover the entire length of the rotor for maximum B_m. Magnet barrier width (m_b) is an air or isolation gap between the permanent magnet and rotor body also denoted as "general".

Finally, the A_{st} of the axial dimension is the length of the stator and rotor iron cores. The value of A_{st} must be kept high to reduce eddy currents induced in the magnet and thus reduce the magnet losses and magnet temperature [59]. Also, the value of S_m is kept at 1 in order that the magnet is not divided due to the fewer number of poles.

7.2.1.2 Input design parameters for machine windings

We have already seen that input design parameters for machine geometry can play a crucial role in estimating output design parameters of the finite element modelling. The second step is to setup the windings of a machine. The machine windings can play a significant role not only to the electromagnetic analysis of a machine but also on the thermal performance of the machine [72]. A list of input design parameters used in magnetostatic FEA for machine windings are provided in Table 15 below.

Input Parameter	Value/Detail	Output Parameter/s
Wire size method	Fill factor	P_{out}, P_{in}, pf, I_a, V_a
Strand diameter (D_s) in mm	9.0	B_m, V_{back}, ϕ_{link}
Winding connection type	Star	β
No. of parallel paths	2	B_m, V_{back}, ϕ_{link}
No. of turns/coil (N_c)	1	P_{out}, P_{in}, pf, I_a, V_a
Number of strands in hand	1	I_a, V_a
Coil fill factor	0.5	B_m, V_{back}, ϕ_{link}
Slot fill factor (λ_s)	0.5	B_m, V_{back}, ϕ_{link}

Coil span	6	I_a, V_a
Winding layout	Automatic	β

Table 15. Input design parameters for machine winding

There are four wire size methods used in MotorXP-PM such as the wire diameter (the wire diameter specified by user), AWG (the wire diameter specified by American wire gauge standard), SWG (the wire diameter specified by standards wire gauge), and fill factor (specified by the user either by coil fill factor or slot fill factor). Here, the fill factor is used because the number of strands in hand and "N_c" are the same. In addition, the slot fill factor specifies the ratio of the area of all conductors of a slot to the total slot area. Whereas the coil fill factor is the ratio of the area of all conductors of a slot to the slot area occupied by the conductors, not including slot isolation [59].

7.2.1.3 Input design parameters for machine mesh

Next, the input design parameters for machine mesh are examined. The mesh quality influences the simulation results accuracy. To enhance the accuracy of the simulation results the triangles of the mesh should be close to the equilateral triangle as much as possible. A summary of the input design parameters for the FEM prototype model is seen in Table 16 below.

Input Parameter	Value/Detail	Output Parameter/s
Max. triangle side in mm	5.0	$B_m, V_{back}, \phi_{link}$
No. of slices	5	$B_m, V_{back}, \phi_{link}$
No. of layers in air-gap	7	$B_m, V_{back}, \phi_{link}$
Air-gap mesh quality	High	$B_m, V_{back}, \phi_{link}$

Table 16. Input design parameters for machine mesh

All four parameters can directly contribute to the output parameters of a machine as well as the final performance analysis of the machines. The value of max. triangle side should be as much minimum as possible to limits the length of the longest triangle side to the specific value. In other words, lower the value of the max. triangle side higher will be the output quantities/parameters. The no. of slices specifies the no. of the machine's cross-sections in which the magnetic field is simultaneously calculated. In other words, the higher the no. of slices the higher the values of output parameters. The no. of layers in the air-gap specifies

the total number of finite elements layers placed in the air-gap. In other words, the higher the number of layers in the air-gap, the higher will be the values of the output parameters. Finally, the air-gap mesh quality specifies the quality of the mesh in the air-gap region. For high-performance PM machines, it is recommended to use high quality in order to analyze the machine's performance accordingly [59].

7.2.1.4 Input design parameters for machine material

A final contribution relating to FEA is estimating the input design parameters for machine material in a finite element prototype model for results and analyses purpose. Table 17 below gives an overview of some of the detail of the input design parameters for machine material chosen for this particular type of HSPMSG.

Input Parameter	Value/Detail	Output Parameter/s
General	Air, Isolation	P_{out}, P_{in}, pf, I_a, V_a
Rotor & stator iron	M-19 29 Si	P_{iron}, β
Stator winding	Copper	B_m, V_{back}, ϕ_{link}
Rotor magnet	N52	P_{iron}, β
Stacking factor	0.95	P_{iron}, β
Winding & magnet temperature (No-load condition) in deg. C	20.0	V_a, ϕ_{link}, T_{cog}, P_c, B_m
Winding & magnet temperature (On-load condition) in deg. C	80.0	I_a, V_{back}, P_c, T, N, P_{out}, P_{iron}

Table 17. Input design parameters for machine material

The input parameters presented in Table 17 above play a dominant role in the variation in performance. At first, the "general" is the air or isolation gap between PM's and rotor body need to include exclusively. Machine analysis shows that the value of "general" can neither be small nor large in order to get electrical quantities and performance appropriately. For this purpose, the value of "general" is kept at 5 mm as mentioned in the rotor dimensions of the machine geometry earlier. As discussed earlier in the material analysis of the analytical method that 6.5% SiFe material is used to construct the rotor and stator material. The "M-19 29 Si" is the material code used in the MotorXP-PM for the identification of 6.5% SiFe material. "Copper" is the most obvious choice while designing stator windings. Therefore, "copper" is chosen to construct the windings of this particular type of HSPMSG. Likewise, the rotor and stator material, the magnet material is carefully chosen to maximize the

performance of the machine. The material code “N52” is used in MotorXP-PM for “NdFeB” permanent magnet material. The “stacking factor” reduces the flux carried by the iron core which is taken into account by MotorXP-PM through the stacking factor value. The value of the stacking factor can neither be too small nor large for the performance analysis of the machine. MotorXP-PM has a value of 0.95 for the stacking factor. Therefore, this value is taken for granted to design HSPMSG accordingly.

The values of winding and magnet temperature vary according to the no-load and on-load conditions. In other words, for no-load conditions, the electrical quantities are measured at 20°C. Whereas, for on-load conditions, the electrical quantities are measured at 80°C in order to analyze the electric machine at different temperatures ranges simultaneously.

7.2.2 Input parameters for electromagnetic analysis

The input design parameters for FEA are used to build a basic prototype model of HSPMSG. In contrast, the design parameters for electromagnetic analysis are used to visualize the electrical quantities/output parameters of the machine respectively. In other words, the magnetostatic FEA is analyzed in the electromagnetic analysis for validation purposes. But, before analyzing output parameters in chapter 8 of this thesis, a few input design parameters for electromagnetic analysis are considered. Table 18 below shows some of the input design parameters used to analyze output design parameters under no-load and on-load conditions.

Input Parameter	Value/Detail	Output Parameter/s
Solver type	Nonlinear	-
Convergence tolerance	0.001	-
Current waveform	Sinusoidal	-
Advance angle (γ_{ad}) in deg. (elect.)	180.0	β
Current input method	RMS supply current	-
Rated speed (N) in rpm	15000	β
RMS supply current (No-load condition) in A	0	V_a, ϕ_{link}, T_{cog}, P_c, B_m
RMS supply current (On-load condition) in A	208.15	I_a, V_{back}, P_c, T, N, P_{out}, P_{iron}
Simulation setup	High accuracy	-
No. of points	96	-

Simulation time	One electrical period	-
Compute cogging torque	Check	T_{cog}

Table 18. Input design parameters for electromagnetic analysis

Solver type in MotorXP specifies whether the linear or nonlinear FEA is used. In this analysis, a nonlinear type of solver is used because *T*, and T_{cog} waveforms are non-sinusoidal. Whereas the nonlinear solver can be used for both sinusoidal and non-sinusoidal current waveforms simultaneously. Convergence tolerance specifies the accuracy of FEA solutions. It means that the smaller the value of convergence tolerance higher can be the results accuracy and vice versa. Current waveform drives simulation results by running simulations for several rotor positions [59]. Almost all types of machine design analysis based on load conditions are conducted under sinusoidal current waveform for high accuracy and low computation speed. It is a fundamental principle to consider γ_{ad} equals to 180° while designing all types of generators as the load is considered to be leading. Whereas the load is considered to be lagging (γ_{ad} = 0°) in designing motor [57]. In addition, the parameters with no output parameters are means to set up simulation only.

The electromagnetic analysis relies heavily on no-load and on-load conditions considered for the field computations of an electric machine. For this purpose, the simulation setup chosen is high accuracy with 96 points to consider the effect of cogging toque on machine performance [59].

A seen from both prototype models (FEA and electromagnetic) that magnetostatic FEA is almost completed by considering no-load and on-load conditions. Similarly, we can analyze air-gap magnetic flux, the harmonic spectrum of torque and cogging torque by considering the same input design parameters from the previous models in the results and analyses chapter of this research work. Therefore, we do not need to present additional parameters for the harmonic analysis of a machine.

As discussed in chapter 5, there are a few considerations presented for the thermal analysis of a machine. MotorXP-PM does not provide field computation for the thermal analysis of a machine. Therefore, there are no input and output design parameters presented in this research work except a few recommendations already presented in chapter 5 of this research work.

Chapter 8

8 Results and Analyses

This research work shows a promising methodology to overcome design challenges associated with a High-speed Permanent Magnet Synchronous Generator in the form of analytical and finite element methods. This part of the thesis presents the results based on the modelling and simulation output design parameters obtained from MATLAB and MotorXP-PM software tools according to their respective analysis type. In addition, a comparative analysis has been made to validate the basic machine requirements for a wind turbine system and machine performance based on data obtained from analytical and finite element modelling and simulation. The following study examines the effect of assumed and collected design parameters according to their respective analysis type.

8.1 Results and Analyses from analytical modelling & simulation

The analytical modelling and simulation approach discussed in chapter 6 and design parameters considered in the prototype model of a machine yields important insight into what dominant parameters are to be selected for result and analysis purposes. The following detail summarizes the output design parameters estimated from the MATLAB software tool to validate the concept of HSPMSG design followed by a brief analysis for each result accordingly.

8.1.1 Results & Analyses for analytical analysis

In order to provide a check on the analytical modelling and simulation and the prototype model of a machine, results are summarized using a combination of equations and modelling and simulation techniques from the MATLAB software tool. A summary of output design parameters w.r.t their machine parts and sections and their values for analytical analysis can be seen in Table 19 below.

Output Parameter	Machine Part or Section	Value
Rated speed "estimated" (N_e) in rpm	Rotor	15000
Rotor radius (r) in m	Rotor geometry	0.127
Rotor stack length (L_{st}) in m	Rotor geometry	0.636
Skew angle (θ_{sk}) in deg. (elect.)	Stator	0.35
Skew factor (K_s)	Rotor magnetic poles	0.995
Number of slots/pole/phase (m)	Stator slots	2
Number of slots with full pitch coil (N_{sfp})	Stator slots	6
Number of slots with actual pitch coil (N_{sap})	Stator slots	5
Slot bottom width (ws_{bottom}) in mm	Stator slot geometry	17
Slot top width (ws_{top}) in mm	Stator slot geometry	15
Average slot width (ws) in mm	Stator slot geometry	16
Area of slot (A_s) in mm^2	Stator slot geometry	0.4
Winding pitch (α) in deg. (elect.)	Stator windings	2.62
Electrical angle (γ) in deg.	Stator windings	0.523
Winding cross-sectional area (A_{ac}) in mm^2	Stator windings	0.1
Number of armature turns/coil (N_a)	Stator windings	8
Electrical frequency "estimated" (f_e) in Hz	Phase	500
Electrical frequency (ω_0) in rad/s	Phase	3.14×10^3
Power factor (pf)	Phase	1.0
Air-gap flux density (B_g) in T	Air-gap between rotor and stator	1.2

Table 19. Output design parameters for analytical analysis

All the unknown design parameters relative to the analytical analysis are grouped together as output design parameters within the results and analyses section. Table 14 shows the output design parameters for the eight different machine parts and sections. Across a wide range of output parameters, the estimated rated speed (N_e), number of slots/pole/phase (m), electrical frequency estimated (f_e), electrical frequency (ω_0), power factor (pf), and air-gap

flux density (B_g) are measured with the analytical design parameters estimation approach adopted in MATLAB only, while the rest of the parameters represents the physical parts and sections of the machine relatively.

The values of the estimated rated speed (N_e), number of slots/pole/phase (m), electrical frequency estimated (f_e), and number of armature turns/coil (N_a) resembled the values assumed in this research work. This shows that the modelling and simulation technique adopted in chapter 6 and the input design parameters from the prototype model of a machine are correctly established.

Generally, a well-suited design often considered to enter into energy market can have a small size and weight [40]. For this purpose, rotor radius (r), rotor stack length (L_{st}) and winding cross-sectional area (A_{ac}) should be kept small as possible. Since the values of these three parameters are well within range, therefore we use these values to estimate the output design parameters of the basic electrical model, machine size and weight and basic losses of the machine accordingly. Conversely, the value of slot bottom width (ws_{bottom}) must be higher than the slot top width (ws_{top}) to achieve the mean value of average slot width (ws) accordingly [39]. Whereas, the rest of the values presented in Table 14, are kept within the acceptable range, corresponding to the requirements as well as the practicality of the machine for high-speed operation during maximum load duration of time.

8.1.2 Results & Analyses for material analysis

For all the modelling and simulation results discussed subsequently in this chapter based on the output design parameters extracted from the MATLAB simulation tool will be used for analyses purpose. This approach certainly provides a significant advantage to judge the performance of a prototype model of a machine, however, that was not the case when it comes to results and analyses for material analysis. Likewise, common design parameters, the input design parameters for material analysis are used to estimate output design parameters for the basic electrical model and basic losses of a machine accordingly.

Three input values from the material analysis are presented in the prototype model of a machine such as the saturation flux density (B_{sat}), recoil permeability (u_{rec}), and electrical resistivity (ρ). It is clear from analytical modelling and simulation that B_{sat} can have a significant effect on determining the basic losses of a machine. The results obtained from hysteresis losses (P_h), eddy current losses (P_e), and iron losses (P_{iron}) heavily rely on B_{sat}.

In other words, the higher the value of B_{sat}, the more will be the losses of a machine and vice versa. The u_{rec} play a significant role for estimating air-gap magnetic flux density (B_{gm}) from the basic electrical model. In order to achieve sufficient B_{gm} the value of u_{rec} needs to be kept low to obtain the desired magnetic flux density (B_m). Finally, the ρ is used to evaluate the P_e of the basic losses of a machine. The value of ρ must be kept large enough to decrease P_e and make the design feasible for high-speed applications.

8.1.3 Results & Analyses for basic electrical model

The results obtained from modelling and simulation of analytical and material analysis offers a number of output design parameters much needed to design HSPMSG. However, we still must estimate the values of output design parameters for the basic electrical model of a machine in order to compute machine performance appropriately. Table 20 below presents the modelling and simulation results for the basic electrical model of a machine for all output design parameters.

Output Parameter	Machine Part or Section	Value
Permeance ($perm$)	Rotor and stator material	7.33×10^{-7}
Permeance coefficient (CP)	Rotor and stator material	14.5
Magnet physical angle (θ_m) in radians	Rotor magnetic poles	0.872
Carter coefficient (K_c)	Air-gap between rotor and stator	1.24
Effective air-gap (g_e) in m	Air-gap between rotor and stator	0.005
Air-gap magnetic flux density (B_{gm}) in T	Air-gap between rotor and stator	0.6
Magnetic flux density (B_m) in T	Air-gap between rotor and stator	0.644
Air-gap inductance (L_{ag}) in mH	Air-gap between rotor and stator	1.15
Magnetic flux linkage (λ_n) in T	Rotor + stator	0.476
Tooth width (w_t) in m	Stator slot geometry	0.0205
Total slot width (τ_s) in m	Stator slot geometry	0.0363
Magnet gap factor (K_g)	Air-gap between stator slots	1.12
Flux concentration factor ($C\phi$)	Stator windings	0.555
End-turn length of an armature conductor "one-end" (l_{eo}) in m	Stator windings	0.11
End-turn length of an armature conductor "half-coil" (l_{eh}) in m	Stator windings	0.347
Length of an armature conductor (l) in m	Stator windings	21.30

Pitch factor (K_p)	Stator windings	0.966
Breadth or distribution factor (K_d)	Stator windings	0.966
Winding factor (K_w)	Stator windings	0.933
Self-slot leakage inductance (L_{as}) in mH	Stator windings	0.0112
Mutual-slot leakage inductance (L_{am}) in μH	Stator windings	1.86
Slot leakage inductance (L_{slot}) in μH	Stator windings	9.33
End-turn inductance (L_e) in μH	Stator windings	0.37
Stator or armature resistance (R_a) in Ω	Phase	0.0036
Phase excitation or internal voltage (E_a) in V	Phase	1057.0
Stator current (I_a) in A	Phase	208.15
Total or synchronous inductance (L_s) in mH	Phase	0.124
Synchronous reactance (X_s) in Ω	Phase	0.4

Table 20. Output design parameters for basic electrical model

All the output design parameters are categorized into eight different machine parts or sections. Among all the parts and sections, the "stator windings" are relatively a major contributor to the basic electrical modelling of a machine. The parameters estimated for stator windings should not be taken too high, because the values estimated for phase must be kept within range in order to get the high performance and efficiency of a machine. For example, the values for flux concentration factor ($C\phi$), pitch factor (K_p), breadth factor (K_d), and winding factor (K_w) are kept below 1 essentially, whereas the rest of the parameter values are likely to be as much small as possible for a low loss design. Most of the highlighted parameters leaving a large impact on the performance of a machine are tabulated under phase. For a good design choice, the generator should have minimum values for armature resistance (R_a), synchronous inductance (L_s), and synchronous reactance (X_s) [57]. In contrast, higher values of phase excitation voltage, and stator current represents a stable design when designing PMSG [57]. Thus, the phase values presented in Table 20 lead to highly motivated values for a generator design to enter into the energy market intuitively.

The values obtained under the "air-gap between rotor and stator" section can play a significant role in the performance of a machine. Unlike stator windings parameters, most of the parameter values for "air-gap between rotor and stator" should be kept high for the optimal performance of the machine. For this purpose, the output design parameters such as the carter coefficient (K_c), effective air-gap (g_e), air-gap magnetic flux density (B_{gm}), and

magnetic flux density (B_m) need to be large, whereas the value of the air-gap inductance (L_{ag}) is kept minimum as shown in Table 15. For most of the generator design work, the values of rotor and stator material are assumed to be constant [35]. The parameters shown under the rotor and stator material section are rationally motivated and estimated from the equations presented in section 3.5.3 of this thesis. Determining the approximate values for stator slot geometry part or section is equally important for the best approximation of electrical modelling of a machine. For this purpose, two parameters such as the tooth width (w_t), and total slot width (τ_s) are estimated appropriately. Both values are within the limit range to optimally distribute the stator slots across the whole length of the stator simultaneously. Finally, three remaining parameters such as the magnet physical angle (θ_m), magnetic flux linkage (λ_n), and magnet gap factor (K_g) are analyzed to judge the suitability of parameters for this particular type of HSPMSG. For this purpose, the values of K_g should be kept in a limit range to evenly distribute the magnet field across the stator windings. Whereas the value of magnetic flux linkage should be kept maximum in order to get maximum performance during high-speed operation. In addition, the value of θ_m is obtained by simply converting angle from degree into radians for the accurate measurement of the B_m accordingly.

Overall, each and every value estimated for the basic electrical model of a machine are equally important and rationally motivated within the range for the optimal performance of the machine. However, as mentioned before, the parameters relevant to the phase part or section of a machine are more viable to judge the suitability of a machine to enter into the energy market successfully.

8.1.4 Results & Analyses for machine size and weight

As discussed in section 6.1 that there are a number of output design parameters that have contributed as an input in order to estimate the output design parameter of the next analysis. For example, the output design parameters for a basic electrical model serve as an input design parameter to estimate the output design parameters for the machine size and weight analysis. The same principle is applied to estimate the output design parameters for machine size and weight. Table 21 below presents the output design parameters used for machine size and weight analysis.

Output Parameter	Machine Part or Section	Value
Stator core back iron depth ($sbid$) in m	Rotor + stator geometry	0.045
Core outside radius (R_{co}) in m	Stator geometry	0.23
Core inside radius (R_{ci}) in m	Stator geometry	0.181
Overall diameter of a machine (D_{mach}) in m	Rotor + stator geometry	0.45
Back iron core mass (M_{cb}) in kg	Rotor + stator	280.0
Teeth core mass (M_{ct}) in kg	Stator slots	60.0
Total core mass (M_c) in kg	Rotor + stator	340.0
Armature conductor mass (M_{ac}) in kg	Stator windings	56.0
Magnet mass (M_m) in kg	Rotor magnetic poles	29.0
Shaft mass (M_s) in kg	Rotor shaft	250.0
Service mass (M_{ser}) in kg	Rotor + stator	101.23
Total mass (M_{tot}) in kg	Rotor + stator + rotor shaft	776.1
Surface current density (K_z) in A/cm^2	Air-gap between rotor and stator	109.21
Terminal voltage (V_a) in V	Phase	1054.0

Table 21. Output design parameters for machine size and weight

There are several ways to analyze the results obtained from machine size and weight modelling and simulation. Here, we will adopt the chronological order to better understand the process and values obtained from modelling and simulation. We see that the value of stator core back iron depth ($sbid$) satisfy the requirements of the machine on one hand. On the other hand, it can impact the value of core outside radius R_{co} accordingly. In other words, the higher the value of *sbid* higher will be the R_{co} and vice versa. The value of R_{co} is appropriate to the selected design as it is the sum of core inside radius (R_{ci}), and *sbid* respectively. Due to the satisfactory value obtained for R_{co}, the value of the overall diameter of a machine (D_{mach}) is also within a limit range in order to justify machine design more practical. Next, the value of total core mass (M_c) is measured with the help of back iron core mass (M_{cb}), and teeth core mass (M_{ct}) accordingly. Here, we see that the value of M_{cb} is relatively higher for this particular type of HSPMSG, but this value can be compensated with the lower value of M_{ct} accordingly. Therefore, the final value of M_c is within the limit range of the machine design. The value of service mass (M_{ser}) is estimated with the help of armature conductor mass (M_{ac}), total core mass (M_c), magnet mass (M_m), and shaft mass

(M_s). The value of M_{ser} is again appropriate to the design as 15% of service mass friction is added due to the assumption made earlier in the machine design analysis phase. Finally, the total mass (M_{tot}) of a machine is estimated to check the feasibility of a design that can be installed in the wind turbine accordingly. The value of M_{tot} provide a good estimation for the relative mass of the machine required by the handler to move the machine from one place to another. Since the size and weight analysis is modelled and simulated successfully, a good estimate of surface current density (K_z), and terminal voltage (V_a) is required to better judge the performance of a machine at high-speed. The value of K_z must be within a limit range in order to draw maximum energy from stator windings [68]. Therefore, we can say that the value of K_z is relatively motivational to accept the simulation results for the final design presented here. Last but not the least, the analysis of terminal voltage (V_a) gives us a better understanding of how well the design is modelled and analyzed to best fit into the energy market. In other words, the higher the value of V_a better will be the performance of the machine. Hence, we can say that the results obtained from machine size and weight analysis are optimal in terms of all parameters analyzed but presenting the best possible solution using analytical modelling and simulation can only be possible if the losses of the machine are also within the range in order to achieve the goal of producing an optimal power generation for the selected PMSG design. Thus, the basic losses of the machine are overviewed under the results and analyses for the basic losses of the machine accordingly.

8.1.5 Results & Analyses for basic losses of a machine

While this analytical method discussed in chapter 4 provides a good estimation suitable for wind turbine operations, a good estimate of the output design parameters for the basic losses of a machine is required to reach the desired performance of a machine in the form of main performance parameters of a machine discussed later. As mentioned earlier, the results obtained for each type of analysis are carefully chosen by selecting appropriate input and common design parameter values from the prototype model of a machine. Therefore, the same technique is applied here to get required values for the basic losses of a machine by adjusting assumed and collected values suitable for this particular type of HSPMSG accordingly. All the output design parameters for basic losses of a machine and their values estimated from modelling and simulation based on machine part or section are presented in Table 22 below.

Output Parameter	Machine Part or Section	Value
Mechanical frequency (ω_m) in rad/s	Rotor	1.6×10^3
Reynold's number (Rey)	Rotor	5.33×10^4
Coefficient of friction (C_f)	Rotor	0.0082
Thickness of material (t) in mm	Rotor + stator material	45
Back iron flux density (B_b) in T	PM material	0.215
Tooth flux density (B_t) in T	Stator slots	2.41
Skin depth (δ)	Rotor + stator material	0.22
Conductor or copper losses (P_a) in W	Stator windings	466.44
Stray losses (P_{stray}) in W	Stator slots	56.0
Hysteresis losses (P_h) in W	Rotor + stator material	174.0
Eddy current losses (P_e) in MW	Rotor	764.0
Iron losses (P_{iron}) in MW	Rotor + stator material	1.5
Core back iron losses (P_{cb}) in W	Stator	123.10
Tooth losses (P_{ct}) in kW	Stator slots	4.5
Total core losses (P_c) in kW	Rotor + stator	4.6
Windage losses (P_{wind}) in kW	Rotor	20.18

Table 22. Output design parameters for basic losses of a machine

The analyses based on the results presented in Table 22 above can be roughly divided into two groups. For example, the parameters used to estimate the basic losses of a machine are grouped together to analyze first, and then the values of machine losses themselves are analyzed in order to understand the suitability of this particular type of HSPMSG to enter into the energy market accordingly.

The value of the mechanical frequency (w_m) of a machine estimated here depends upon the f_e of the machine. As discussed in section 4.1.1, that the value of f_e is validated correctly. Therefore, we can say that the value of w_m is also estimated correctly in order to estimate Reynold's number (Rey), and windage losses (P_{wind}) simultaneously. The value of Rey, and coefficient of friction (C_f) depends upon each other. For a good design estimation, the value of C_f must be kept lower in order to minimize P_{wind} as much as possible [54]. Thus, we can say that the value of Rey is appropriate within the design criteria. Likewise, the thickness of material (t) must also be kept lower as much as possible to minimize the eddy current losses

(P_e) of a machine [55]. The value of "t" obtained from this analytical modelling and simulation is appropriate and support the theory of the machine design analysis presented in this research work. Similarly, the values of back iron flux density (B_b), and tooth flux density (B_t) can also be kept smaller in order to estimate core back iron losses (P_{cb}), and teeth losses (P_{ct}) within the limit range. Therefore, the values presented in Table 16 for B_b, and B_t are appropriate and fulfil the required design criteria accordingly. As mentioned earlier the lower the basic losses of a machine, the higher will be the machine performance and vice versa. With this principle, the value of skin depth (δ) must also be kept smaller in order to satisfy the basic requirements of the machine as shown in Table 22 above.

The values of the basic losses of a machine are estimated in such a way that the efficiency of the machine must be kept higher to produce a maximum amount of energy from the wind turbine. For this purpose, the conductor losses (P_a), total core losses (P_c), and windage losses (P_{wind}) are the main losses, which contribute the most to the performance analysis of a machine.

From Table 22 we can observe that the value of P_a is much smaller than P_c, and P_{wind}. It is because the P_a can only be calculated from stator windings. Also, the P_{wind} are estimated from the rotor of the machine. It is to be assumed that the losses estimated from the rotor part of a machine are relatively higher than the other part of the machine [54]. Therefore, the estimated value of P_{wind} is higher than the P_a. But the value of P_c is well under the limit range of this particular type of HSPMSG. It means that the values assumed and collected in the prototype model are appropriate and motivated to accept the design consideration used in this research work. In addition, the values of stray losses (P_{stray}), hysteresis losses (P_h), and P_{cb} are well within the range to justify the design consideration suitable for this particular type of HSPMSG. However, the value of P_{ct} is higher than P_{cb}. But as we discussed earlier that the value of P_c is well under the limit range of the design. Therefore, we can say that the value of P_{cb} is also acceptable to analyze the main performance parameters of a machine accordingly. Finally, we will analyze the suitability of eddy current losses (P_e), and iron losses (P_{iron}) to better match the basic requirement criteria of a machine. Here, we see that the value obtained for P_e is much higher than the other losses of a machine. Normally, while designing a high-speed generator the value of P_e is almost always very much high during the analytical design estimation of an electric machine [55]. The effect of P_e on the performance of a machine is typically negligible because, it is not used for the final performance estimation of a machine. Similarly, the P_{iron} is also neglected for the efficiency estimation of this particular type of HSPMSG, unless it is required to estimate the essential parameters in some other type of applications such as solar,

and auxiliary power supply systems [69]. Hence, we can say that the values obtained for the basic losses of a machine are well suited to ensure the realistic design required to perform the performance analysis of a machine eventually.

8.1.6 Main performance parameters of a machine

The main reason behind the output design parameter extraction is to validate the machine design consideration performed in the machine design analysis and prototype modelling phase of the thesis. However, the results presented in section 8.1 above are applicable only if the output of the main design parameters are well within range and matched under full capacity conditions. Table 23 below shows input and output design parameters helpful to better understand the suitability of this machine design to enter into the energy market.

Type of Parameter	Parameter	Machine Part or Section	Value
Input	Slot height (h_s) in cm	Stator slot geometry	2.5
Output	Stator current density "estimated" (J_o) in A/cm^2	Stator	874.0
	Power input (P_{in}) in kW	Phase	685.26
	Efficiency (β)	Phase	0.963

Table 23. Main performance parameters of a machine

The performance of a machine is examined using output design parameters extracted from the analytical design parameters estimation in MATLAB. There are four parameters presented in Table 17 above of which three of them are output parameters and one of them presents the input design parameter. The input design parameter is merely the slot height (h_s) in centimetres. This parameter is converted first (m→cm) in order to estimate stator current density (J_o) for comparison purposes. Therefore, it is presented here as an input design parameter. The output design parameters are analyzed one by one to determine the generator performance accordingly. For J_o, the suitable range estimated for this particular type of HSPMSG is between 800 to 1200 A/cm^2 as discussed in section 4.1.3.3 earlier. Therefore, the value obtained from this modelling and simulation approach is well suited within the limit range defined in this research work. The power input (P_{in}) is the combination of power output (P_{out}) and the basic losses of a machine. The value of P_{in} is considered feasible only if it is close to the value of P_{out} in order to extract maximum efficiency from a machine [39]. Again, we can say that the value of P_{in} is acceptable

to analyze the maximum performance of a machine in terms of efficiency. Finally, the maximum performance efficiency (β) of a machine is analyzed here to complete the results and analyses section from analytical modelling and simulation. A machine is said to be a high-performance unit if its efficiency is close to 100%. It is clear from Table 17 that the efficiency obtained is 96.3% after thorough estimation of all design parameters assumed and collected during the entire analytical design process. This efficiency value gives good confidence in terms of design robustness and agility simultaneously.

In the end, we can say that all parameters established during the entire analytical design process of HSPMSG are of practical interest and can be implemented in the wind turbine industry as a future essential unit of the wind turbine system. Since all the output design parameters suggest that the analytical design is well within the performance range, but these results do not guarantee the wind turbine operation within a good control operating condition. For this purpose, the output design parameters from finite element modelling & simulation are presented and analyzed in the next section of this chapter accordingly.

8.2 Results & Analyses from FE modelling & simulation

Detailed formulation of analytical design parameters for the analytical method has been developed in the previous section. In this section, the results and analyses of magnetostatic FEA and electrical quantities of HSPMSG under no-load and on-load conditions are presented. In the finite element prototype model, the machine geometry is constructed with the help of input design parameters. In order to validate the prototype model, the simulation results are analyzed and compared with results obtained from analytical modelling and simulation.

8.2.1 Results & Analyses for No-load conditions

After finalizing input design parameters and variables, no-load simulation is performed in MotorXP-PM which is based on analytical calculations calibrated in FEA of the simulating software tool. A number of resulting graphs such as the terminal voltage, flux linkage, cogging torque, magnetic flux density, and total core losses are presented and analyzed below in Figures 21 – 26.

Before discussing these figures, we introduce a number of electrical quantities that are used to validate the prototype model of a machine. These quantities are referred to as the voltage output (V_{out}), and electrical frequency (f_e) that is used to validate the basic requirement of a machine

exclusively. Figure 21 below shows some of the quantities used to validate the prototype model of a machine.

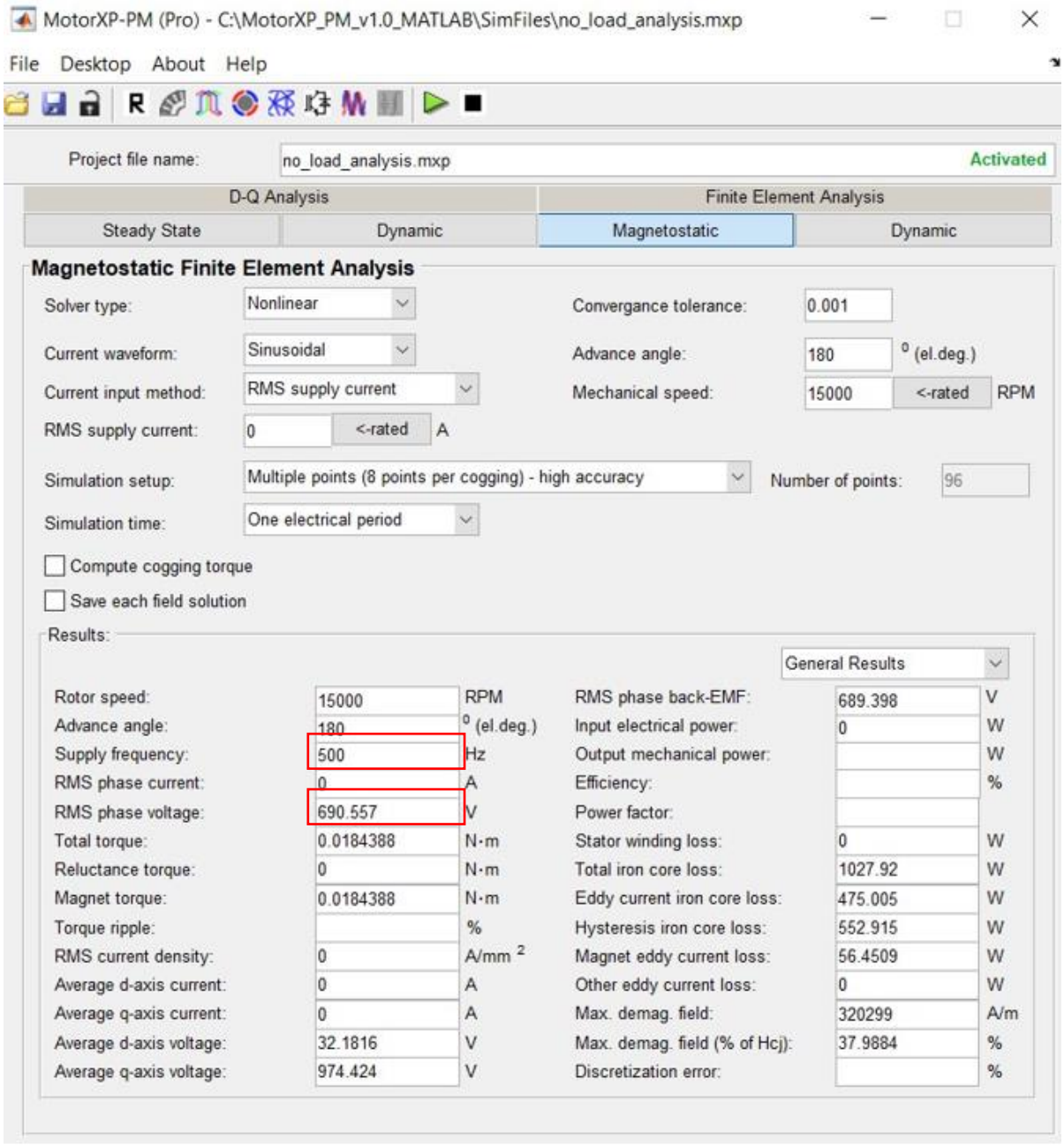

Figure 21. Electrical quantities obtained from no-load magnetostatic FEA

Figure 21 shows the impact of input design parameters from electromagnetic and FEA on machine design. The f_e and V_{out} depicts the input design parameters values relative to the required output design values. The value of f_e taken from the analysis validates the accuracy of the FE prototype model of a machine. Whereas the value of V_{out} gives us the basic machine requirements for a wind turbine system. These results are more representative of the no-load conditions that the prototype model would be employed in. Thus, more quantities can be plotted

that represents the output design parameters for this particular type of HSPMSG. Figure 22 below shows the line-to-line terminal voltage graph plotted in MotorXP-PM.

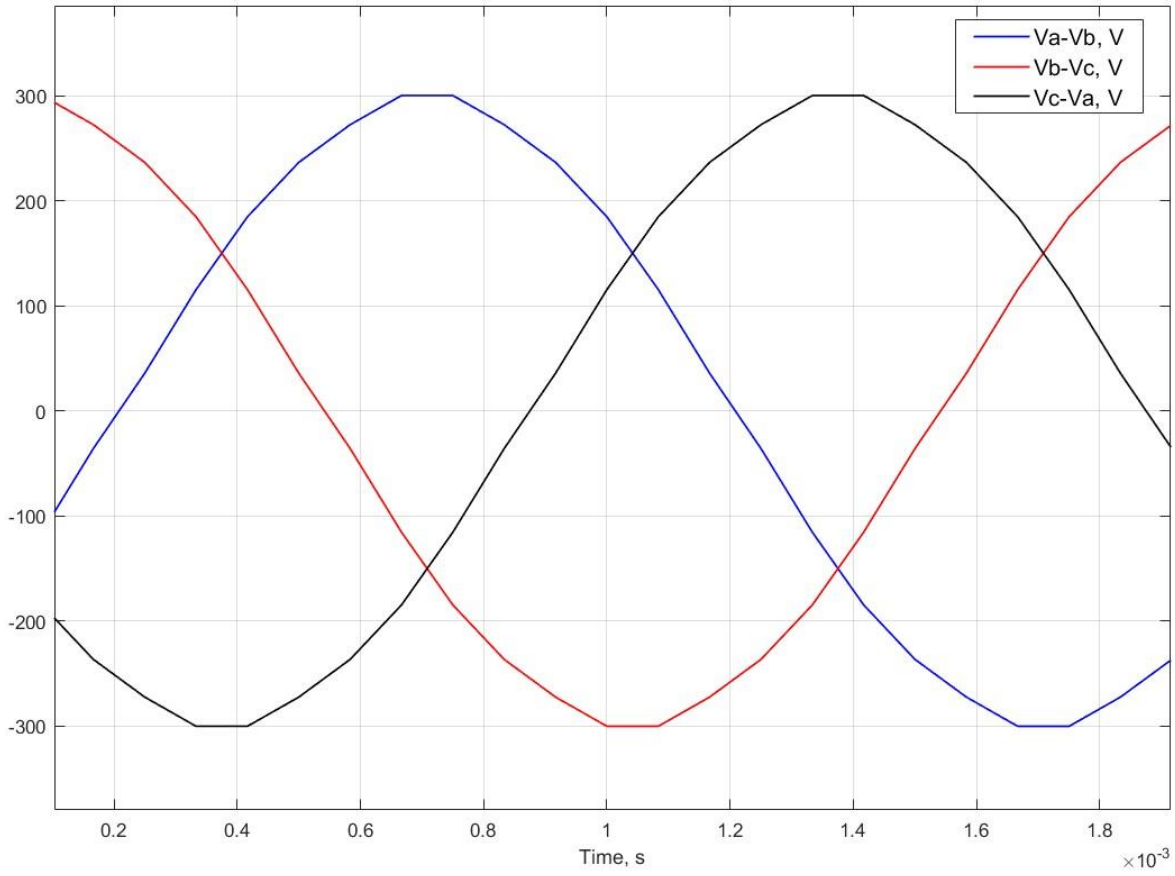

Figure 22. Terminal voltage (V_a) in V

Figure 22 above shows V_a waveform close to sinusoidal, extracted by subtracting line-to-line V_{out}. If we compare figure 21 with 22, then we can observe some difference in values of V_{out} and V_a. Because of some torque ripples, harmonic contents of the line-to-line voltage, and skew factor in the air-gap flux density, it shows some deviation from the required output needed to perform at higher efficiency [69]. These factors can be eliminated by reducing torque ripples to enhance the machine life and to get good behavior towards noise cancellation and reduced vibration. However, it shows good agreement between analytical and FEA results. Therefore, this waveform is accepted and matched closely with the flux linkage (ϕ_{link}) waveform.

By solving the electromagnetic model, the flux linkage in the rotor and stator of the machine can be analyzed. Figure 23 below shows the results obtained from the flux linkage plot after performing high accuracy simulation setup for 96 points in MotorXP.

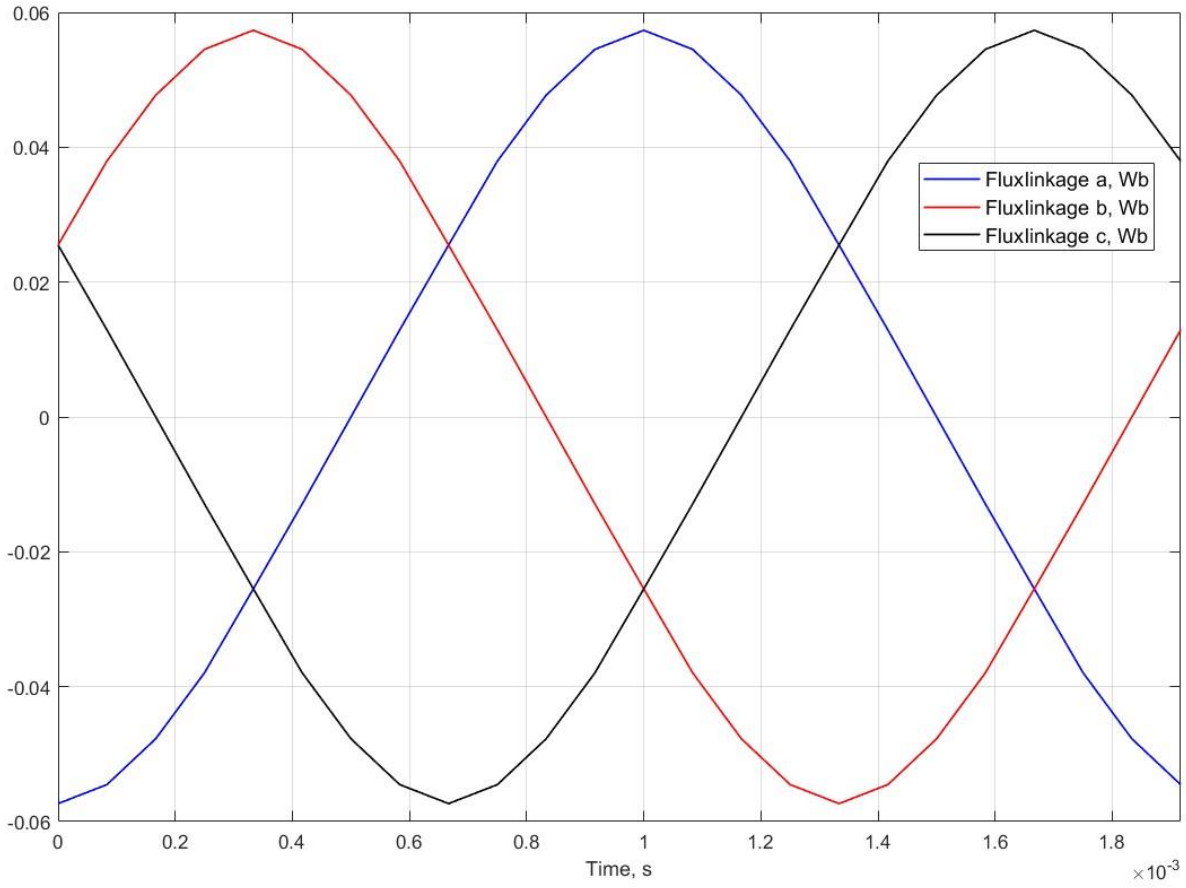

Figure 23. Flux linkage (ϕ_{link}) in Wb

It is validated from figure 23 above that the tooth and stator slot dimensions are good to get the design objectives. As it can be seen that all the flux from the rotor can easily be linked into the stator tooth, indicates that the flux linkage waveform is sinusoidal, symmetrical as well as good to calibrate into the design process successfully.

Another parameter that is due to the alignment of magnetic poles and the edges of the stator tooth is the cogging torque (T_{cog}). Figure 24 below shows the MotorXP output results for T_{cog} after processing the FE and electromagnetic prototype model of a machine.

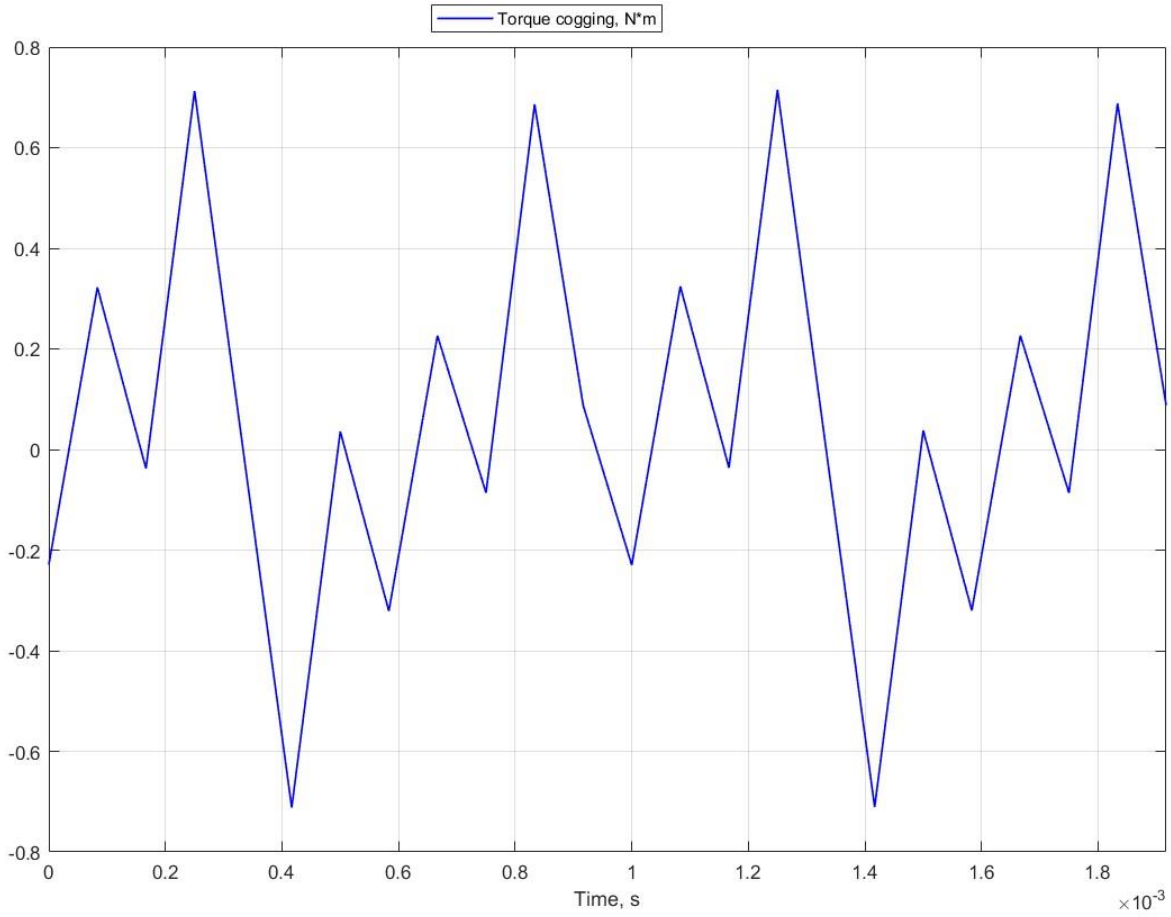

Figure 24. Cogging torque (T_{cog}) in Nm

It is found from figure 24 that the maximum value of T_{cog} is less than 1 Nm. This shows that the magnetic poles are properly aligned with the edges of the stator tooth, and if the rotor changes its position, the value of T_{cog} can also change simultaneously. In contrast, we observe some undesirable spikes in the plot. These un-wanted fluctuations in the waveform can be reduced by selecting an appropriate skewing angle. The cogging torque curve can be smoothened by choosing the value of skew angle one-half of the slot pitch [69].

Another important result drawn from the no-load electromagnetic analysis is the distribution of magnetic flux passing through the core of a machine. Figure 25 below shows the magnitude and direction of magnetic flux density (B_m) passing through a certain area.

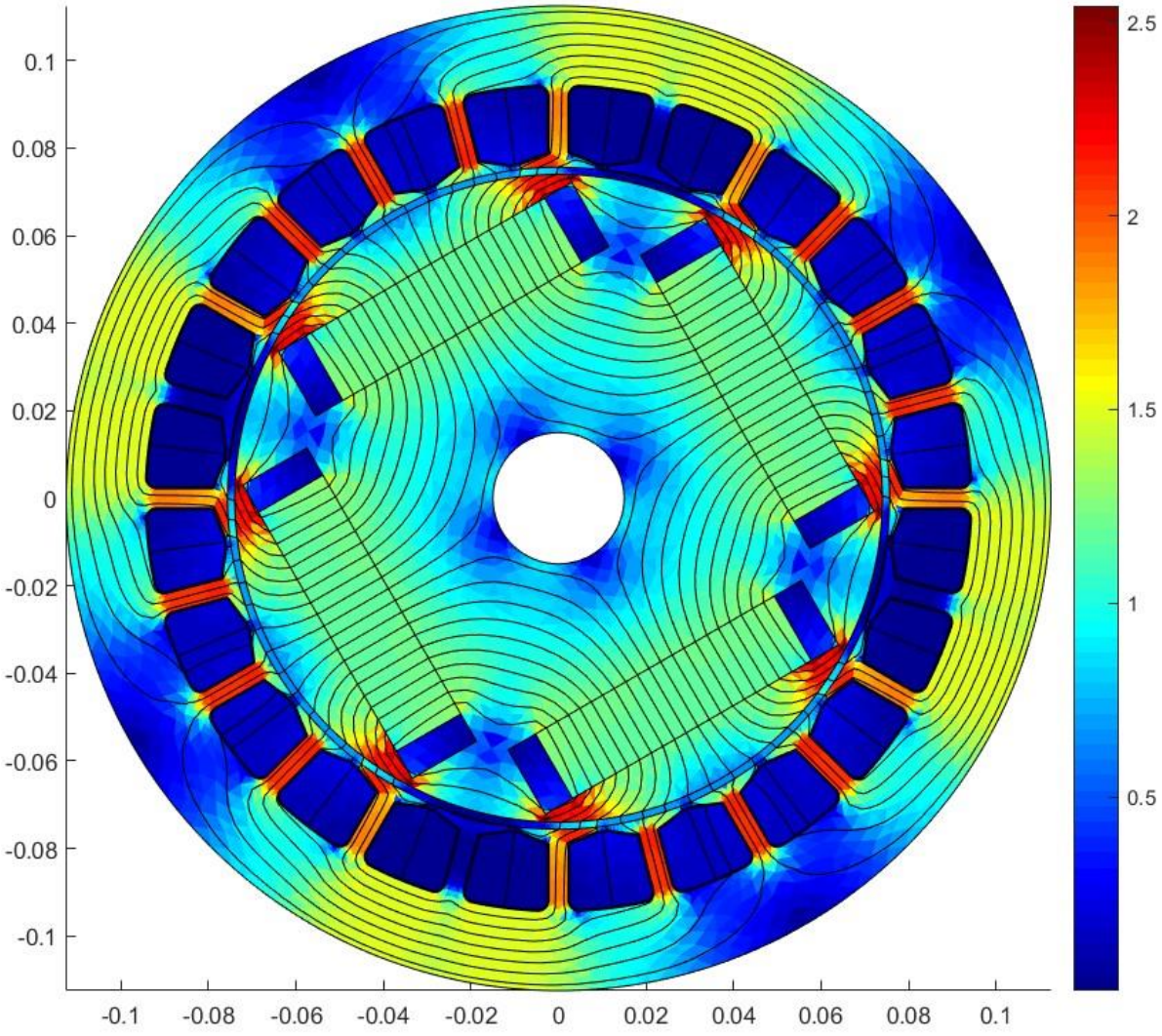

Figure 25. Magnetic flux density (B_m) in T

We can observe two important results from figure 25 above. First, the magnetic flux lines are leaving the rotor poles nearly perpendicularly which means that rotor and stator dimensions are properly aligned to neglect the axial field components. In the two-dimensional e-magnetic field, the electromagnetic force for the rotation of rotor is generated by the tangential component of force [17]. Second, the magnitude of the magnetic flux density does not reach its saturation level in most parts of the machine. In other words, the value of B_m is below 1.8 T except for the "general" part of the machine at the maximum rated speed which can be overcome by employing the cooling method properly.

Finally, the no-load e-magnetic analysis can be validated by observing total core losses (P_c) in the rotor and stator parts accordingly. Figure 26 below shows losses in the rotor and stator material and how well they are suited to this particular type of HSPMSG.

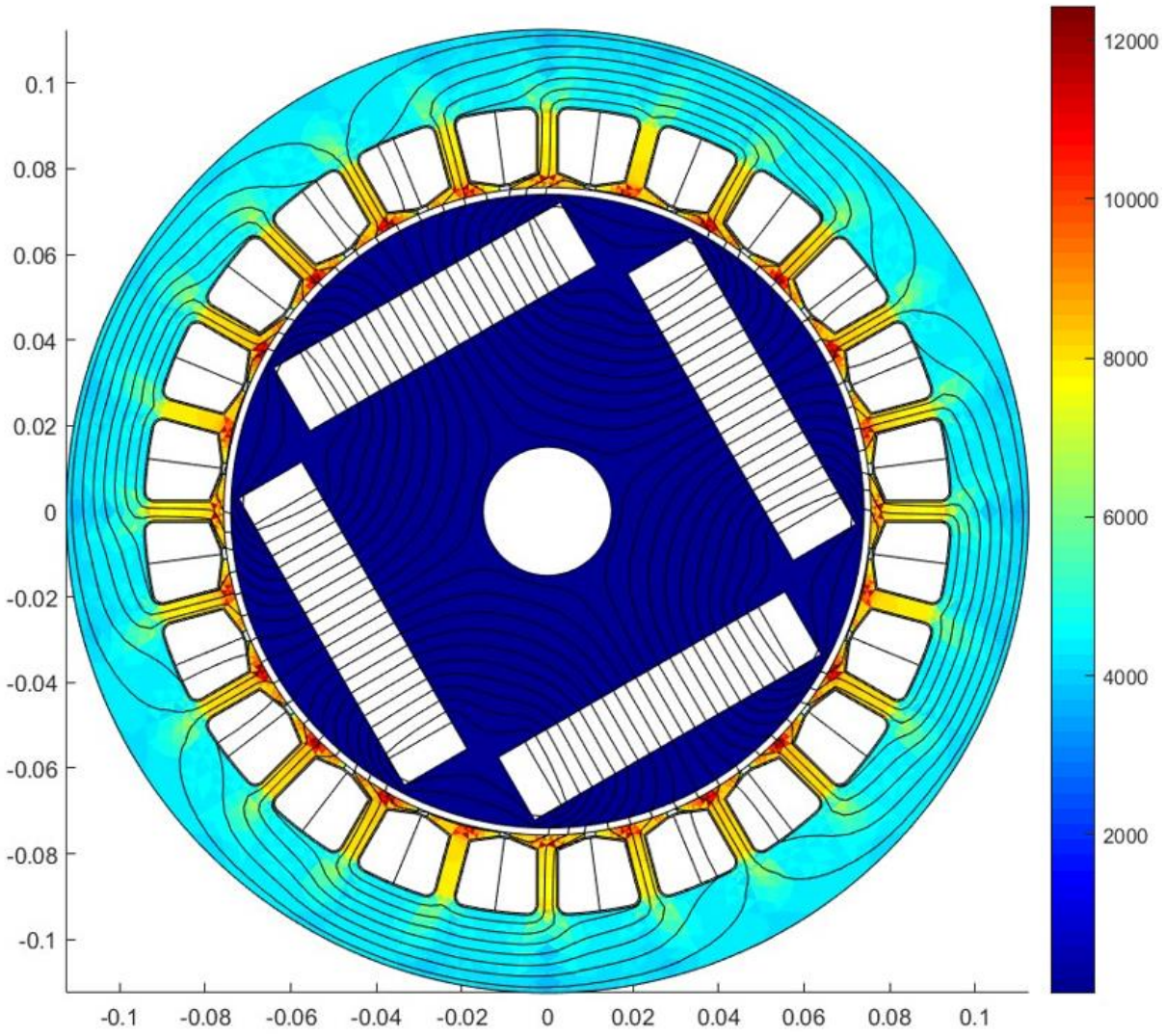

Figure 26. Core losses (P_c) in W

The core losses (P_c) results obtained from figure 26 above can validate that the losses are well within the range which is 4.6 kW. Higher losses can be observed in the stator yoke due to some harmonic current going through the armature windings. Another factor that can cause these higher losses may be the skin effect resulting from the same source conductor. It is suggested that the core losses can be reduced by replacing core material with an amorphous alloy [60]. Overall, the result is good and replicate the rigorous methodology adopted to design HSPMSG accordingly.

8.2.2 Results & Analyses for On-load conditions

No-load e-magnetic analysis suggests that the optimal design solution is significantly appropriate to analyze on-load conditions. Since there is no change in the physical geometry of the machine, the stator current (I_a) is supplied to the armature windings. A number of resulting

graphs such as the back-emf (V_{back}), stator phase current (I_a), and tooth losses (P_{ct}) are presented and analyzed below in figures 28 – 30. Before discussing these figures, we introduce a number of output electrical quantities derived when a 3-phase balanced current is injected in armature windings to get output design parameters and validate analytical results as well as the basic requirements of the machine are presented in figure 27 below.

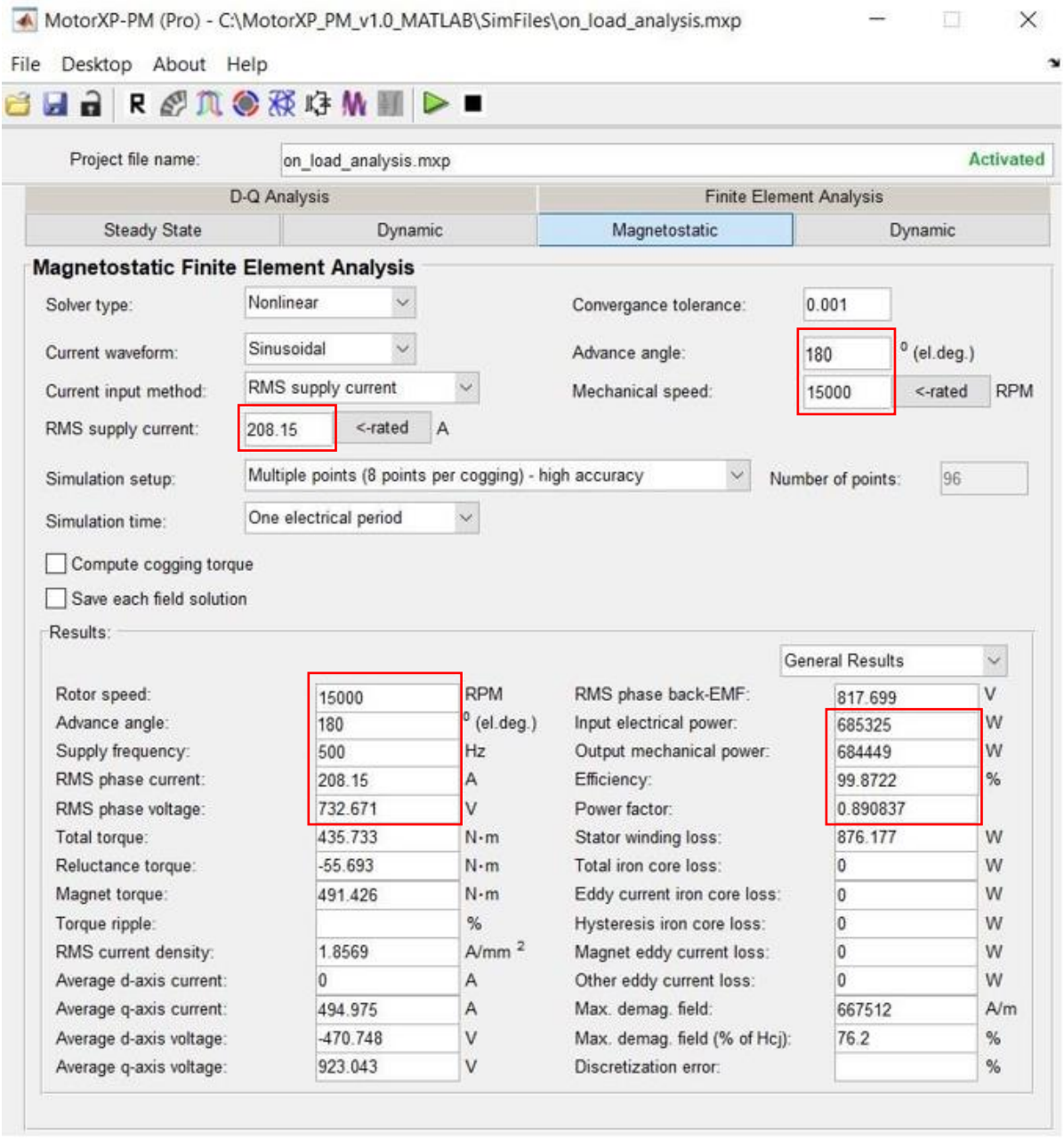

Figure 27. Electrical quantities obtained from on-load magnetostatic FEA

Figure 27 shows the variation in V_{out} as the I_a increase. But this variation can be overcome with the help of pulse width modulation (PWM) [59]. The values of estimated P_{out}, and P_{in} suggest that the maximum efficiency can be yielded to get the high-performance benefit. Any value of

power factor (*pf*) between 0.8 and 1 is acceptable while designing a PM generator [39]. Therefore, the value of *pf* suggests that the geometrical construction in MotorXP and analytical calculation in MATLAB are within the calculated range and boundary limits.

A good estimate of back-emf is required because it is an important indicator of the ability of the generator to produce torque and speed [17]. In this experiment, the back-emf is analyzed by subtracting the line-to-line back-emf value from another phase value. Figure 28 below shows the back-emf (V_{back}) waveform for on-load finite element electromagnetic analysis.

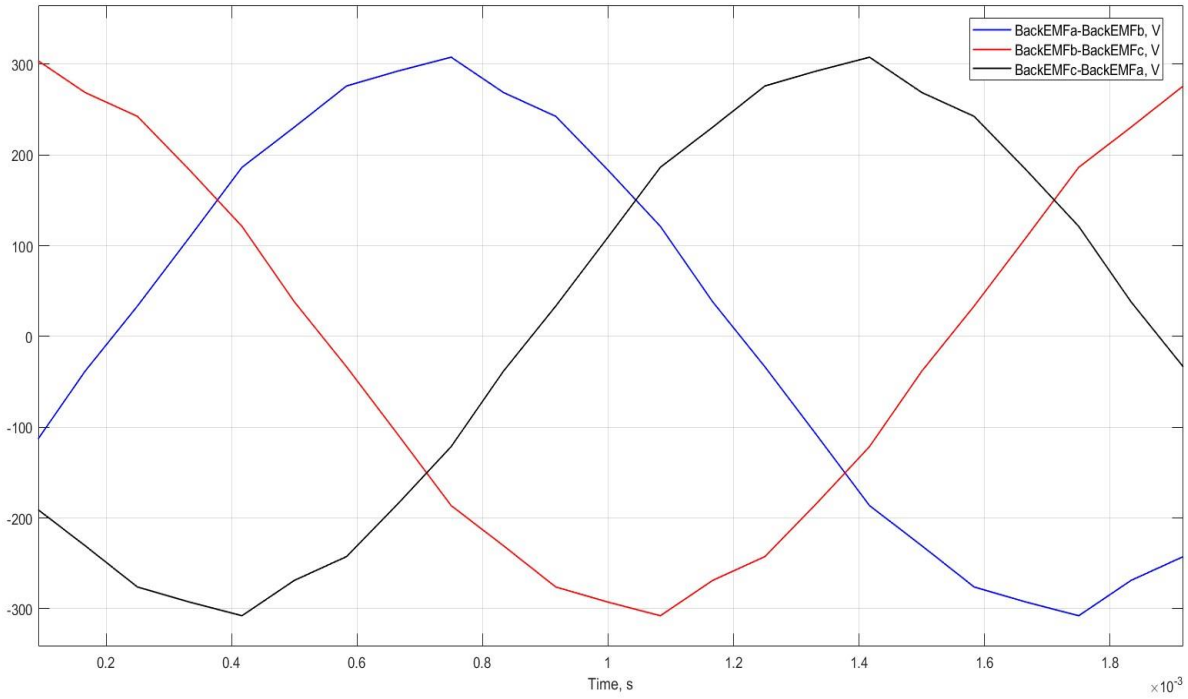

Figure 28. Back-emf (V_{back}) in V

The output back-emf waveform exhibit nearly sinusoidal with some fluctuation observed in figure 28 above. Whereas the values of V_{back} and V_{out} is almost the same which suggest that the induced voltage of the stator windings is in the steady-state conditions when the generator is running at full-load capacity. In addition, the plotted graph can be smoothened by amorphous alloy instead of SiFe material [60].

Another significant quantity that leads to the validation of the prototype model w.r.t the input and output design parameters is the measurement of stator phase current across the entire generator operation under full-load conditions. Figure 29 below shows the MotorXP output waveform for stator phase current.

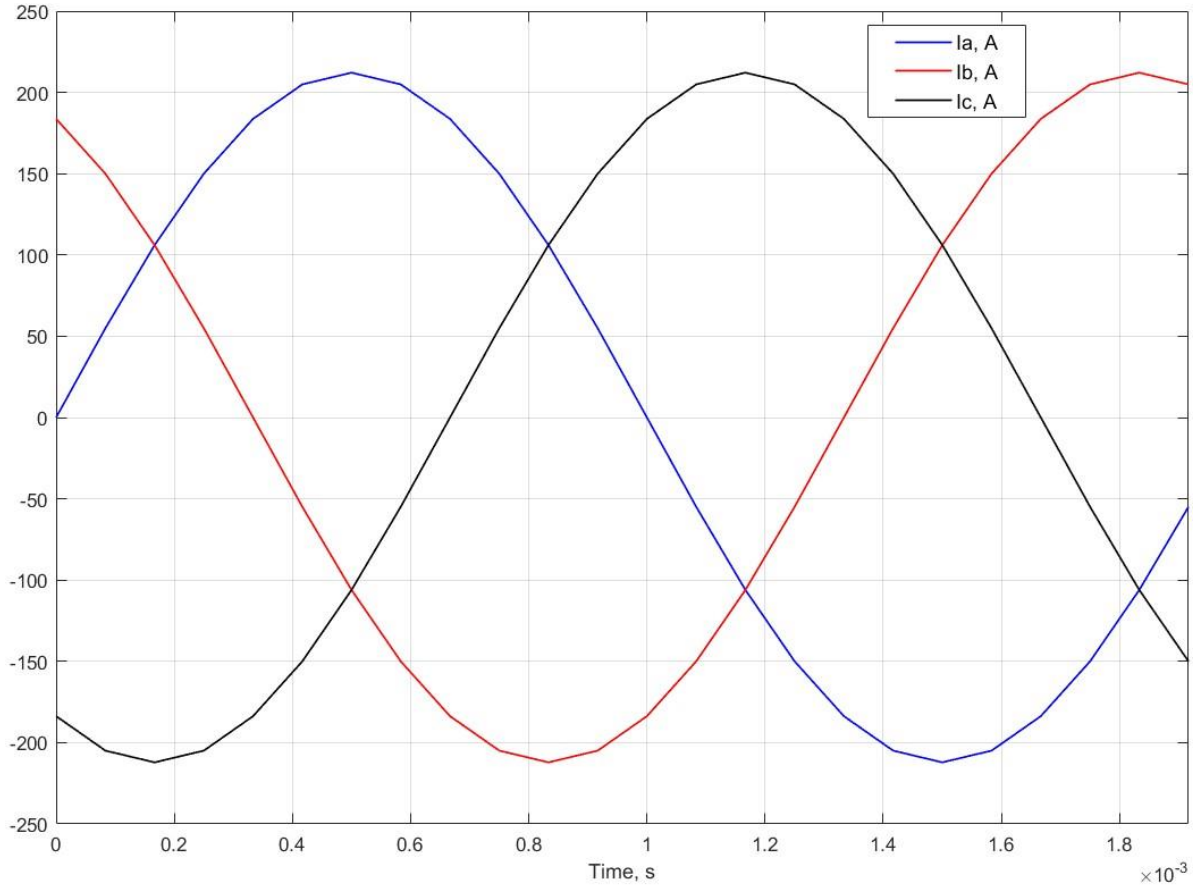

Figure 29. Stator phase current (I_a) in A

The waveform of the I_a is obtained directly by selecting stator phase current for each phase in the plot wizard of the MotorXP software tool. The waveform presented in figure 29 above exhibits almost sinusoidal across the entire full-load operation. The sinusoidal phase current behavior is important to enhance machine life and noise cancellation to reduce vibration [19]. In addition, the value of I_a is almost the same as determined in the analytical results from MATLAB. It indicates a good match between the analytical and MotorXP field calculation simultaneously.

In an on-load flux distribution, the machine losses are comparatively higher than in no-load conditions. Hence, the value of magnetic flux density is close to saturation level such as 1.8 T. In order to analyze rotor and stator dimensions, stator tooth losses (P_{ct}) are plotted for a good correlation between FE and e-magnetic analysis. Figure 30 below shows the stator tooth losses when the machine is supplied by maximum phase current.

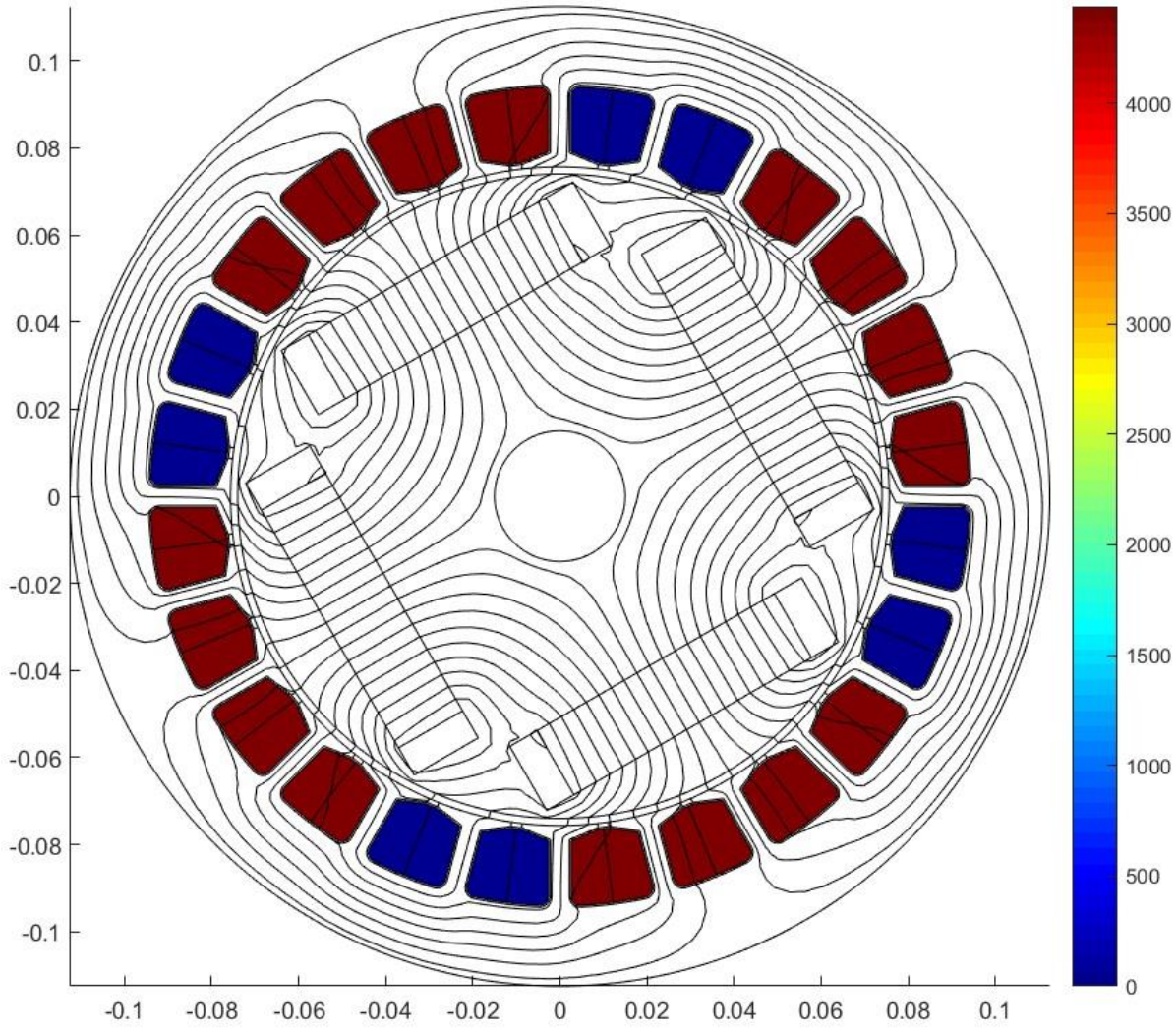

Figure 30. Tooth losses (P_{ct}) in W

From figure 30 above, we can observe that the losses are at their minimum level when close to "general" and maximum when close to PM material. It is obvious because air or insulation is a non-magnetic part of a machine whereas the PM material conduct field and electricity. Another important result obtained from figure 30 is that the average value of P_{ct} is 4.5 kW approximately. It means that the field calculations of MotorXP matched with the analytical results to obtain design objectives accordingly.

8.2.3 Results & Analyses for harmonic analysis

Machine harmonics are the main cause of all types of losses including eddy-current losses [73]. In order to investigate harmonic components of the machine, air-gap magnetic flux (ϕ_{gm}) is chosen on one hand. On the other hand, the harmonic spectrum of torque (T), and cogging torque (T_{cog}) are presented. The ϕ_{gm} is analyzed with each rotor angular position

and harmonic numbers. Whereas T, and T_{cog} are analyzed at different frequency levels. Figure 31 below shows two parallel graphs of the air-gap magnetic flux under no-load conditions.

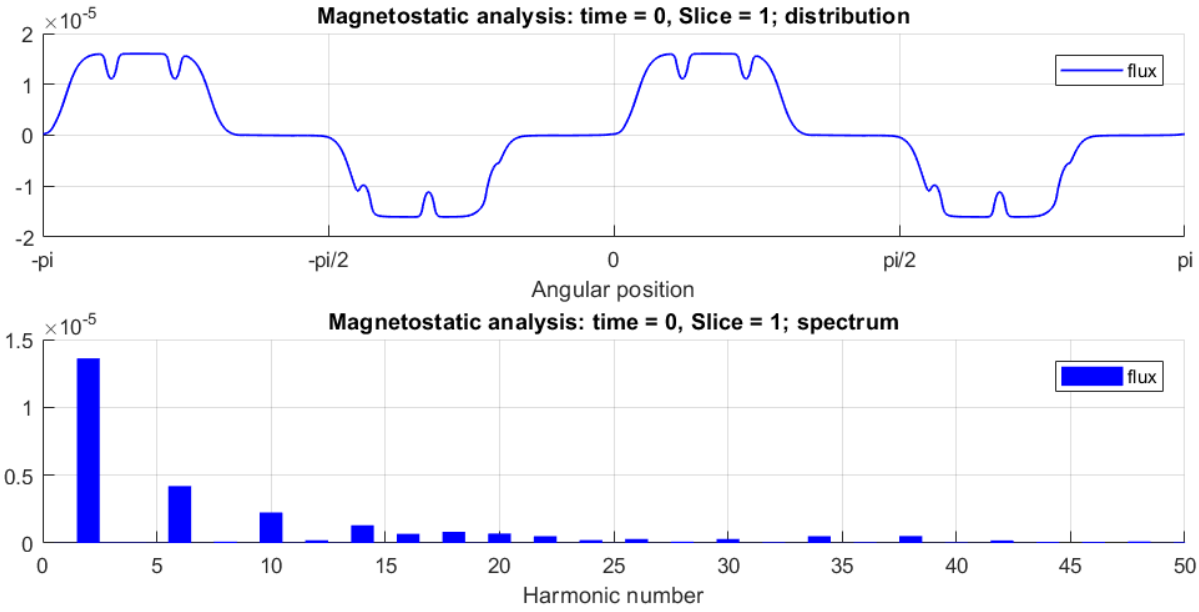

Figure 31. Air-gap magnetic flux distribution (upper), Air-gap magnetic flux spectrum (lower) in Wb

The upper ϕ_{gm} plot is distributed evenly across the wide range of rotor angular positions. There are some unwanted degradations in the output result, but they can be eliminated by using power electronics combinations such as the PWM accordingly [59]. It can be observed from the lower ϕ_{gm} plot that even harmonic numbers have the highest values, which implies that the first flux spectrum appears at the 2nd harmonic, the second spectrum appears at the 6th harmonic and so on. This result validates that the 24/4 machine is correctly constructed with low spectrum values appearing after every five harmonic numbers and slowly disappearing after the 10th harmonic number. In other words, as the speed of the machine increase, the harmonics will disappear to get maximum benefits from an electrical point of view because differential inductance leakage decreases when sub-harmonic disappears [74]. The harmonic spectrum of torque and cogging torque is also analyzed in detail in figure 32 below.

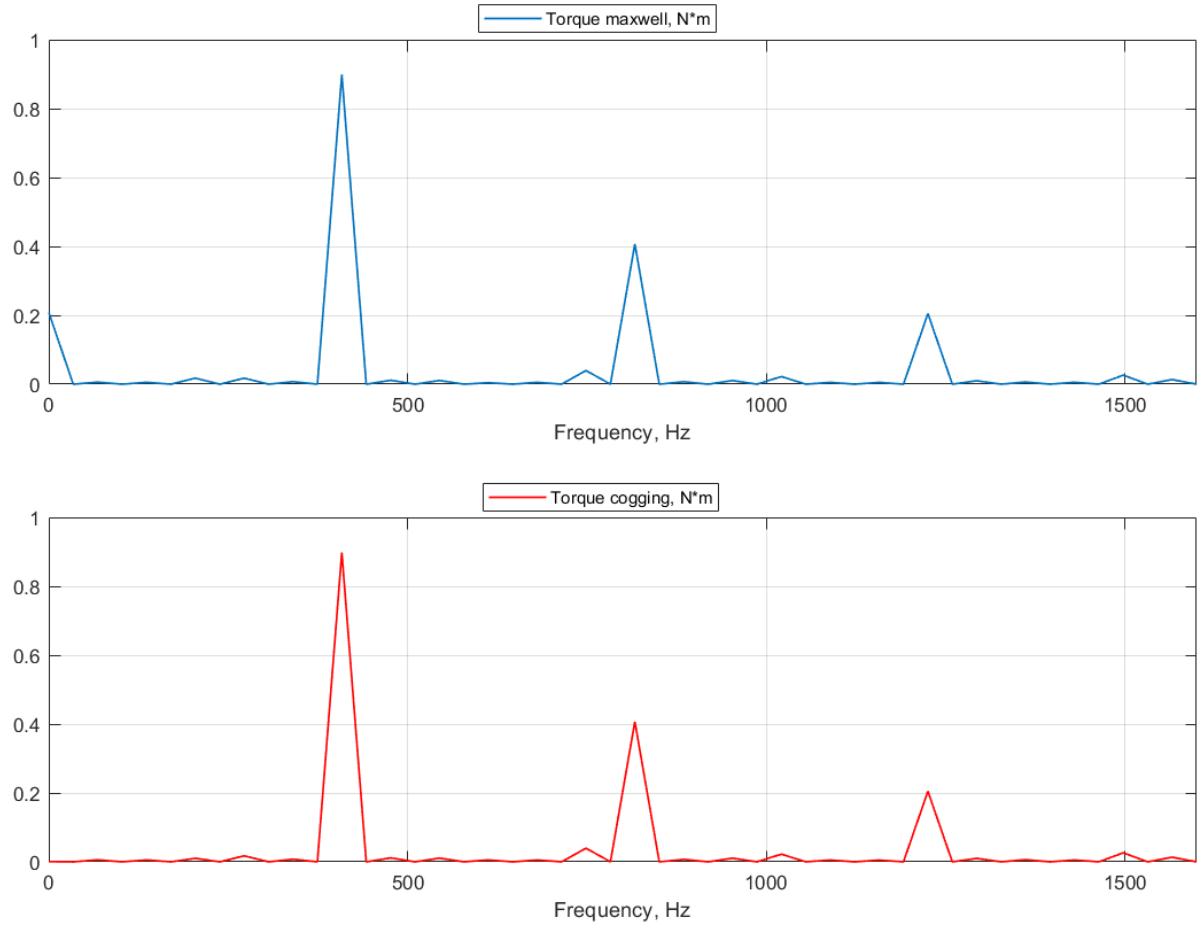

Figure 32. Harmonic spectrum of torque T (upper), Harmonic spectrum of cogging torque T_{cog} (lower) in Nm

It is important for a high-performance machine that the value of cogging torque does not exceed the rated torque value. A good design parameter consideration and proper selection of PM material along with the combination of rotor and stator alignment technique make sure that the value of cogging torque exactly follows the rated torque initially and disappears if the speed or frequency increases [64]. Figure 30 above suggest that the cogging torque attains exactly the same pattern w.r.t the rated torque and disappear as the frequency increase. This means that the parameters assumed and collected from the analytical method meets the design specification of the machine.

8.2.4 Performance analysis of a machine

PM synchronous machines are used to generate energy at a constant speed and hence can be easily controlled by adjusting the speed control mechanism. The best way to gain an understanding of the performance characteristics of an HSPMSG is to study the speed and torque relationship [17]. The performance plot for speed, torque, and power is obtained by selecting steady state D-Q analysis in MotorXP-PM. The steady state D-Q model is built using input design parameters to ensure that the generator has enough torque, and power at all speeds

without exceeding any thermal or electrical limits. Next, the iron loss (P_{iron}), and efficiency (β) maps are plotted against speed that can be used in the iterative design process. The following detail summarizes the input and output design parameters for the performance analysis of a machine under on-load conditions.

8.2.4.1 Input design parameters for the performance analysis of a machine

In MotorXP-PM, it is possible to calculate output performance parameters in order to satisfy the most basic functional requirements of the machine against speed. More detail on each input design parameter in steady-state D-Q analysis is shown in the Table 24 below.

Input Parameter	Value/Detail	Output Parameter/s
For Speed, Torque, and Power		
Convergence tolerance of FEA solution	0.001	-
Max. RMS supply current (I_a) in A	208.15	T, N, P_{out}, P_{in}
Current step	0.02	-
Advance angle step	5	-
Number of rotor positions	10	-
Include iron losses	Check	P_{iron}
X-axis quantity	Speed	-
Rotor speed values in rpm	0:50:15000	-
Max. phase voltage selection method	Vdc and PWM	-
Field-weakening control	Const-advance-angle	-
Model Type	D-Q with sinusoidal supply	-
D-Q parameters interpolation	Nonlinear	-
DC supply voltage (V_a) in V	690.0	T, N, P_{out}, P_{in}
Drive type	Current hysteresis PWM	-
For Iron losses and Efficiency		
Control method	Max. Efficiency	P_{iron}, β
Advance angle values in deg. (elect.)	0:90:180	P_{iron}, β
Max. RMS phase voltage (V_a) in V	690.0	P_{iron}, β
Max. RMS phase current (I_a) in A	208.15	P_{iron}, β
Maximum speed (N) in rpm	15000	P_{iron}, β

Torque step in Nm	20	P_{iron}, β
Speed step in rpm	50	P_{iron}, β
Model type	D-Q with sinusoidal supply	P_{iron}, β
D-Q parameters interpolation	Nonlinear	P_{iron}, β

Table 24. Input design parameters for performance analysis of a machine

In short circuit (on-load) conditions, efficient field calculations are performed to validate the FE prototype model for the optimal design solution. In contrast, 2-D time-stepping steady-state D-Q calculations are needed with a large number of operating points for the entire envelope. For this purpose, current step and advance angle positions are kept minimum, whereas the number of rotor positions are kept high accordingly. The rotor speed values are in between (0→15000) rpm with a speed step of 50 for detail plotting. The value of advance angle covers 180° with advance angle step of 90° to cover sinusoidal waveform entirely for a good simulation result. The values of torque and speed steps are kept average to complete simulation iteration in a measured time duration accordingly. Whereas the remaining input parameters are kept the same as of electromagnetic FE no-load analysis. The results of torque, power, speed, iron losses and performance efficiency based on these input parameters can be seen clearly in the output design parameters for the performance analysis of a machine.

8.2.4.2 Output design parameters for the performance analysis of a machine

Once the input parameters are correctly established, the output design parameters can be easily plotted to analyze the performance analysis of a machine. In this section, three main electrical quantities are plotted to establish the integrity of the machine design methodology adopted to design HSPMSG. Figure 33 below represent the first curve of speed versus torque (in blue), and speed versus P_{in} (in red).

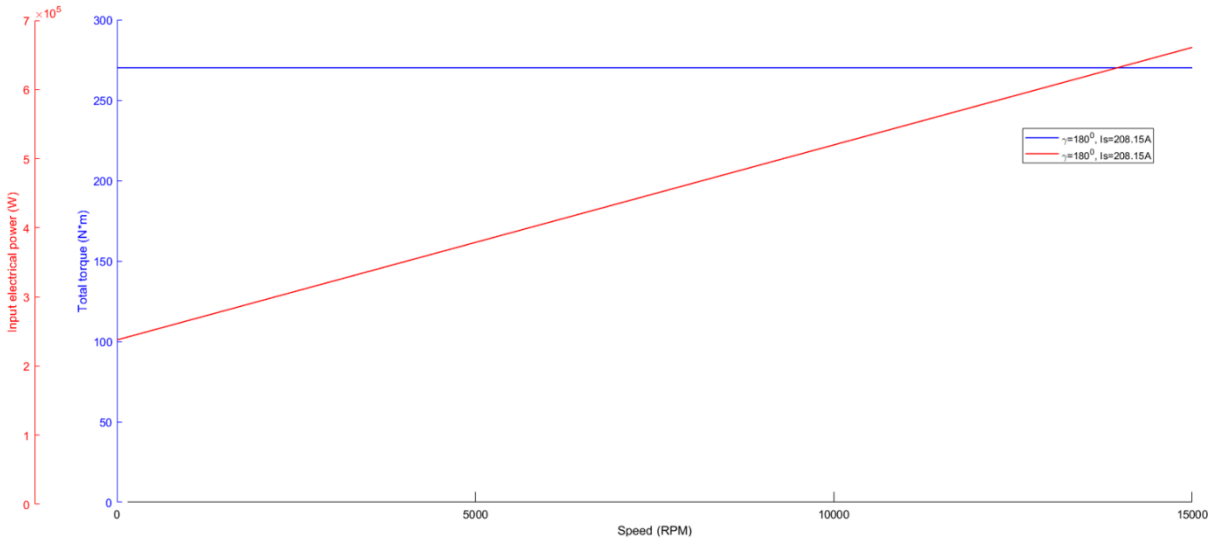

Figure 33. Speed *N* versus Torque *T* (in blue), Speed *N* versus Power input P_{in} (in red)

It is clear from figure 33 above that the value of *T* remains unchanged with the increase of *N*. In other words, the torque is independent of the variation of speed. In contrast, the value of P_{in} increase with the increase of speed until it reaches the generator rated speed. This precise determination of P_{in} and *T* is of great importance in the sense that more than ~685 kW of power is achieved to satisfy the basic requirement of the wind turbine system. Another conclusion can be extracted that, the generator can be easily controlled due to constant torque value under on-load conditions.

Secondly, the iron losses map is computed across the entire speed versus torque envelope. Figure 34 below shows the iron losses map and the region in which iron losses are computed for analyses purpose.

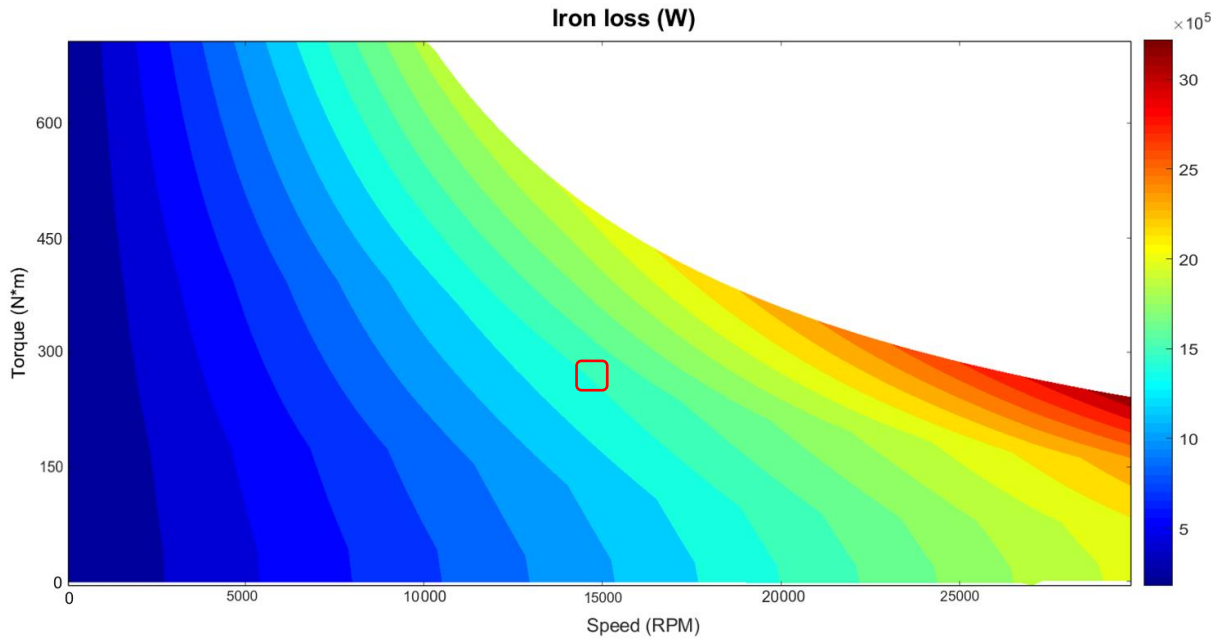

Figure 34. Iron losses (P_{iron}) map in W

Typically, the iron losses are predicted high as the machine operate mostly at rated speed. However, we are interested to measure P_{iron} when torque is 270 Nm at 15000 rpm. The region inside the triangle shows the value of P_{iron} is 1.5 MW approximately. This predicted value is almost the same as it was calculated in the analytical modelling and simulation. Thus validate the accuracy of input design parameters discussed in the FE prototype model. As the machine operates only at the rated speed, therefore, higher values of iron losses at higher speed at eliminated and the machine is safe to operate at the rated speed of the generator.

Finally, the efficiency map is plotted to determine the ideal region where the design is laying. Figure 35 below represents the efficiency map in percentage to envelop the ideal region to operate the machine for maximum efficiency.

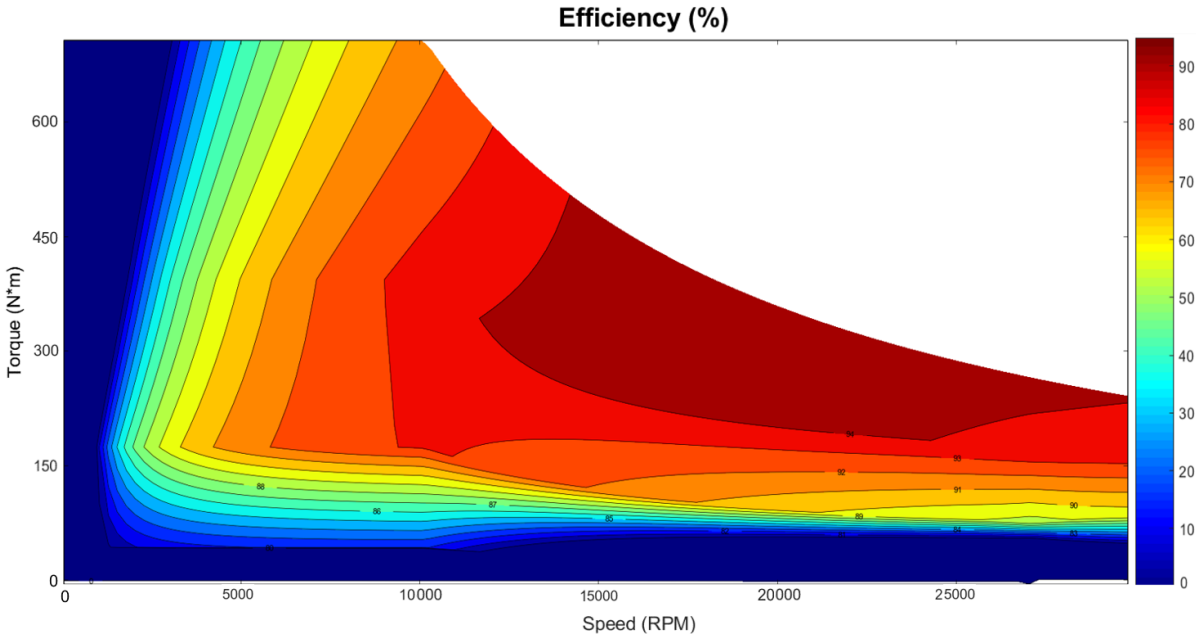

Figure 35. Efficiency (β) map in percentage

We can observe from figure 35 that a large area is covered by a higher percentage of efficiencies. In other words, if the generator reaches its rated speed and torque value then the generator efficiency is reached up to 94% approximately. The contour plot shows a big area above 94% of efficiency which is a very good result mainly in peak power at corner speed when the machine is at maximum losses. The contour plot also shows that it is possible to attain such results with a good margin. This margin is particularly comfortable and gives good prospects of renewable energy over the fossil fuel industry.

Chapter 9

9 Conclusion and Future Work

This research work presents a complete virtual prototype model of a brushless High-speed Permanent Magnet Synchronous Generator with U-shaped interior magnets. This design was made after an intense literature review in the last two years to achieve the necessary knowledge and tools to fulfil the basic requirements of a wind turbine system after combining two different approaches.

PM synchronous machine allows for much safer use, while still retaining much of the losses reduction benefits for high-speed operations. The wind turbine generator design presented in the past studies is not appropriate for on-shore and off-shore wind turbine systems. This work first details the development of a prototype model appropriate for analyzing the performance of machine in the results and analyses section. The machine design process adopted by this research work agrees well with the machine design analyses for a variety of configurations. Due to the extensive modelling and simulation approach the output design parameters, variables, and electrical quantities are estimated using machine design methodology. These analyses establish practical limits for design, highlight which parameters contribute most to the variation in performance, and describe some of the fundamental differences in the two methodologies.

The second contribution of this thesis is the steady-state D-Q analysis on the performance analysis of a machine. Most past studies of PM synchronous machines have been using analytical and finite element analyses, leaving the impact of power, torque, and speed on the machine's performance not well understood. This research work describes a separate section that allows for efficient 2-D time-stepping steady-state D-Q calculations with a large number of operating points for the entire spectrum to envelope iron losses and performance efficiency effectively.

The final contribution of this thesis is the examination of gaps between analytical and finite element methods. Previous work in this area has included only limited potential in the computational analysis's mitigation. In other words, the two methods are used solely with many unrealistic assumptions. In this thesis, the analytical design parameters are first validated in MATLAB and then used to construct the geometry of a machine in MotorXP-PM. Hence, identifying key performance parameters to predict the optimal design solution.

9.1 Summary of conclusion

The following findings of these two methodologies summarize the most important conclusions described in this research work.

- The performance efficiency is reasonable up to 96% on average. Whereas increasing values for current-step, advance angle step, and rotor positions, the value of generator efficiency decreases which can be overcome by running the generator at the synchronous speed which is the main objective of this study.

- The value of power input estimated in the analytical part is validated in the finite element part of the thesis. Whereas the value of power output assumed in the analytical part is validated in the finite element part accordingly. In other words, 660 kW of output power is a good agreement for a 776 kg machine. This accomplishment is only possible due to the silicon-iron alloy used in this work with sintered NdFeB magnets.

- Maximum flux density (B_m) achieved is well below the saturation level "B_{sat}". At the same time stator current density (J_o) is well below the maximum current density (J_a). It means that high power densities are achieved with low iron losses as well as high saturation polarization.

- The electromagnetic design is acceptable for this type of application as torque ripple waveform eliminate at 15000 rpm. Although some spikes are observed in the cogging torque graph which results in electromagnetic noise and vibration which is acceptable to this type of application. However, for other types of moving vehicles such as cars, or trains, these ripples are not acceptable as they use servomotor for high precision accuracy with a slotless machine.

- The mechanical problems can be eliminated by introducing a skew angle. The skew angle filters cogging torque, harmonic contents, flux leakage, and torque ripples on one hand. On the other hand, it produces better emf waveform and flux linkage for a guaranteed better design.

- 2-D computational analysis is better than a 3-D analysis due to the small computational time. In contrast, the thermal analysis is ideally experimented with and tested in 3-D software tools. The sensitive analysis is performed in 3-D modelling and simulation by dimensioning water jackets channels and air ducts to better estimate the main performance parameters of a machine.

- Determining intensive cooling strategy and the thermal class of the machine can improve the self-ventilation, allowing to achieve the high-power densities at high-speed operations.

- PM machines produce a higher torque-to-weight ratio as compared to the similar rated induction machine. The PM machines are 30% smaller and 10 – 15% more efficient than equivalent rated induction machines [77]. The wind turbine industry can apply brushless PM generators to get lightweight, higher efficiency, and reduced cost inverters for the renewable market.

- Vestas produced V47 – 660 kW wind turbine generator for medium and large-scale wind turbine systems with an efficiency of ~88% [75]. The prototype model produced in this research work suggests more than 96% performance efficiency for the same rated machine. It proves that this type of machine is easily adaptable to the renewable energy market.

9.2 Future work

The presented design is based on the input and output parameters analyzed in simple MATLAB and MotorXP-PM software tools. However, other sophisticated tools are already tested and implemented in the power industry for rotatory applications. Nevertheless, more work needs to be done on this topic but with a different approach.

Different ways of investigating optimum design solutions are being developed all around the world. One good example is Siemens Gamesa off-shore wind-to-hydrogen project. They used ANSYS software to achieve the optimum electromagnetic design, based on the definition of the design variables, constraints, and objectives.

It is possible to avail some of the benefits in the MotorXP-PM software mainly with the DXF interface to make some machine geometry in order to integrate the magnetostatic FEA with the electromagnetic analysis together. In this research work, only the magnetostatic and steady-state D-Q analyses are investigated. Whereas MotorXP-PM can permit dynamic FEA and D-Q analysis to solve analytical and EM design challenges more objectively.

The second possibility is to get benefits of availing "ActiveX interface", to make some script with SIMULINK or Microsoft Excel as a black box, synchronized with ANSYS or COMSOL Multiphysics software to combine analytical and finite element models for thermal and electromagnetic analysis purpose. In this way, the thermal model of an HSPMSG become possible to automate and integrate into the design process.

The third possibility for future work, which has been alluded already, is the operational analysis and maintenance durability. While some of the tradeoffs in rotor positions, advance angle setup, and speed range were discussed in the results and analyses chapter, proper selection of design conditions needs to be done in the context of the fully operational phase of installing inverter in the wind turbine site to observe various parameters to better estimate the entire system of a wind turbine.

In the end, such applications and field tests boost the machine projects, exploring other solutions to the designers and engineers in less time. For example, an interior permanent magnet with a V-shaped magnet or classical IPM with slits used to bury in rotor slots and protect them against magnet losses can be a good alternative. The ultimate goal is to find the best configuration with less weight gives some initial constants and constraints can define machine design objectives more simple to investigate. In addition, the comparative analysis of the final results of different studies could be interesting to check what the best machine is: the one with non-massive rotor steel like used in this thesis or other IPM with high saliency and slits? The answer might be the next machine design and development.

10 Reference List

[1] U.S. Energy Information Administration, “Wind explained, History of wind power,” Washington, D. C., U.S.A., 1977, [Online] Available: https://www.eia.gov/energyexplained/wind/history-of-wind-power.php, [Accessed: 31. 04. 2020]

[2] J. K. Lee, K. Y. Oh, J. Y. Kwak, and J. Y. Park, “Design and Analysis of Permanent Magnet Synchronous Generator for Small Wind Turbine”, The Korean Society for New and Renewable Energy, AFORE, Nov. 2014, pp. 308 – 308

[3] A. Verde, O. Lastres, G. Hernàndez, G. Ibañez, L. Verea, and P. J. Sebastian, “A new method for characterization of small capacity wind turbines with permanent magnet synchronous generator: An experimental study,” Heliyon 4, 2018, e00732, DOI: http://doi.org/10.1016/j.heliyon.2018.e00732

[4] L. Qinghua, “Analysis, Design and Control of Permanent Magnet Synchronous Motors for wide-speed operation,” Ph.D. dissertation, Dept. Elect. Engg., National Univ. of Tech., Singapore, 2005.

[5] O. Anaya-Lara, D. Campos-Gaona, E. Moreno-Goytia, and G. Adam, “Offshore wind energy generation: control, protection, and integration to electrical systems,” Chichester, U.K.: Wiley, 2014.

[6] T. P. M. Bazzo, J. F. Kolzer, R. Carlson, F. Wurtz, and L. Gerbaud, “Multiphysics Design Optimization of a Permanent Magnet Synchronous Generator” in Proc. IEEE Transactions on Industrial Electronics., Dec. 2017, Vol. 64 (12), pp. 9815 – 9823.

[7] P. C. Putnam, “Power from the wind” New York, U.S.A., Van Nostrand Reinhold Publishing Company, 1948.

[8] W. Shephard, L. Zhang, “Electricity Generation Using Wind Power”, Singapore. World Scientific Publishing Company, 2010.

[9] F. R. Eldridge, “Wind Machines”, 2nd ed., New York, U.S.A., Van Nostrand Reinhold Publishing Company, 1980.

[10] J. L. F. van der Veen, L. J. J. Offringa, A. J. A. Vandenput, “Minimizing rotor losses in high-speed high-power permanent magnet synchronous generators with rectifier load”, IEE Proceedings – Electric Power Applications, Sept. 1997, Vol. 144 (5), pp. 331 - 337, DOI: https://doi.org/10.1049/ip-epa:19971354.

[11] A. B. Proca, A. Keyhani, A. EL-Antably, “Analytical Model for Permanent Magnet Motors with Surface Mounted Magnets” Sixth International Conference on Electrical Machines and Drives, Nov. 1999, Vol. 2, pp. 767 – 769

[12] K. F. Rasmussen, “Analytical Prediction of Magnetic Field from Surface Mounted Permanent Magnet Motor”, International Conference on Electric Machines and Drives, May 1999, pp. 34 – 36

[13] Z. Q. Zhu, D. Howe, C. C. Chan, "Improved Analytical Model for Predicting the Magnetic Field Distribution in Brushless Permanent-Magnet Machines", IEEE Transactions on Magnetics, Jan. 2002, Vol. 38 (1), pp. 229 – 238, DOI: https://doi.org/10.1109/20.990112

[14] A. B. Proca, A. Keyhani, A. EL-Antably, W. Lu, and M. Dai, "Analytical Model for Permanent Magnet Motors with Surface Mounted Magnets", IEEE Transactions on Energy Conversion, Sep. 2003, Vol. 18 (3), pp. 386 – 391

[15] Y. Zhilichev, "Analysis of Permanent Magnet Machines Using Crossing Macro-Elements", IEEE Transactions on Magnetics, Sep. 2000, Vol. 36 (5), pp. 3122 – 3124, DOI: https://doi.org/10.1109/20.908706

[16] A. Mahmoudi, N. A. Rahim, and W. P. Hew, "Axial-flux Permanent-Magnet Machine Modeling, Design, Simulation and Analysis", Scientific Research and Essays, June 2011, Vol. 6 (12), pp. 2525 – 2549

[17] N. H. Phyu, Numerical Analysis of a Brushless Permanent Magnet DC Motor Using Coupled Systems", Ph.D. dissertation, Dept. Elect. & Comp. Engg., National Univ. of Tech., Singapore, 2004.

[18] S. R. Guda, C. Wang, and M. H. Nehrir, "Modeling of Microturbine Power Generation Systems", Elect. Power Compon. Syst., Aug. 2006, Vol. 34 (9), pp. 1027 - 1041, DOI: https://doi.org/10.1080/15325000600596767

[19] A. Zachas, Y. Duan, R. G. Harley, and T. G. Habetler, "Knowledge Based Permanent Magnet Machine Design-Literature Survey", Grainger Center for Electric Machinery and Electromechanics, Dept. of Elect. & Comp. Engg., Univ. of Illinois at Urbana-Champaign, Rev. 3, Illinois, U.S.A., 2007.

[20] C. Y. Hsiao, S. N. Yeh, and J. C. Hwang, "Design of High Performance Permanent-Magnet Synchronous Wind Generator", Energies, Nov. 2014, Vol. 7 (11), pp. 7105 – 7124, DOI: http://doi.org/10.3390/en7117105

[21] J. J. H. Paulides, G. W. Jewell, and D. Howe, "An Evaluation of Alternative Stator Lamination Materials for a High-Speed, 1.5 MW, Permanent Magnet Generator", IEEE Transactions on Magnetics, Aug. 2004, Vol. 40 (4), pp. 2041 – 2043, DOI: http://doi.org/10.1109/TMAG.2004.832172

[22] A. Arkkio, T. Jokinen, E. Lantto, "Induction and Permanent-Magnet Synchronous Machines for High-Speed Applications", Proceedings of the 8th International Conference on Elect. Machines and Systems, Oct. 2005, Vol. 2, pp. 871 – 876, DOI: http://doi.org/10.1109/ICEMS.2005.202668

[23] Z. Kolondzovski, A. Arkkio, J. Larjola, and P. Sallinen, "Power Limits of High-Speed Permanent-Magnet Electrical Machines for Compressor Applications", In IEEE Transactions on Energy Conversion, March 2011, Vol. 26 (1), pp. 73 - 82, DOI: http://doi.org/10.1109/TEC.2010.2089459

[24] Wind-turbine-models, “The big portal for wind energy, 660kW V47, Vestas Wind Systems A/S”, Germany, 2011, [Online] Available: https://en.wind-turbine-models.com/turbines/13-vestas-v47#datasheet, [Accessed: 31.10.2020]

[25] Engineering ToolBox, “Resources, Tools and Basic Information for Engineering and Design of Technical Application”, U.S.A., 2001, [Online] Available: https://www.engineeringtoolbox.com/synchronous-full-load-speed-induction-motors-d_1448.html, [Accessed: 01.11.2020]

[26] H. Y. Isaac-Du, L. Hao, and H. Lin, “Modeling and Analysis of Electromagnetic Vibrations in Fractional Slot PM Machines for Electric Propulsion”, IEEE Energy Conversion Congress & Exposition, Sept. 2013, pp. 5077 – 5084, DOI: http://doi.org/10.1109/ECCE.2013.6647386

[27] J. F. Gieras, and U. Jonsson, “Design of a high-speed permanent-magnet brushless generator for microturbines”, Electromotion, July 2005, Vol. 12, pp. 86 – 91

[28] A. Jain, S. Shankar, and V. Vanitha, Power Generation Using Permanent Magnet Synchronous Generator (PMSG) Based Variable Speed Wind Energy Conversion System (WECS): An Overview”, Journal of Green Engineering, March 2018, Vol. 7 (4), pp. 477 – 504, DOI: http://doi.org/10.13052/jge1904-4720.742

[29] A. El Shahat, A. Keyhani, and H. El Shewy, “400kW Six Analytical High Speed Generator Design for Smart Grid Systems”, International Journal of Energy and Power Engineering, Sept. 2010, Vol. 4 (3), pp. 676 – 693

[30] MotorXP, “MotorXP-PM”, VEPCO TECHNOLOGIES INC., California, U.S.A, 2020, [Online] Available: https://motorxp.com/#motorpm, [Accessed: 01.11.2020]

[31] Z. Guo, and L. Chang, "FEM study on permanent magnet synchronous generators for small wind turbines," Proceedings of CCECE, 1-4 May 2005, pp. 641 – 644, DOI: 10.1109/CCECE.2005.1557012

[32] A. Kiyoumarsi, P. Moallem, M. Hassanzadeh, and M. Moallem, “Application of the Finite Element Method in Design and Analysis of Permanent-Magnet Motors”, Published by WSEAS press, 2007, pp. 138 – 152

[33] J. Ma and Z. Q. Zhu, "Magnet Eddy Current Loss Reduction in Permanent Magnet Machines," IEEE Transactions on Industry Applications, March – April 2019, Vol. 55 (2), pp. 1309 – 1320, DOI: 10.1109/TIA.2018.2874350

[34] J. Q. Xing, L. Chen, Q. Zhang, and Y. F. Ma, “Design and Analysis of Fan-Cooling for High Speed Permanent Magnet Machine Rotor,” Trans Tech Publ, Advanced Materials Research, Nov. 2012, Vol. 591–593, pp. 3-6, DOI: 10.4028/www.scientific.net/AMR.591-593.3

[35] C. C. Hwang, C. M. Chang, S. P. Cheng, C. K. Chan, C. T. Pan, and T. Y. Chang, “Comparison of performances between IPM and SPM motors with rotor eccentricity,” Journal of Magnetism and Magnetic Materials, Vol. 282, May 2004, pp. 360 – 363, DOI: doi.org/10.1016/j.jmmm.2004.04.084

[36] K. J. Tseng and S. B. Wee, "Analysis of flux distribution and core losses in interior permanent magnet motor," IEEE Transactions on Energy Conversion, Dec. 1999, Vol. 14 (4), pp. 969 – 975, DOI: 10.1109/60.815015

[37] J. Kolehmainen and J. IkÄheimo, "Motors With Buried Magnets for Medium-Speed Applications," IEEE Transactions on Energy Conversion, March 2008, Vol. 23 (1), pp. 86 – 91, DOI: 10.1109/TEC.2007.914331

[38] R. H. Staunton, P. J. Otaduy, J. M. Mckeever, S. C. Nelson, J. M. Bailey, and S. Das, R. L. Smith, "PM Motor Parametric Design Analyses for a Hybrid Electric Vehicle Traction Drive Application-Interim Report," Engineering Science and Technology Division, U. S. Department of Energy, July 2004

[39] J. E. Rucker, "Design and analysis of a permanent magnet generator for naval applications," Master Thesis, Dept. of Ocean Engg. and the Dept. of Elect. Engg. & Comp. Sc., Massachusetts Institute of Technology, June 2005

[40] A. El Shahat, A. Keyhani, and H. M. El Shewy, "Optimized Sizing of High Speed PM Generator for Renewable Energy Applications," 14th Int. Middle East Power Systems Conference (MARCON'10), Dec. 2010, pp. 550 - 558

[41] J. R. Hendershot, Jr. & T. J. E. Miller, "Design of Brushless Permanent Magnet Motors", Oxford, U.K., Magna Physics Publishing and Clarendon Press, 1994

[42] W. Fengxiang, Z. Wenpeng, Z. Ming, and W. Baoguo, "Design considerations of high-speed PM generators for micro turbines," IEEE Proceedings. International Conference on Power System Technology, Kunming, China, 2002, Vol. 1, pp. 158 – 162, DOI: 10.1109/ICPST.2002.1053524

[43] P. George, J. Gogue & Joseph, and Jr. Stupak, "G2 Consulting," Course in magnetics, electromagnetics, and motors, etc., Chapter 7, Beaverton, U.S.A., [Online] Available: www.consult-g2.com/course/chapter7/chapter.html, [Accessed: 06.12.2020]

[44] M. Rahman, and G. Slemon, "Promising applications of neodymium boron iron magnets in electrical machines," IEEE Transactions on Magnetics, Vol. 21 (5), Sept. 1985, pp. 1712 – 1716, DOI: 10.1109/TMAG.1985.1064113

[45] O. Aglen and A. Andersson, "Thermal Analysis of a High-Speed Generator," IEEE Transactions, 2003

[46] D. C. Hanselman, "Brushless Permanent Magnet Motor Design," 2nd ed., The Writer's Collective, Magna Physics Publishing Press, 2003

[47] M. Rippy, "An Overview Guide for the Selection of Lamination Material," Proto Laminations, Inc., 2004

[48] D. Pavlik, V. K. Garg, J. R. Repp, and J. Weiss, "A Finite Element Technique for Calculating the Magnet Sizes and Inductances of Permanent Magnet Machines," IEEE Transactions of Energy Conversion, Vol. 3 (1), March 1988, pp. 116 – 122, DOI: 10.1109/60.4211

[49] D. H. Kang, P. Curiac, Y. H. Jeong, and S. J. Jung, “Prospects for magnetization of large PM rotors: conclusions from a development case study,” IEEE Transactions on Energy Conversion, Sept. 2003, Vol. 18 (3), pp. 409 – 416, DOI: 10.1109/TEC.2003.815847

[50] Magnetic Component Engineering, “A website for permanent magnet material,” California, U.S.A., 1973, [Online] Available: Neodymium Iron Boron Magnets (NdFeB) | MCE (mceproducts.com) [Accessed: 28. 12. 2020]

[51] JFE steel, “A steel manufacturing company,” Tokyo, Japan, 2002, [Online] Available: JFE Steel Corporation (jfe-steel.co.jp) [Accessed: 30. 12. 2020]

[52] A. H. Isfahani, A. H. S. Boroujerdi, and S. Hasanzadeh, “Multi-objective design optimization of a large-scale direct-drive permanent magnet generator for wind energy conversion systems,” Frontiers in Energy, May 2014, Vol. 8(2), pp. 182 – 191, DOI: https://doi.org/10.1007/s11708-014-0320-z

[53] S. M. Abu-Sharkh, M. R. Harris, and N. T. Irenji, “Calculation of rotor eddy-current loss in high-speed PM alternators,” 8th International Conference on Electrical Machines and Drives (Conf. Publ. No. 444), Cambridge, U. K., 1997, pp. 170 – 174, DOI: 10.1049/cp:19971061

[54] C. Huynh, L. Zheng, D. Acharya, “Losses in High Speed Permanent Magnet Machines Used in Microturbine Applications,” Journal of Engineering for Gas Turbines and Power, Mar. 2009, Vol. 131 (2), pp. 022301 (6 pages), DOI: https://doi.org/10.1115/1.2982151

[55] E. S. Hamdi, “Design of Small Electrical Machines,” NY, John Wiley & Sons, 1998

[56] O. Aglen and A. Andersson, "Thermal analysis of a high-speed generator," 38th IAS Annual Meeting on Conference Record of the Industry Applications Conference, Salt Lake City, UT, U.S.A., 2003, Vol. 1, pp. 547-554, DOI: 10.1109/IAS.2003.1257554

[57] P. Kiameh, "Power Generation Handbook: Selection, Applications, Operation, Maintenance," 1st ed., McGraw-Hill, 2003

[58] J. Pepi, and P. Mongeau, "High Power Density Permanent Magnet Generators," DRS Electric Power Technologies, Inc., 2004

[59] V. Kuptsov, “Design and Analysis of Permanent Magnet Machines,” MotorAnalysis-PM User Manual, Ver. 1.1, 2017, [Online] Available: MotorAnalysis – Electric Machine Design and Analysis Software [Accessed: 24. 04. 2021]

[60] G. Sarumol, and S. V. Reeba, “Minimisation of losses in permanent magnet synchronous generator for high speed applications,” International Conference on Control Communication & Computing India (ICCC), 2015, pp. 200 – 205, DOI: 10.1109/ICCC.2015.7432892

[61] F. Caricchi, F. Crescimbini, F. Mezzetti and E. Santini, "Multistage axial-flux PM machine for wheel direct drive," IEEE Transactions on Industry Applications, July-Aug. 1996, Vol. 32 (4), pp. 882-888, DOI: 10.1109/28.511645

[62] P. Mongeau, "High Torque Density Propulsion Motors," DRS Electric Power Technologies, Inc., 2004

[63] M. Comanescu, A. Keyhani, and M. Dai, "Design and Analysis of 42-V Permanent Magnet Generator for Automotive Applications," IEEE Transactions on Energy Conversion, Mar. 2003, Vol. 18 (1), pp. 107-112, DOI: 10.1109/TEC.2002.808380

[64] L. GAŠPARIN, and R. FIŠER, "Sensitivity of Cogging Torque to Permanent Magnet Imperfections in Mass-produced PM Synchronous Motors," Przegląd Elektrotechniczny, 2013, n. pag., pp. 80-83

[65] Z. Tan, X. G. Song, B. Ji, L. Zheng, J. E. Ma, W. P. Cao, "3D thermal analysis of a permanent magnet motor with cooling fans ," Journal of Zhejiang University-SCIENCE A (Applied Physics & Engineering), Aug. 2015, Vol. 16 (8), pp. 616-621, DOI: https://doi.org/10.1631/jzus.A1400293

[66] B. R. D. F. Marques, "Virtual Prototyping of a Brushless Permanent Magnet AC Motor-Electromagnetic and Thermal Design using CAD Software," Instituto Superior Técnico Lisbon, Portugal, Nov. 2012, DOI: https://fenix.tecnico.ulisboa.pt/downloadFile/395145026134/dissertacao.pdf

[67] A. Tassi, G. Zanocchi, and D. Staton, "FEM and Lumped Circuit Thermal Analysis of External Rotor Motor," 32nd Annual Conference on IEEE Industrial Electronics, 2006, pp. 4825-4828, DOI: 10.1109/IECON.2006.348144

[68] M. A. Khan, P. Pillay, and K. D. Visser, "On Adopting a small PM Wind Generator for a Multiblade, High Solidity Wind Turbine", IEEE Transaction on Energy Conversion, Sept. 2005, Vol. 20 (3), pp. 685 – 692, DOI: 10.1109/PES.2005.1489540

[69] K. Shahzad, Y. Guo, L. Li, and D. Dorrell, "Design of High Speed Permanent Magnet Generator for Solar Co-Generation System Using Motor-CAD", 20th International Conference on Electrical Machines and Systems (ICEMS), Aug. 2017, DOI: 10.1109/ICEMS.2017.8056036

[70] K. Sitapati, and R. Krishnan, "Performance comparisons of radial and axial field, permanent-magnet, brushless machines," IEEE Transactions on Industry Applications, Sept.-Oct. 2001, Vol. 37 (5), pp. 1219-1226, DOI: 10.1109/28.952495

[71] H. A. Khazdozian, "Improved design of permanent magnet generator for large scale wind turbines," Ph. D. Thesis, Dept. of Elect. Engg., Iowa State University, 2016

[72] M. Polikarpova, P. Ponomarev, P. Lindh, I. Petrov, W. Jara, V. Naumanen, J. A. Tapia, and J. Pyrhönen, "Hybrid Cooling Method of Axial-Flux Permanent-Magnet Machines for Vehicle Application," IEEE Transactions on Industrial Electronics, 2015, Vol. 62 (12), pp. 7382 – 90, DOI: 10.1109/TIE.2015.2465354

[73] J. Li, D.-W. Choi, D.-H. Son, and Y.-H. Cho, “Effects of MMF Harmonics on Rotor Eddy-Current Losses for Inner-Rotor Fractional Slot Axial Flux Permanent Magnet Synchronous Machines,” IEEE Transactions on Magnetics, Feb. 2012, Vol. 48 (2), pp. 839 – 42, DOI: 10.1109/TMAG.2011.2173923

[74] T. J. E. Miller, “SPEED’s Electric Motors,” Dept. of Electronics & Electrical Engineering, University of Glasgow, 2002

[75] Vestas Wind Systems A/S, “V47 – 660 kW,” General Specification 660 kW Variable Slip Wind Turbines brochure, Denmark, 2000, pp. 1 – 27

[76] W. Zhu, S. Pekarek, B. Fahimi, and B. J. Deken, “Investigation of Force Generation in a Permanent Magnet Synchronous Machine,” IEEE Transactions on Energy Conversion, Sept. 2007, Vol. 22 (3), pp. 557 – 565, DOI: 10.1109/TEC.2006.888034

[77] J. F. Gieras, “New Applications of Synchronous Generators,” PRZEGLAD ELEKTROTECHNICZNY, Sept. 2012, Vol. 88 (9a), pp. 150 – 157

Appendices

Appendix 1

MATLAB Codes for the analytical design parameters estimation

```
% Danish Mukhtar Novia Thesis
% High speed permanent magnet synchronous generator for a wind turbine
% Modelling & Simulation for Analytical method
% Analytical design parameters estimation
%%%%%%%%%%%%%%%%%%%%%%%%%%%%%%%%%%%%%%%%%%%%%%%%%%%%%%%%%%%%%%%%%%%%%%%%%%%%
%%
% common design parameters assumed & collected for analytical modelling &
simulation
uo = 4*pi*1e-7;                                         % free space permeability
p = 2;                                                  % no. of pole pairs
q = 3;                                                  % no. of phases
Ns = 24;                                                % no. of stator slots
% slot depression width in m
wd = 1e-6;
g = .004;                                               % air-gap in m
% magnet height (10% higher than air-gap) in m
mh = .04;
% slot depression height in m
hd = 1e-4;
mw = 0.025;                                             % magnet width in m
tf = 0.5;                                               %    peripheral    tooth
fraction
% angle between RMS voltage & current or power factor angle in deg.
phi = 0;
Nc = 1;                                                 % no. of turns per coil
hs = 0.025;                                             % slot height in m
Nsp = 1;                                                %  no.  of  slots  short
pitched
% magnet remnant flux density in T
Br = 1.2;
% stator winding conductivity in s/m
psi_cap = 6.0e+7;
sbir = 0.7;                                             % stator back iron ratio
% input parameters for analytical analysis
% rated speed (assumed) in rpm
N = 15000;
% electrical frequency (assumed) in Hz
f = 500;
LDr = 2.50;                                             % L/D ratio
vtip = 200;                                            % maximum tip speed in m/s
% magnetic skew angle in deg. (mech.)
thmsk = 10;
lambda_s = 0.5;                                         % slot fill factor
Ncs = 224;                                              % no. of conductors/slot
% stator current density (assumed) in A/cm^2
Ja = 1200;
% output parameters estimation for analytical analysis
% electrical frequency in Hz
fe = p*N/60;
% electrical frequency in rad/s
wo = 2*pi*fe;
r = p*vtip/wo;                                          % rotor radius in m
% rated speed (estimated) in rpm
Ne = 60*wo/(2*pi*p);
Lst = 2*LDr*r;                                          % rotor stack length in m
% skew angle in deg. (elect.)
```

```
thsk = ((p*thmsk)+wd)*(pi/180);
ks = sin(thsk/2)/(thsk/2);                          % skew factor
ws_bottom = 2*pi*(r+g+wd+hd)*(1-tf)/Ns;             % slot bottom width in m
ws_top = ws_bottom*(r+g+wd+hd)/(r+g+mw+hd);         % slot top width in m
ws = (ws_top + ws_bottom)/2;                        % average slot width in m
Bg = (mh/mh+g)*Br;                                  % air-gap flux density in
T
pf = cos(phi);                                      % power factor
% no. of slots per pole per phase "estimated"
m = Ns/(2*p*q);
% no. of slots with full pitch coil
Nsfp = Ns/(2*p);
% no. of slots with actual pitch coil
Nsap = Nsfp - Nsp;
% winding pitch or pitch factor angle in deg. (elect.)
alpha = pi*Nsap/Nsfp;
% electrical angle in degrees
gamma = 2*pi*p/Ns;
As = ws*hs;                                         % slot area in m^2
% winding cross-sectional area in m^2
Aac = (As*lambda_s)/(2*Nc);
% no. of armature turns per coil
Na = 2*p*m*Nc;
% input parameters for material analysis
% stator saturation flux density in T
Bsat = 1.8;
urec = 1.05;                                        % recoil permeability
% electrical resistivity of the material in ohm.m
rho = 1.43e-6;
% input parameters for basic electrical model
Pout = 660000;                                      % power output in W
% magnet physical angle in deg. (mech.)
thm = 50;
kl = 0.95;                                          % leakage factor
kr = 1.05;                                          % reluctance factor
% inner magnetic boundary in m
Ri = r;
% outer magnetic boundary in m
Rs = r+mw+g;
% inner boundary of magnet in m
R1 = r;
% outer boundary of magnet in m
R2 = r+mw;
% output parameters estimation for basic electrical model
% end-turn length of an armature conductor (one-end) in m
leo = pi*(r+g+mw+hd+0.5*hs)*Nsap/Ns;
% end-turn length of an armature conductor (half-coil) in m
leh = pi*leo;
% length of an armature conductor in m
l = 2*Na*(Lst+2*leh);
% stator/armature resistance in ohms
Ra = l/(psi_cap*Aac);
kp = sin(alpha/2)*sin(pi/2);                        % pitch factor
% breadth/distribution factor
kd = sin(m*gamma/2)/(m*sin(gamma/2));
kw = kp*kd;                                         % winding factor
% magnet gap factor
kg=((Ri^(p-1))/(Rs^(2*p)-Ri^(2*p)))*((p/p+1))*(R2^(p+1)-
R1^(p+1))+(p*Rs^(2*p)/(p-1))*(R1^(1-p)-R2^(1-p));
wt = 2*pi*(r+g+mw+hd)*tf/Ns;                        % tooth width in m
taus = ws+wt;                                       % total slot width in m
kc = 1/(1-(1/((taus/ws)*((5*g/ws)+1))));            % carter coefficient
ge = kc*g;                                          % effective air-gap in m
```

```
Cphi = (p*thm)/180;                                % flux concentration factor
CP = mh/(ge*Cphi);                                  % permeance coefficient
% air-gap magnetic flux density in T
Bgm = ((kl*Cphi)/(1+kr*urec/CP))*Br;
% magnet physical angle in radians
thmrad = thm*(pi/180);
% magnetic flux density in T
Bm = (4/pi)*Bgm*kg*sin(p*thmrad/2)*sin(pi/2);
% Magnetic flux linkage in T
lambda_n = 2*Rs*Lst*Na*Bm*kw*ks/p;
% RMS phase excitation voltage or internal voltage in V
Ea = wo*lambda_n/sqrt(2);
Ia = Pout/(q*Ea);                                   % stator current in A
% air-gap inductance in H
Lag = (q/2)*(4/pi)*(uo*Rs*Lst*Na^2*kw^2)/(p^2*(g+mw));
perm = uo*((1/3)*(hs/ws_top)+hd/ws_top);            % permeance
% self-slot leakage inductance in H
Las = 2*p*Lst*perm*(4*Nc^2*(m-Nsp)+2*Nsp*Nc^2);
% mutual-slot leakage inductance in H
Lam = 2*p*Lst*Nsp*Nc^2*perm;
% slot leakage inductance in H
if q==3
      Lslot = Las+2*Lam*cos(2*pi/q);                % for 3-phase windings
else
% for multiple phase windings
Lslot = Las-2*Lam*cos(2*pi/q);
end
% end-turn inductance in H
Le = ((uo*Nc*Na^2*taus)/2)*log(wt*sqrt(pi)/sqrt(2*As));
% total inductance or synchronous inductance in H
Ls = Lag+Lslot+Le;
% synchronous reactance in ohms
Xs = wo*Ls;
% input parameters for machine sizing and weight
cov = 703.0696;                                     %  conversion  factor  in
N/m^2 per psi
tau = 10;                                           % shear stress in psi
% magnetic flux density in cT
BmcT = 100*Bm;
ds = 7700;                                          % steel density in kg/m^3
dm = 7400;                                         % magnet density in kg/m^3
% conductor density in kg/m^3
dc = 8900;
% output parameters estimation for machine sizing and weight
% surface current density in A/cm^2
kz = (tau*cov)/BmcT;
% stator core back iron depth in m
sbid = (sbir*r)/p;
Rci = r+mw+g+hd+hs;                                 % core inside radius in m
Rco = Rci+sbid;                                      % core outside radius in
m
% overall diameter of a machine in m
Dmach = 2*Rco;
Mcb = ds*pi*(Rco^2-Rci^2)*Lst;                       % back iron core mass in
kg
Mct = ds*Lst*(Ns*wt*hs+2*pi*r*hd-Ns*hd*wd);         % teeth core mass in kg
% terminal voltage in V
Va = sqrt(Ea^2-((Xs+Ra)*Ia*cos(phi))^2)-(Xs+Ra)*Ia*sin(phi);
% armature conductor mass in kg
Mac = q*l*Aac*dc;
Mc = Mcb+Mct;                                       % total core mass in kg
Mm = 0.5*(p*thmrad)*((r+mw)^2-r^2)*Lst*dm;          % magnet mass in kg
Ms = pi*r^2*Lst*ds;                                 % shaft mass in kg
```

```
% service mass with 15% service fraction in kg
Mser = 0.15*(Mac+Mc+Mm+Ms);
Mtot = Mac+Mc+Mm+Ms+Mser;                          % total mass in kg
% input parameters for basic losses of a machine
Cr = 1.12;                                         % resistance coefficient
etea = 0.1;                                        % material constant
% density of air at 20 deg. C in kg/m^3
Jair = 1.205;
Ch = 0.0275;                                     % coefficient of hysteresis
losses in W/Hz.T^2.kg
% coefficient of excess eddy current losses in W/Hz.T^2.kg
Ce = 0.000277;
% coefficient of classical eddy current losses in W/Hz.T^2.kg
Cc = 1.83;
% kinematic viscosity of air at 20 deg. C in m^2/s
epsilon = 1.5e-5;
Pb = 36.79;                                        % base power in W/lb
Bo = 1.0;                                          % base flux density in T
n = 2.12;                                          % flux density exponent
fo = 1000;                                         % base frequency in Hz
nf = 1.68;                                         % frequency exponent
% output parameters estimation for basic losses of a machine
% conductor or copper losses in W
Pa = q*Ia^2*Ra;
delta = sqrt(2/wo*uo*psi_cap);                     % skin depth
Pstray = Pa*(Cr-1);                                % stray losses in W
Ph = etea*Bsat^n*fe;                               % hysteresis losses in W
% thickness of the material in m
t = (sbir*r)/p;
% eddy current losses in W
Pe = (pi^2*Bsat^2*t^2*fe^2)/(rho*CP);
% iron losses in W
Piron = Ch*(Bsat^2)*fe+Cc*((Bsat*fe)^2)+Ce*((Bsat*fe)^1.5);
% back iron flux density in T
Bb = Bg*r*p*sbir;
% core back iron losses in W
Pcb = Mcb*Pb*abs(Bb/Bo)^n*abs(fe/fo)^nf;
Bt = Bg/tf;                                        % tooth flux density in T
Pct = Mct*Pb*abs(Bt/Bo)^n*abs(fe/fo)^nf;           % teeth losses in W
Pc = Pcb+Pct;                                      % total core losses in W
% mechanical frequency in rad/s
wm = wo/p;
Rey = (wm*r*g)/epsilon;                            % Reynold's number
Cf = 0.0725/Rey^0.2;                               % coefficient of friction
Pwind = Cf*pi*Jair*wm^3*r^4*Lst;                   % windage losses in W
% remaining performance parameters
% input parameter for machine performance
hscm = 100*hs;                                     % slot height in cm
% output parameters for machine performance
% stator current density (estimated) in A/cm^2
Jo = 10*kz/(hscm*lambda_s);
Pin = Pout+Pa+Pc+Pwind;                            % power input in W
beta = Pout/Pin;                                   % efficiency
```

Appendix 2

JFE

Super Core™

Electrical steel sheets for high-frequency application

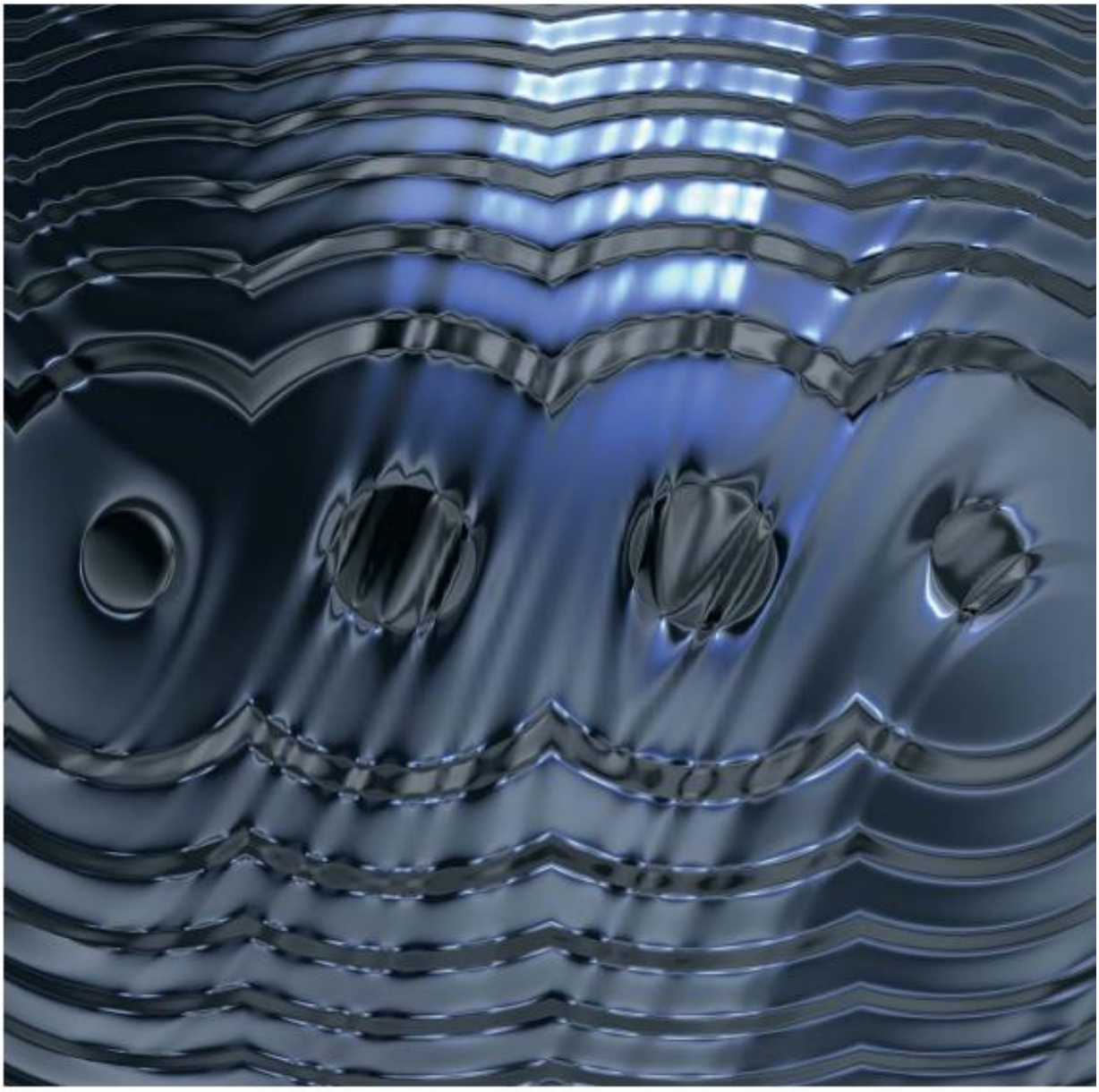

JFE Steel Corporation

Super Core™

Super Core™ is manufactured using an innovative process that is completely different from that for conventional silicon steel sheets. These are the highest grade, non-oriented magnetic steel sheets available.

Conventional silicon steel sheets have a Si (silicon) content of 3.5% or less. It has long been known that the magnetic characteristics of a silicon steel sheet improve as the Si content increases, peaking at 6.5%. However, it has been impractical to produce thin steel sheets with a Si content of over 3.5% because the steel tends to harden and become brittle. In 1993 JFE Steel solved this production problem through the adoption of a process called the CVD process, and successfully introduced the first 6.5% Si steel sheets (JNEX-Core) to the world.

In order to meet new demands, this technology has continued to be developed, leading to the commercial production of gradient high-silicon steel sheets with superior high-frequency characteristics (JNHF-Core).

Super Core™ Production Process

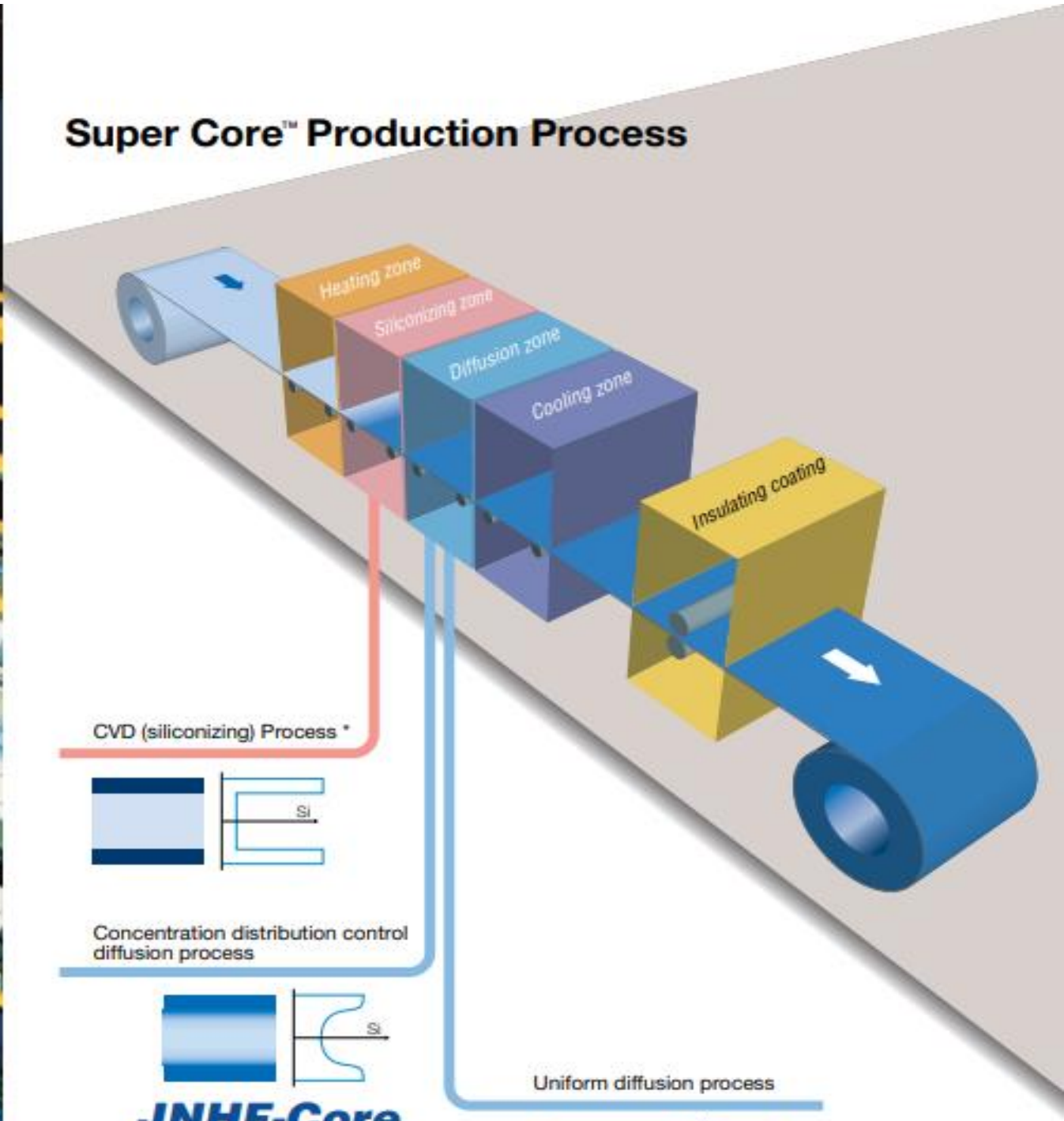

CVD (siliconizing) Process *

Concentration distribution control diffusion process

JNHF-Core

Gradient high-silicon steel sheet with low silicon content at the center portion and 6.5% silicon near the outer surface areas

Uniform diffusion process

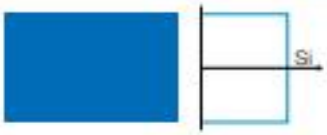

JNEX-Core

6.5% silicon steel sheet. (A high-silicon steel sheet with a uniform silicon content of 6.5% throughout the sheet)

* CVD Chemical Vapor Deposition

JNEX-Core

JNEX-Core is the highest-grade non-oriented magnetic steel sheets manufactured with a production method (CVD process) that is completely different from that for conventional silicon steel sheets, allowing a previously impossible Si content of 6.5%.

Low Core Loss

Core loss in high-frequency ranges is extremely low. This allows for low heat generation and size reductions for magnetic components such as high-frequency reactors and transformers.

Low Magnetostriction

Magnetostriction which causes noise and vibration is nearly zero. This enables significant noise reductions for magnetic components such as reactors and transformers.

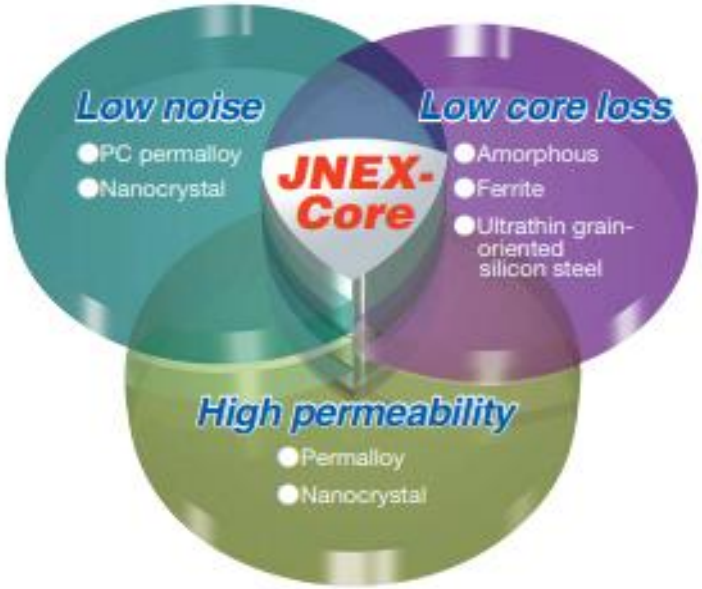

High Permeability

The permeability is extremely high across a wide range of frequencies, making it highly suitable for use in shield applications and CT.

Stable Quality

The high-temperature processing provides thermal stability. Since there is minimal deterioration of the properties due to machining, so stress-relieving anneals are not required.

Non-oriented

There is virtually no difference in the characteristics between the rolling direction (L-direction) and the transverse (C-direction). Therefore, this can be used in a wide range of applications, from stationary machines to rolling machines.

10JNEX900

●High-frequency core loss curve

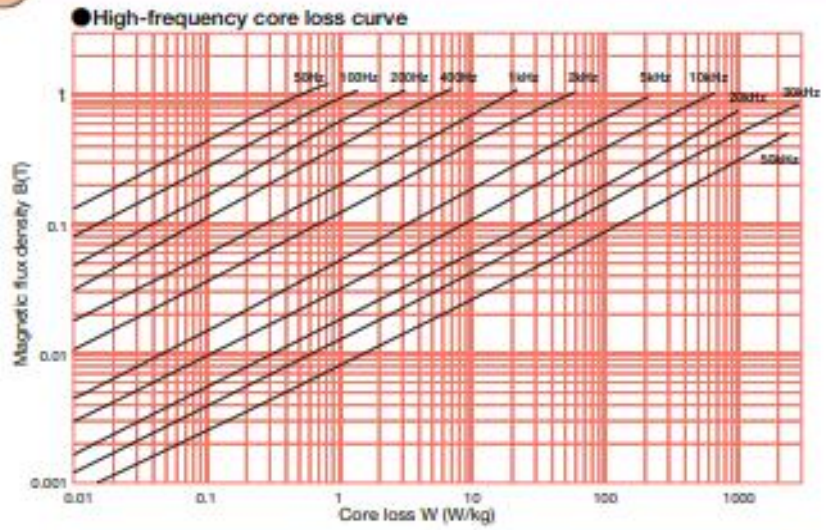

Measurement : 25 cm Epstein test
Rolling direction, shear cross-section

Variation in magnetic properties of silicon steel by Si content

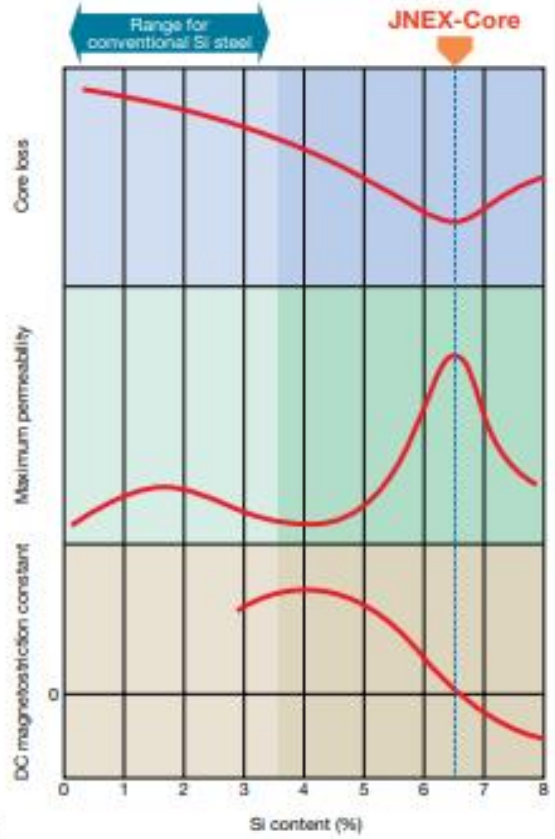

Characteristics

■Material core loss W1/10k (W/kg)* (in-house data)

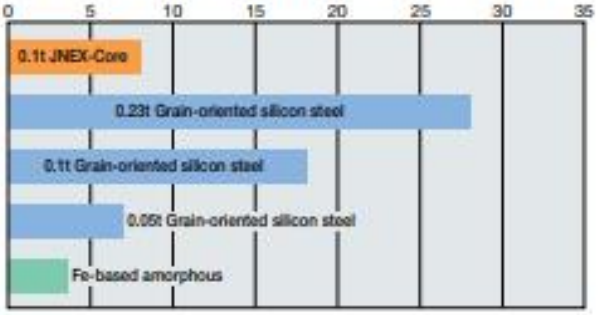

■Cut core (CS500 core loss W1/10k (W/kg)* (in-house data)

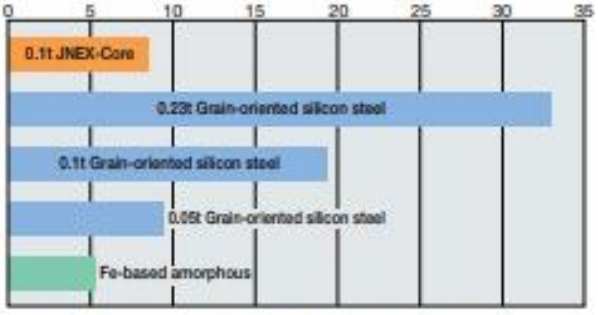

* W1/10k is the core loss at 10kHz, 0.1T(=1kG) when the magnetic flux sine wave is excited.

Sample Characteristics Table

■Comparison of magnetic characteristics (JFE in-house data) : Rolling direction, shear cross-section

Material	Thickness (mm)	Specific resistance (μΩ-m)	DC max. relative permeability	Saturation magnetization (T)	Magnetic flux density B8(T)	Magnetic flux density B25(T)	Magneto-striction λ10/400 (×10⁻⁶)	Core loss (W/kg)						
								W10/50	W10/400	W10/1k	W5/2k	W2/5k	W1/10k	W0.5/20k
JNEX-Core	0.10	0.82	23,000	1.80	1.29	1.40	0.1	0.5	5.7	18.7	13.7	11.3	8.3	6.9
Grain-oriented silicon steel	0.05	0.48	–	2.03	1.75	–	−0.8	0.8	6.4	17.2	13.5	9.2	7.1	5.2
	0.10		24,000		1.84	1.91		0.7	6.0	22.7	22.0	20.0	18.0	14.0
	0.23		92,000		1.92	1.96		0.3	7.8	35.0	33.0	33.0	30.0	32.0
	0.35		94,000		1.92	1.96		0.4	12.2	55.0	49.5	49.5	47.0	49.0
Non-oriented silicon steel	0.10	0.57	12,500	2.05	1.58	–	7.8	0.8	8.5	27.1	22.4	16.5	13.3	–
	0.20		15,000	2.03	1.44	1.53		0.7	11.0	38.5	33.2	26.2	23.0	–
	0.35		18,000	1.96	1.45	1.56		0.7	14.4	62.0	50.2	38.0	33.0	–
Fe-based amorphous	0.025	1.30	300,000	1.50	1.38	–	27.0	0.1	1.5	5.5	8.1	4.0	3.6	3.3
Ferrite	Bulk	–	3,500	–	0.37	–	21.0	–	–	–	–	2.2	2.0	1.8

* W10/50 is the core loss at 50Hz, 1T(=10kG) when the magnetic flux sine wave is excited.
* B8 is the magnetic flux density at 800A/m.
* λ10/400 is the magnetostriction at 400Hz, 1T when the magentic flux sine wave is excited.

JNHF-Core

For the JNHF-Core, the siliconization technology (CVD process) used for JNEX-Core has been further developed, leading to even greater lower core loss in the high-frequency ranges.

Low Core Loss

For high-frequencies in excess of 5 kHz, outshines even JNEX-Core for low core loss.

Highly Workable

Excellent workability for pressing, bending, stamping, etc.

Non-oriented

There is virtually no difference in the characteristics between the rolling direction (L-direction) and the transverse direction (C direction).
Therefore, this can be used in a wide range of applications, from stationary machines to rolling machines.

High-saturation magnetic flux density

Has a high saturation magnetic flux density of 1.85 – 1.94 T Using this material in a reactor takes full advantage of the superior DC superimposition characteristics.

10JNHF600

●High-frequency core loss curve

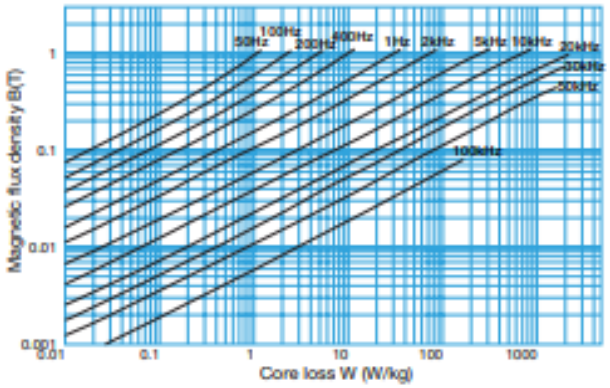

Measurement: 25 cm Epstein test
Rolling direction, shear cross-section

20JNHF1300

●High-frequency core loss curve

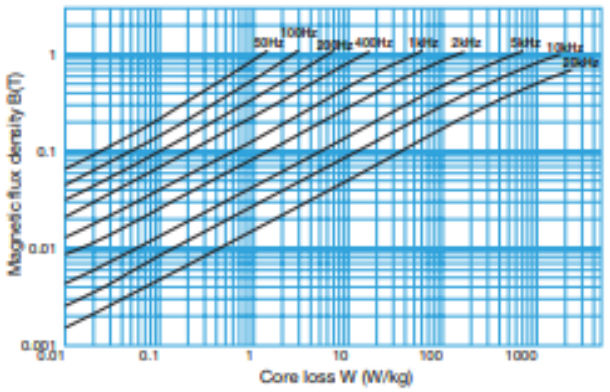

Core Loss Comparison between JNHF-Core and JNEX-Core (0.10 mm thick)

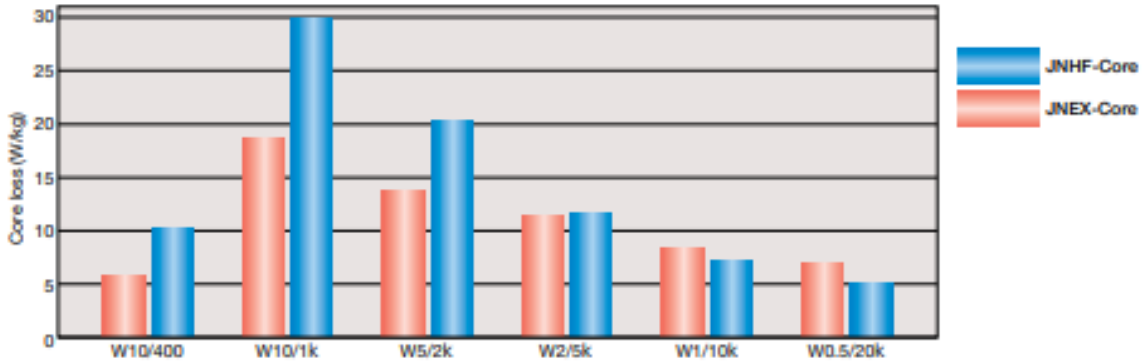

* W10/400 is the core loss at 400Hz, 1T(=10kG) when the magnetic flux sine wave is excited.

Comparison of reactor DC superimposition characteristics

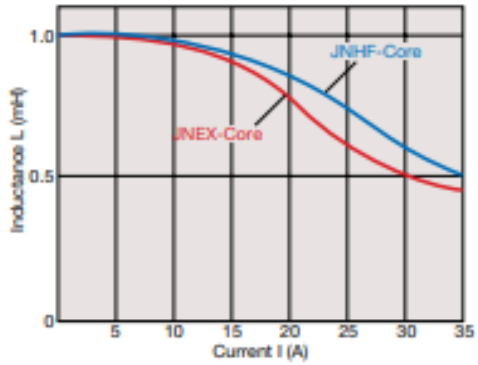

* Using a multi-layer block core (sheet thickness 0.1 mm)
* 20 kHz, 0.05 T equivalent ripple current applied

Press machined sample (0.2 mm thick)

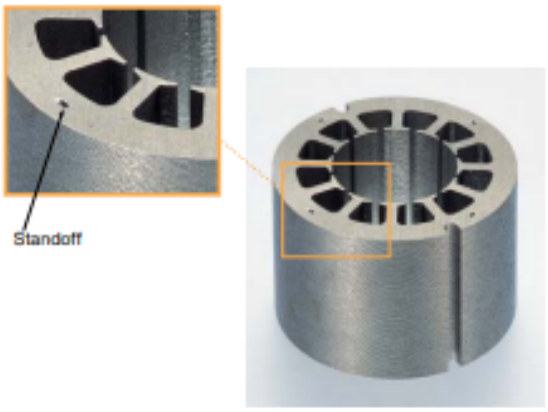

Sample Characteristics Table

■Comparison of magnetic characteristics (JFE in-house data) : Rolling direction, shear cross-section

Material	Thickness (mm)	DC max relative permeability	Saturation magnetization (T)	Magnetic flux density Ba(T)	Magnetic flux density Bzs(T)	Core loss (W/kg)						
						W10/50	W10/400	W10/1k	W5/2k	W2/5k	W1/10k	W0.5/20k
JNHF-Core	0.10 0.20	4,100 3,900	1.88 1.94	1.15 1.09	1.44 1.47	1.1 1.2	10.1 14.5	30.0 51.6	20.2 29.1	11.5 17.9	7.1 12.7	5.0 9.5
JNEX-Core	0.10	23,000	1.80	1.29	1.40	0.5	5.7	18.7	13.7	11.3	8.3	6.9
Grain-oriented silicon steel	0.10	24,000	2.03	1.84	1.91	0.7	6.0	22.7	22.0	20.0	18.0	14.0
Non-oriented silicon steel	0.35	18,000	1.96	1.45	1.56	0.7	14.4	62.0	50.2	38.0	33.0	–
Amorphous	0.025	300,000	1.50	–	–	0.1	1.5	5.5	8.1	4.0	3.6	3.3

* W10/50 is the core loss at 50 Hz, 1 T (=10kG) when the magnetic flux sine wave is excited
* Bs is the magnetic flux density at 800A/m.

Uses for Super Core™

Super Core™ Applications

JNEX-Core

Reduced noise and low core loss for high-frequency magnetic components

JNHF-Core

Further core loss reduction in high frequency ranges beyond 5 kHz

High-frequency transformer

Transformers

The low core loss characteristics at high-frequency of Super Core™ allow it to be effectively used for a wide range of transformers, driven from several hundred Hz to several tens of kHz.
Super Core™ allow the transformer to generate less heat, and provide higher design induction than conventional silicon steel sheets, enabling transformer size to be reduced. This then reduces the quantities of other required transformer materials, such as the copper wire, leading to overall cost reductions.
By taking full advantage of the low magnetostriction characteristics of JNEX-Core, it is also possible to reduce transformer noise dramatically.

●Examples of noise and size reduction for high-frequency transformers (for fixed core loss)

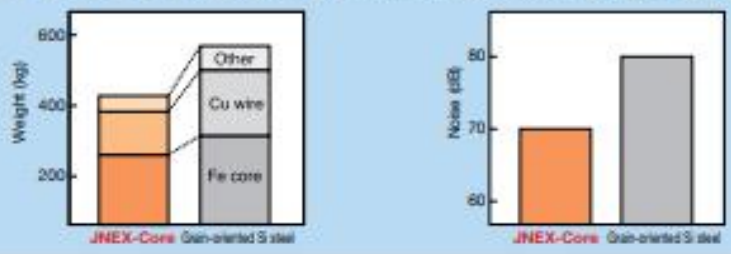

●High-frequency transformer noise and core loss comparison

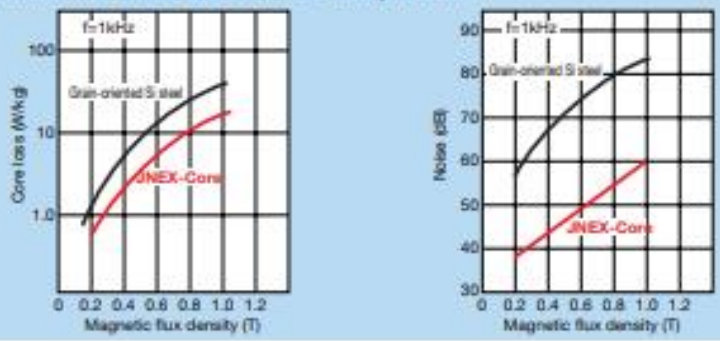

Reactors (Chokes, Inductors)

Due to the high saturation magnetic flux density, the low core loss at high-frequency and the high-permeability of Super Core™ , it is ideal for applications in high-frequency reactors with high-frequency current superimposition over a broad range of frequencies.
Because Super Core™ meets all high frequency wave regulations and power factor improvements, demand is on the increase for its use in not only inverter output reactors but also in active filters and in PWM converter reactors in the market sectors from consumer electronics to industrial, renewable power generation and automotives.
Diagram below shows the characteristics of general magnetic cores and Super Core™ (JNHF-Core and JNEX-Core) from the perspective of the magnetic characteristics required for a high-frequency reactor, i.e., core loss and saturation flux density. In this diagram, the iron loss is compared under a ripple frequency of 20 kHz. The data shows that JNHF-Core and JNEX-Core both have the necessary characteristics for a high-frequency reactor, and indicate superior total balance compared to the other magnetic cores.

●Typical magnetic properties of soft magnetic core materials applied for switched mode power supplies using IGBT, MOS-FET

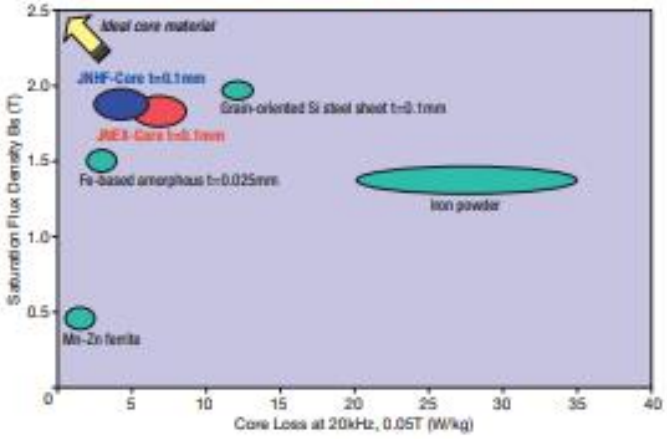

Diagram below indicates the power supply and the switching frequency (ripple frequency) that are suitable for Super Core™. As the data shows, Super Core™ is suitable for medium-capacity inverter and converter reactors of 3 kHz, 1 kVA or 10A or higher. Particularly with this power supply, Super Core™ effectively brings such benefits as high efficiency, compact size, and low noise.

●Suitable core materials for transformers and reactors in switched mode power supplies

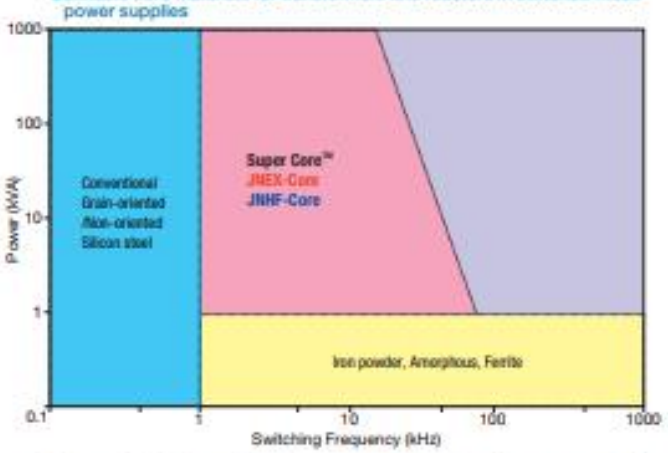

Super Core™ meets a diverse range of customers needs since it can be formed into wound cores, such as C-cores and toroidal cores, as well as into lamination cores and glued block cores of various shapes by cutting or pressing.
For example, as illustrated in the figure on the bottom right, a reactor with 4-point gaps, consisting of a combination of glued-lamination core and a flat, vertically wound coil, with excellent impedance-frequency characteristics, shows DC superimposition characteristics that are far superior to conventional wound core with one or two gaps.
Furthermore, the low magnetostriction characteristics of JNEX-Core reduce high frequency noise in the audible ranges of 20kHz or less, and therefore provide quiet power sources for inverters and converters.

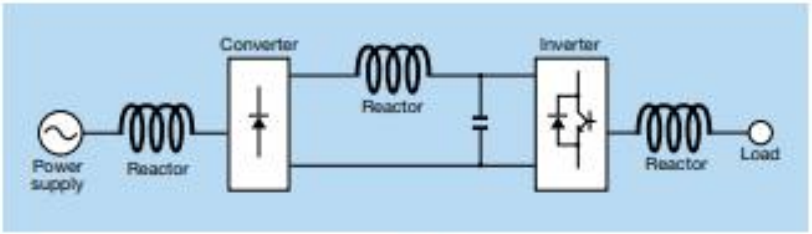

●Comparison of DC superimposition characteristics

High-frequency reactors

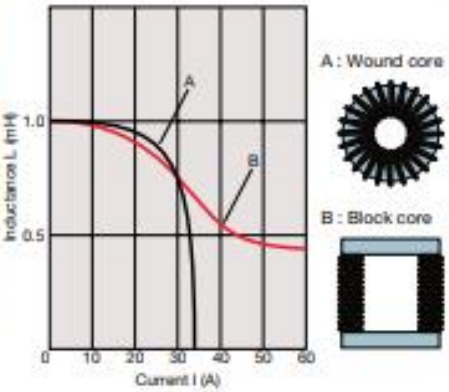

Motors & Generators

Because of its superior low core loss characteristics, Super Core™ has many advantages in high-speed motors and power generator applications -- stator, rotor, and yoke -- and contributes greatly to efficiency.
It is also effective in reducing noise that is caused in part by magnetostriction.
Super Core™ has attracted the attention for its use in electric and hybrid car motors, power generators, as well as the motors for OA devices.

Other applications

Applications are diverse, including magnetic shields, which take advantage of the excellent permeability into high-frequency ranges, magnetic yokes used at high-frequencies, heating equipment inductors, and CT(Current Transformer). Other applications include inductors and filters that reduce high-frequency noise.

PRODUCTS

Base Coil

*The base coil is made on a continuous production line with a siliconizing process.

Slit Coil

*The base coil goes through a slitter line, slits are cut and the coil is hooped.
*After a paper sleeve is put around its inner circumference, the slit coil is wound with rust-preventing paper used for packaging. It is then placed on skids for shipment.

Product Dimensions and Specifications

Product name	Thickness (mm)	Code number	Core loss (W/kg)	Dimensions (mm)	Space factor (%)	Density (g/cm³)
JNEX-Core	0.10	10JNEX900	W10/400 9.0 or less	Sheet width 20–600	90 or more	7.49
JNHF-Core	0.10	10JNHF600	W0.5/20k 6.0 or less	Core outer diameter Max 900	90 or more	7.53
	0.20	20JNHF1300	W0.5/20k 13.0 or less	Core inner diameter Std. 508	92 or more	7.57

* W10/50 indicates the core loss at 50 Hz, 1 T (=10kG) when the magnetic flux sine wave is excited. Similarly, W10/400 indicates for 400 Hz, 1 T (=10kG), and W0.5/20k indicates the core loss for 20 kHz, 0.05 T (=500G).

Insulating Coating

A mixture of organic and inorganic type of coating is available.

Substances of Environmental Concern Data

In JFE's Electrical Steel Sheet products, substances of environmental concern listed below are not detected in the results of analyses conducted by following methods.

Analytical method

Substance	Preparation	Analytical method	Minimum limit of determination
Hg	Wet digestion	Atomic absorption spctrometric method after reduction-generation as Mercury gas	1ppm
Cd	Wet digestion (dissolved completely)	Atomic absorption spectrometric method	10ppm
Pb	Wet digestion (dissolved completely)	Atomic absorption spectrometric method	10ppm
Cr^{6+}	Extraction in boiling water	Diphenylcarbazide spectrophotometric method	0.01μg/cm²

Note:1.Insulation coating contains Cr^{3+}
Please pay attention when heating in the oxidizing atmosphere or using in the high temperature conditions.
2.Chemical substances such as PBB and PBDE are neither intentionally added nor used in our production processes.

Processed Goods

●Wound Cores (C-core and Toroidal core)

- After the steel coil is formed and annealed, it is soaked in varnish and fixed.
- The sheet thickness is 0.05 mm or 0.1 mm.
- Please contact us regarding the available size.

●Laminated Cores

- A core produced with a stamping-lamination process to take full advantage of the features of non-oriented Super Core™.
- Unlike products using conventional 3% Si electrical steel sheets, these can be used up to high-frequency ranges.
- Please contact us regarding the available size.

■Block Core

●Block cores are small and medium sized cores for reactors and transformers. They are highly effective for reducing costs when mass-producing such equipment.

●The standard lamination fixing method is adhesive fixation.

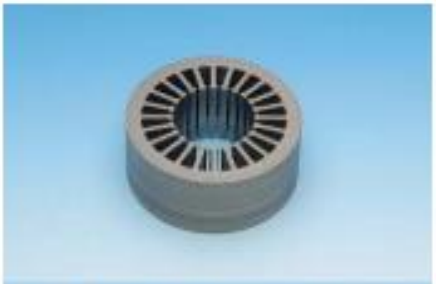

■Adhesive-Laminated Core for Motors

●A core that has been adhesive-laminated and solidified

●Provide significant reduction in high-frequency core loss due to high-speed rotation

■Block Core with Rounded Corners

●A laminated core made in virtually the same shape as a cut core, so that it is possible to use the same washers and clamp bands

●Stacked Cores

- These cores are used mainly with medium- and large-sized transformers and reactors. The user stacks the strips and affixes them using bolts.
- The possible range of production varies somewhat depending on the processing maker, so check before proceeding.
- Please contact us regarding the available size.

●Cores for Motors and Power Generators

- Motors and power generators using Super Core™, the best non-oriented magnetic steel sheets available, demonstrate superior performance.
- The core manufacture is determined separately in consultation with each customer according to their design plans.

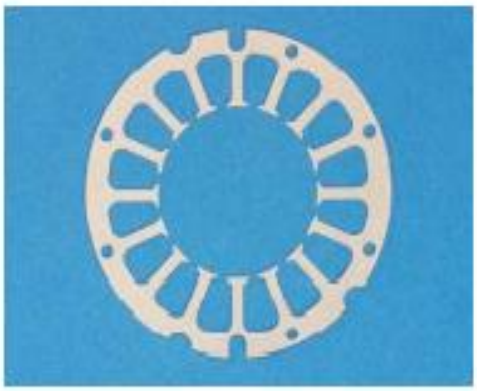

■For inquiries or orders, contact the office listed below or your nearest JFE Steel Corporation office.

2-2-3 Uchisaiwaicho, Chiyoda-ku, Tokyo 100-0011 (Hibiya Kokusai Bldg)
Electrical Steel Section TEL +81-3-3597-4099 FAX +81-3-3597-4779
URL : http://www.jfe-steel.co.jp/en/supercore

Cat.No.F1E-002-02

JFE Steel Corporation

http://www.jfe-steel.co.jp/en/

TOKYO HEAD OFFICE Hibiya Kokusai Building, 2-3 Uchisaiwaicho 2-chome, Chiyodaku, Tokyo 100-0011, Japan
Phone : (81)3-3597-3111 Fax : (81)3-3597-4860

NEW YORK OFFICE JFE Steel America, Inc.
600 Third Avenue, 12th Floor, New York, NY 10016, U.S.A.
Phone : (1)212-310-9320 Fax : (1)212-308-9292

HOUSTON OFFICE JFE Steel America, Inc., Houston Office
10777 Westheimer, Suite 230, Houston, TX 77042, U.S.A.
Phone : (1)713-532-0052 Fax : (1)713-532-0062

BRISBANE OFFICE JFE Steel Australia Resources Pty Ltd.
Level 19, CPA Centre, 307 Queen St, Brisbane, QLD 4001, Australia
Phone : (61)7-3229-3855 Fax : (61)7-3229-4377

RIO DE JANEIRO OFFICE JFE Steel do Brasil LTDA / JFE Steel Corporation, Rio de Janeiro Office
Praia de Botafogo, 228 Setor B, Salas 508 & 509, Botafogo, CEP 22250-040, Rio de Janeiro-RJ, Brazil
Phone : (55)21-2553-1132 Fax : (55)21-2553-3430

LONDON OFFICE JFE Steel Europe Limited
15th Floor, The Broadgate Tower, 20 Primrose Street, London EC2A 2EW, U.K.
Phone : (44)20-7426-0166 Fax : (44)20-7247-0168

DUBAI OFFICE JFE Steel Corporation, Dubai Office
P.O.Box 261791 LOB19-1208, Jebel Ali Free Zone Dubai, U.A.E.
Phone : (971)4-884-1833 Fax : (971)4-884-1472

NEW DELHI OFFICE JFE Steel India Private Limited
1101, 11th Floor, Unitech's Signature Tower, Tower-A, South City-I, NH-8, Gurgaon, Haryana, 122002, India
Phone : (91)124-426-4981 Fax : (91)124-426-4982

MUMBAI OFFICE JFE Steel India Private Limited Mumbai Office
308, A Wing, 215 Atrium, Andheri - Kurla Road, Andheri (East), Mumbai - 400093, Maharashtra, India
Phone : (91)22-3076-2760 Fax : (91)22-3076-2764

SINGAPORE OFFICE JFE Steel Asia Pte. Ltd.
16 Raffles Quay, No. 15-03, Hong Leong Building, 048581, Singapore
Phone : (65)6220-1174 Fax : (65)6224-8357

BANGKOK OFFICE JFE Steel (Thailand) Ltd.
22nd Floor, Abdulrahim Place 990, Rama IV Road, Bangkok 10500, Thailand
Phone : (66)2-636-1886 Fax : (66)2-636-1891

VIETNAM OFFICE JFE Steel Vietnam Co., Ltd.
Unit 1401, 14th Floor, Kumho Asiana Plaza, 39 Le Duan Street, Dist 1, HCMC, Vietnam
Phone : (84)8-3825-8576 Fax : (84)8-3825-8562

JAKARTA OFFICE JFE Steel Corporation, Jakarta Office
16th Floor Summitmas II, JL Jendral Sudirman Kav. 61-62, Jakarta 12190, Indonesia
Phone : (62)21-522-6405 Fax : (62)21-522-6408

MANILA OFFICE JFE Steel Corporation, Manila Office
23rd Floor 6788 Ayala Avenue, Oledan Square, Makati City, Metro Manila, Philippines
Phone : (63)2-886-7432 Fax : (63)2-886-7315

SEOUL OFFICE JFE Steel Korea Corporation
6th Floor. Geumgang-Tower. 889-13, Daechi-dong, Gangnam-gu, Seoul, 135-570, Korea
Phone : (82)2-3468-4130 Fax : (82)2-3468-4137

BEIJING OFFICE JFE Steel Corporation Beijing
1009 Beijing Fortune Building No.5, Dongsanhuan North Road, Chaoyang District, Beijing, 100004, P.R.China
Phone : (86)10-6590-9051 Fax : (86)10-6590-9056

SHANGHAI OFFICE JFE Consulting (Shanghai) Co., Ltd.
Room 801, Building A, Far East International Plaza, 319 Xianxia Road, Shanghai 200051, P.R.China
Phone : (86)21-6235-1345 Fax : (86)21-6235-1346

GUANGZHOU OFFICE JFE Consulting (Guangzhou) Co., Ltd./ JFE Steel Corporation, Guangzhou Office
Room 3901, Citic Plaza, 233 Tian He North Road, Guangzhou 510613, P.R.China
Phone : (86)20-3891-2467 Fax : (86)20-3891-2469

1403R (0708) SP

Appendix 3

MAGNETICS

Magnetics XFLUX® cores

6.5% SiFe cores for high current applications

XFLUX® cores offer an economical high saturation (1.6 Tesla) solution for use in low and medium frequency inductors and chokes. The high saturation is advantageous in applications where inductance under load is critical such as inverters for renewable energy and Uninterruptable Power Supplies (UPS).

XFLUX distributed air gap cores are made from 6.5% silicon iron powder. A true high temperature material, with no thermal aging, XFLUX offers lower losses than powdered iron cores and superior DC bias performance. The soft saturation of XFLUX material offers an advantage over ferrite cores.

XFLUX can be a lower cost alternative to High Flux, in situations where the higher core losses of XFLUX are acceptable.

Material Properties	
Composition	Fe Si
Saturation Flux Density	1.6 Tesla
Typical Core Loss (50kHz, 100mT)	650 mW/cm³
Curie Temperature	700°C
Operating Temperature Range	-55°C to 200°C
DC Bias (80%)	60 A-T/cm min
DC Bias (50%)	120 A-T/cm min

Material	Alloy Composition	Core Loss	DC Bias	Relative Cost	Saturation Flux Density (Tesla)	Curie Temperature	Operating Temperature Range	60 μ μ flat to...
XFlux	**Fe Si**	**High**	**Best**	**Low**	**1.6**	**700° C**	**-55° C to 200° C**	**500 kHz**
High Flux	Fe Ni	Moderate	Best	Medium	1.5	500° C	-55° C to 200° C	1 MHz
AmoFlux	Fe Si B C	Low	Better	Medium	1.5	400° C	-30° C to 155° C	2 MHz
Kool Mu	Fe Si Al	Low	Good	Low	1.0	500° C	-55° C to 200° C	900 kHz
MPP	Fe Ni Mo	Very Low	Better	High	0.75	460° C	-55° C to 200° C	2 MHz
Iron Powder	Fe	Highest	Good	Lowest	1.2 - 1.5	770° C	-30° C to 75° C	500 kHz
Ferrite	Ceramic	Lowest	Poor	Lowest	0.45	100 - 250° C	Variable	Variable

XFlux®
Permeability vs. AC Flux Density

26µ Toroids $(\Delta\mu/\mu i) = 3.846*10^{-4} + (4.288*10^{-1} B) - (1.853 B^2) + (3.132 B^3) - (2.138 B^4)$

60µ Toroids $(\Delta\mu/\mu i) = 1.584*10^{-3} + (7.074*10^{-1} B) - (2.782 B^2) + (4.403 B^3) - (2.621 B^4)$

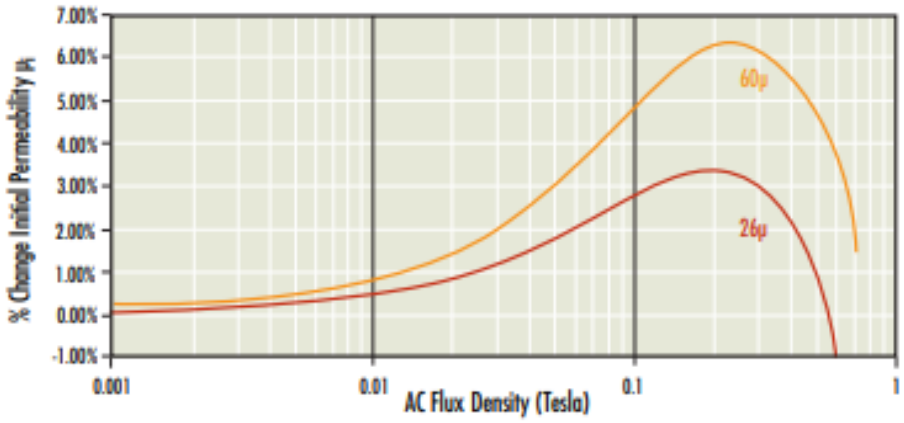

XFlux® Permeability vs. Frequency

26µ Toroids $(\Delta\mu/\mu i) = 3.000*10^{-4} - (3.132*10^{-2} F) + (4.902*10^{-3} F^2) - (1.015*10^{-3} F^3) + (5.543*10^{-5} F^4)$

60µ Toroids $(\Delta\mu/\mu i) = 6.805*10^{-3} - (7.575*10^{-2} F) + (1.206*10^{-2} F^2) - (1.607*10^{-3} F^3) + (7.524*10^{-5} F^4)$

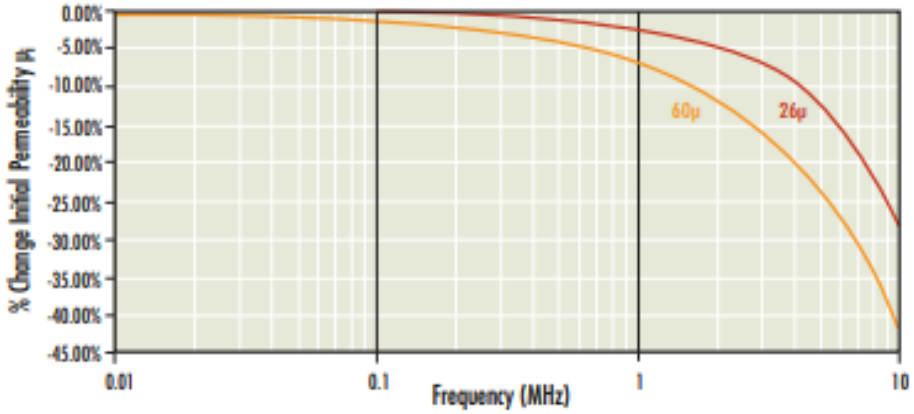

XFlux® Permeability vs. Temperature

26µ Toroids $(\Delta\mu/\mu i) = -3.879*10^{-3} + (1.356*10^{-3} T) + (1.228*10^{-7} T^2) - (1.739*10^{-8} T^3) + (4.35*10^{-10} T^4)$

60µ Toroids $(\Delta\mu/\mu i) = -4.01*10^{-3} + (1.553*10^{-4} T) + (1.875*10^{-8} T^2) + (3.907*10^{-8} T^3) - (1.213*10^{-11} T^4)$

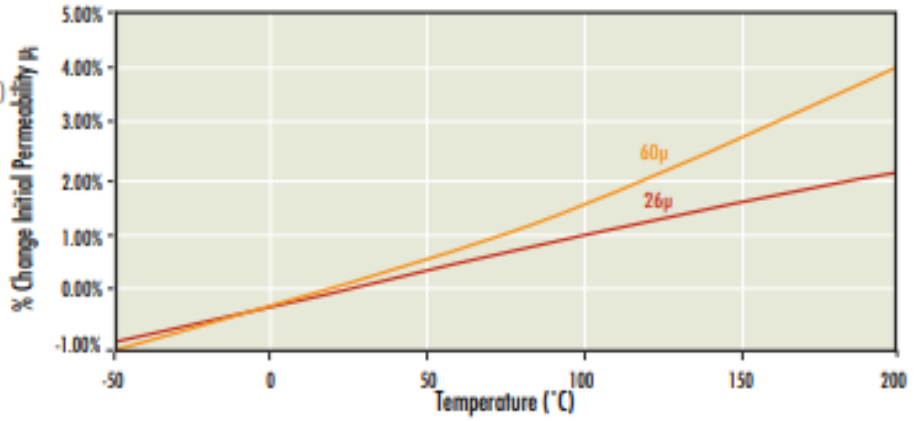

XFlux® Magnetization Curves

26µ Toroids $B = \{(4.445*10^{2} + 2.547*10^{2} H + 5.153*10^{4} H^2) / (1 + 9.162*10^{2} H + 3.510*10^{4} H^2)\}^2$

60µ Toroids $B = \{(2.455*10^{2} + 8.789*10^{2} H + 6.444*10^{3} H^2) / (1 + 4.188*10^{1} H + 4.668*10^{3} H^2)\}^2$

26µ Shapes $B = \{(2.275*10^{5} + 6.400*10^{2} H + 2.615*10^{3} H^2) / (1 + 3.654*10^{1} H + 1.972*10^{3} H^2)\}^2$

40µ Shapes $B = \{(6.495*10^{3} + 7.939*10^{2} H + 4.816*10^{3} H^2) / (1 + 4.312*10^{1} H + 3.647*10^{3} H^2)\}^2$

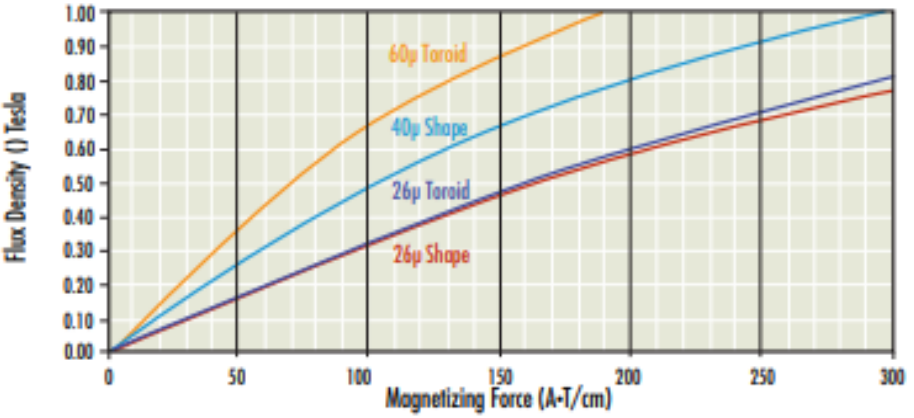

XFlux® Permeability vs. DC Bias

26µ Toroids $(\mu/\mu i) = 0.9970 + (5.006*10^{-4}\ H) - (1.510*10^{-5}\ H^2) + (3.917*10^{-8}\ H^3) - (3.396*10^{-11}\ H^4)$

60µ Toroids $(\mu/\mu i) = 0.9887 + (2.740*10^{-3}\ H) - (1.091*10^{-4}\ H^2) + (6.052*10^{-7}\ H^3) - (1.058*10^{-9}\ H^4)$

26µ Shapes $(\mu/\mu i) = 0.9940 + (1.062*10^{-3}\ H) - (2.317*10^{-5}\ H^2) + (6.612*10^{-8}\ H^3) - (6.511*10^{-11}\ H^4)$

40µ Shapes $(\mu/\mu i) = 0.9870 + (3.530*10^{-3}\ H) - (8.498*10^{-5}\ H^2) + (3.830*10^{-7}\ H^3) - (5.508*10^{-10}\ H^4)$

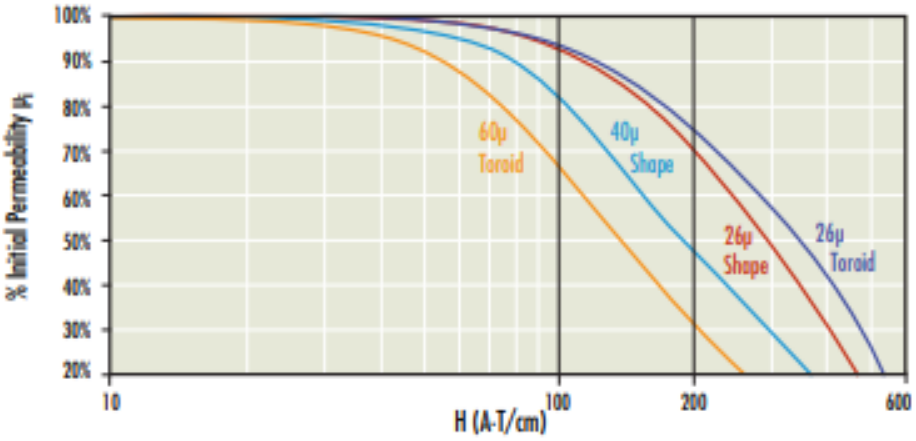

XFlux® Core Loss Density Toroids 26µ

26µ Toroids 1kHz–20kHz $P_L = 335\ B^{1.825}\ F^{1.332}$

>20kHz $P_L = 510\ B^{1.830}\ F^{1.180}$

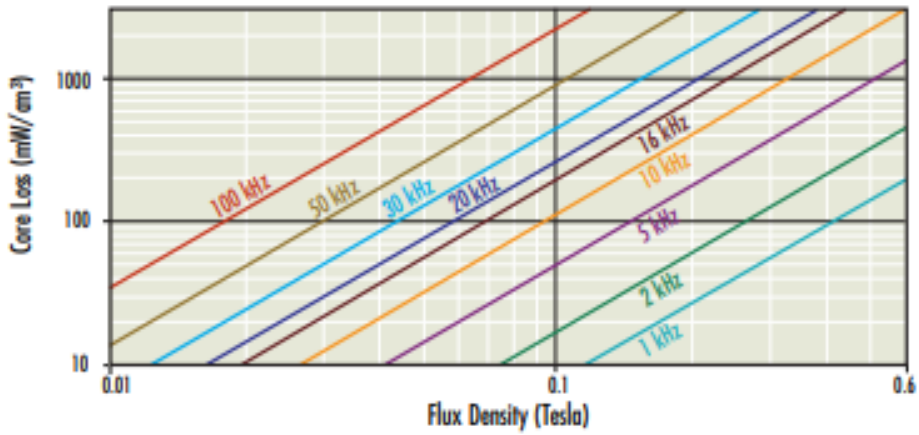

XFlux® Core Loss Density Toroids 60µ

60µ Toroids 1kHz–10kHz $P_L = 335\ B^{1.865}\ F^{1.283}$

>10kHz $P_L = 505\ B^{1.865}\ F^{1.153}$

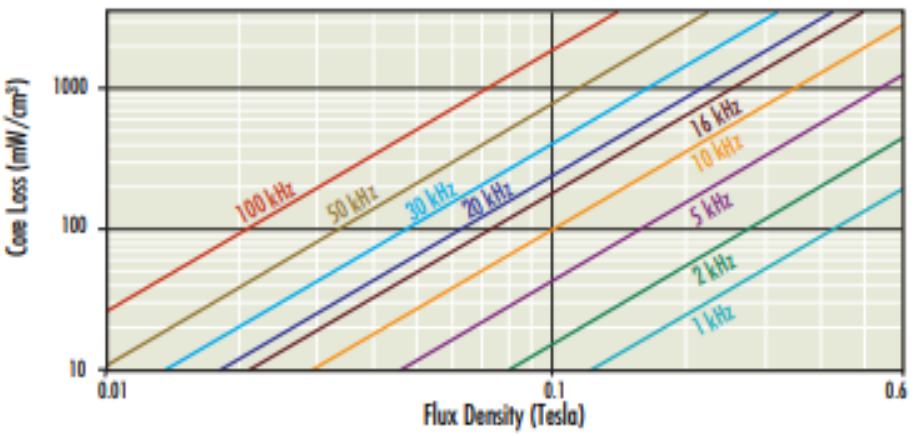

XFlux®
Core Loss Density Shapes 26µ, 40µ

26µ Shapes $P_L = 429\ B^{2.034}\ F^{1.287}$

40µ Shapes $P_L = 429\ B^{2.034}\ F^{1.287}$

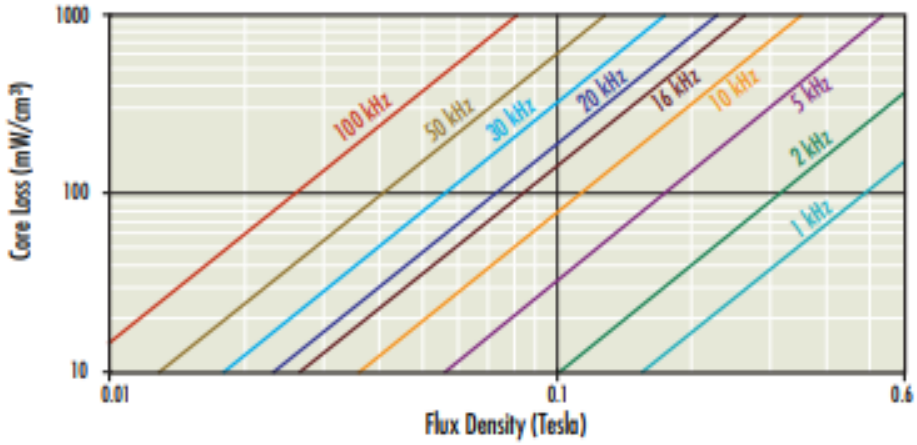

XFlux® Dimensions and Magnetic Data

Dimensions (after coating)			60µ		26µ		Magnetic Data				
OD (mm) max	ID (mm) min	HT (mm) max	Part Number	A_L±8% (nH/T²)	Part Number	A_L±8% (nH/T²)	W_e (mm²)	L_e (mm)	A_e (mm²)	V_e (mm³)	60µ Weight (g)
13.5	6.98	5.52	0078051A7	27			38.3	31.2	10.9	340	2.5
17.3	9.52	7.12	0078121A7	35			71.2	41.2	19.2	791	5.6
18.1	9.01	7.12	0078381A7	43			63.8	41.4	23.2	960	7.2
21.1	12	7.12	0078848A7	32			114	50.9	22.1	1,120	7.9
23.7	13.3	8.39	0078059A7	43			139	56.7	31.7	1,800	13
24.4	13.7	9.66	0078351A7	51			149	58.8	38.8	2,280	16
27.7	14.1	12	0078894A7	75	0078932A7	32	156	63.5	65.4	4,150	29
27.7	14.1	15	0078894A7HT15	94			156	63.5	82.1	5,210	37
33.7	19.4	11.5	0078071A7	61			297	81.4	65.6	5,340	38
35.2	22.5	9.78	0078586A7	38			399	89.5	46.4	4,150	29
36.7	21.5	11.4	0078076A7	56			364	89.8	67.8	6,090	43
40.8	23.3	15.4	0078083A7	81			427	98.4	107	10,600	78
47.6	27.9	16.2	0078090A7	86	0078091A7	37	610	116	134	15,600	110
47.6	23.3	19	0078439A7	135	0078440A7	59	427	107	199	21,300	151
51.7	30.9	14.4	0078716A7	73			751	127	125	15,900	110
58	34.7	14.9	0078110A7	75	0078111A7	33	948	143	144	20,700	150
58	25.6	16.2	0078192A7	138	0078191A7	60	514	125	229	28,600	200
62.9	31.7	25.9	0078617A7	189	0078615A7	82	789	144	360	51,800	380
69.4	34.7	21.4	0078072A7	143			945	158	314	49,700	360
75	44.4	35.9	0078737A7	204	0078735A7	88	1,550	184	497	91,400	660
79	48.2	13.9	0078867A7	68	0078868A7	30	1,820	196	176	34,500	240
79	48.2	17.1	0078907A7	85	0078908A7	37	1,820	196	221	43,400	320
103	55.8	17.9	0078099A7	111	0078102A7	48	2,470	243	358	86,900	620
134	77.2	26.8			0078337A7	68	4,710	324	678	220,000	1400

E Core		Dimensions			Magnetic Data				
Part Number	A_L±8% (nH/T²)	Length (mm) max	Leg Length (mm) min	Height (mm) max	W_e (mm²)	L_e (mm)	A_e (mm²)	V_e (mm³)	Weight (g)
00X4022E026	104	43.5	21.4	20.3	276	98.4	237	23,300	63
00X4022E040	140	43.5	21.4	20.3	276	98.4	237	23,300	65
00X6527E026	162	66.4	32.9	27.4	530	147	540	79,400	210
00X6527E040	230	66.4	32.9	27.4	530	147	540	79,400	220
00X8020E026	103	81.2	38.7	20.2	1110	185	389	72,000	200
00X8020E040	145	81.2	38.7	20.2	1110	185	389	72,000	210

Block	Dimensions			Magnetic Data	
Part Number	Length (mm) max	Width (mm) min	Height (mm) max	V_e (mm³)	Weight (g)
00X4741B026	48.1	41.5	27.9	53,600	330
00X4741B040	48.1	41.5	27.9	53,600	340
00X5030B026	51	30.6	15.3	23,000	140
00X5030B040	51	30.6	15.3	23,000	140
00X6030B026	60.3	30.3	15.3	27,000	170
00X6030B040	60.3	30.3	15.3	27,000	170
00XB030B026	81	30.8	20.1	48,800	300
00XB030B026HT15	81	30.8	15	36,000	230
00XB030B040	81	30.8	20.1	48,800	310

MAGNETICS®

NAFTA SALES
Toll-Free: 1 800 245 3984
Phone: 412 696 1333 • Fax: 412 696 0333
Web: www.mag-inc.com
Email: magnetics@spang.com

INTERNATIONAL SALES
Phone: +852 3102 9337
Fax: +852 3585 1482
Email: asiasales@spang.com
China Hotline +86 139 1147 1417

Appendix 4

United States Patent

Willyoung

[15] **3,660,705**

[45] **May 2, 1972**

[54] POLYPHASE GENERATOR WINDINGS

[72] Inventor: **David M. Willyoung**, Scotia, N.Y.

[73] Assignee: **General Electric Company**

[22] Filed: **Apr. 24, 1970**

[21] Appl. No.: **31,496**

[52] **U.S. Cl.** **310/198**, 310/205

[51] **Int. Cl.** **HO2k 3/00**

[58] **Field of Search** 310/198, 199, 195, 202, 203, 310/205, 206, 207, 179, 171

[56] **References Cited**

UNITED STATES PATENTS

2,015,562	9/1935	Kilgore	310/202
2,778,962	1/1957	Taylor	310/202
2,778,963	1/1957	Habermann	310/202
3,152,273	10/1964	Harrington	310/198
3,201,627	8/1965	Harrington	310/198
3,408,517	10/1968	Willyoung	310/202
3,470,409	9/1969	Scheda	310/202

Primary Examiner—J. D. Miller
Assistant Examiner—R. Skudy
Attorney—William C. Crutcher, Frank L. Neuhauser, Oscar B. Waddell and Joseph B. Forman

[57] **ABSTRACT**

Each phase of a polyphase armature winding is constituted by a pair of phase belts, each belt consisting of three segments of the winding. The first and third segments in each belt are connected in series with one another and the remaining segment is series-connected with a corresponding segment of the opposite phase belt. Each phase is thus constituted by three separate circuits, but only a single connection ring per phase is necessary to connect segments laying on opposite sides of the armature.

3 Claims, 6 Drawing Figures

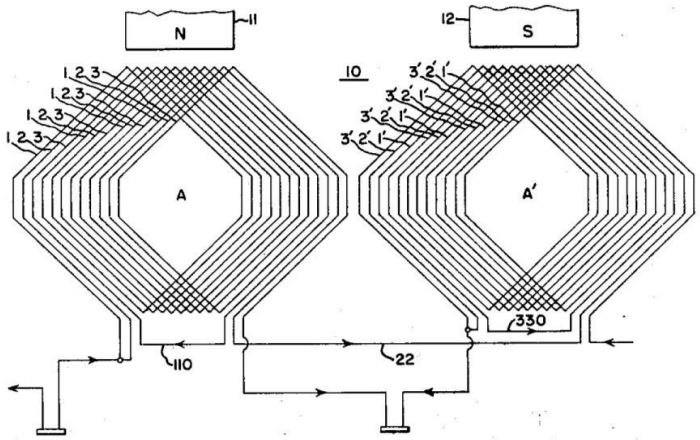

Patented May 2, 1972 **3,660,705**

2 Sheets-Sheet 1

FIG.1

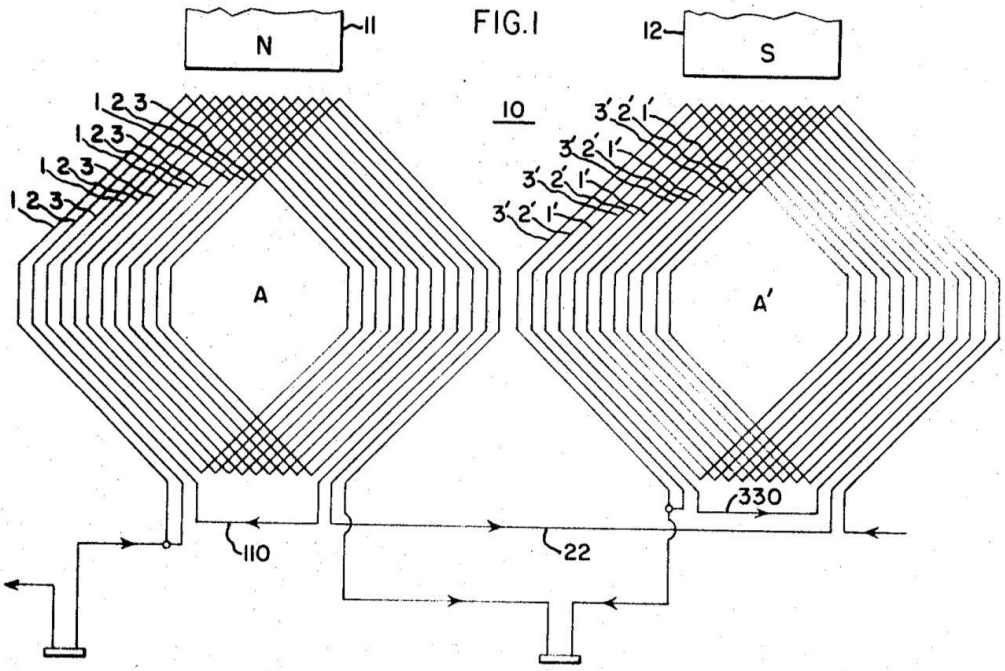

FIG.2

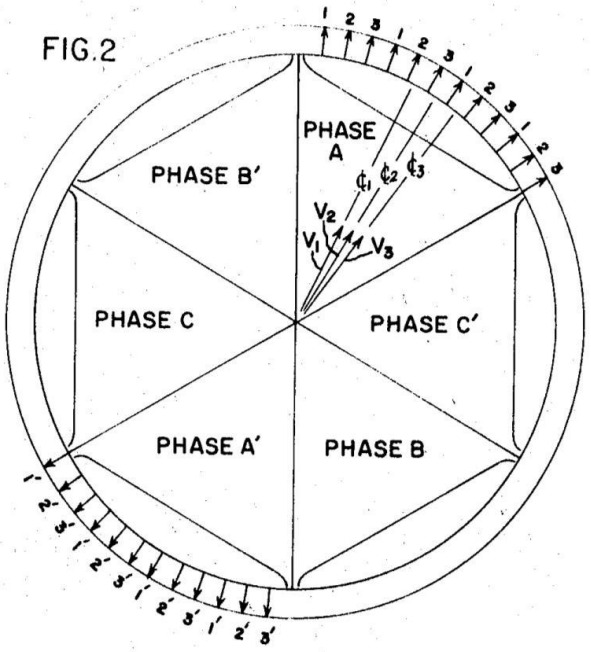

INVENTOR:
DAVID M. WILLYOUNG,
BY W.C. Cutchen
HIS ATTORNEY.

Patented May 2, 1972 **3,660,705**

2 Sheets-Sheet 2

FIG.3 (PRIOR ART)

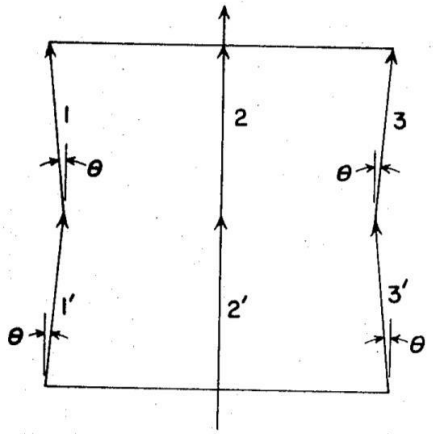

FIG.4 (PRIOR ART)

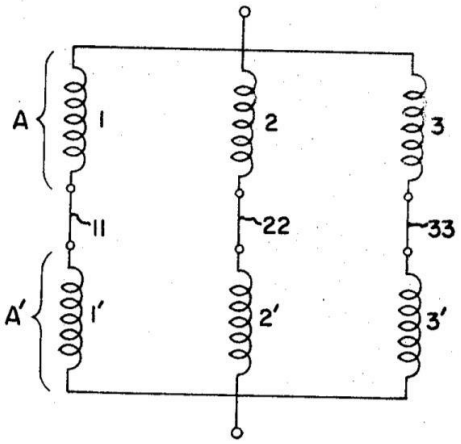

FIG.5

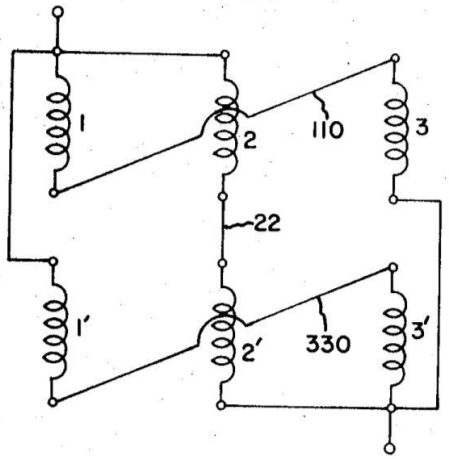

FIG.6

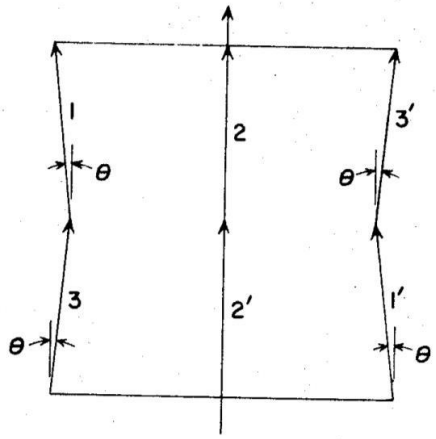

INVENTOR:
DAVID M. WILLYOUNG,
BY W. C. Crutcher,
HIS ATTORNEY.